Electronic Supplementary Material (ESI) for Chemical Science.
This journal is © The Royal Society of Chemistry 2020

Electronic Supplementary Information (ESI)

Conformational editing of intrinsically disordered protein by α-methylation

Valentin Bauer[a†], Boris Schmidtgall[a†], Gergő Gógl[b], Jozica Dolenc[c], Judit Osz[b], Yves Nominé[b], Camille Kostmann[b], Alexandra Cousido-Siah[b], André Mitschler[b], Natacha Rochel[b], Gilles Travé[b], Bruno Kieffer[b] and Vladimir Torbeev[a,1]

[a] Institut de Science et d'Ingénierie Supramoléculaires (ISIS), International Center for Frontier Research in Chemistry (icFRC), University of Strasbourg, CNRS (UMR 7006), Strasbourg, France. *Correspondence should be addressed to V. T. (torbeev@unistra.fr)

[b] Institut de Génétique et de Biologie Moléculaire et Cellulaire (IGBMC), INSERM (U964), University of Strasbourg, CNRS (UMR 7104), Illkirch, France

[c] Chemistry | Biology | Pharmacy Information Center, ETH Zurich, Zurich, Switzerland

[†] - these authors equally contributed to this work

Table of contents:

Supplementary Discussion

Non-optimal helix-helix interfaces observed in [1055meLeu;1076meLeu]ACTR/NCBD complex

The structural information obtained by X-ray crystallography made possible to analyze helix-helix packing and relevant interatomic contacts in the [1055meLeu;1076meLeu]AD1-ACTR/NCBD complex. The structure of the complex represents a noncanonical six-helical bundle (Figure S18). While this is a non-symmetric helix bundle, the helix-helix interactions can be considered in a pairwise manner, allowing their parametrization using the generalized Crick parameters (1). This mathematical framework previously developed for description of any arbitrary helical structure, is helpful for analysis and comparison with the other structures containing helix-helix interaction motifs. The fitted parameters are listed in Table S15.

Interactions between H1-ACTR and H1-NCBD as well as H1-NCBD and H2-NCBD helices follow the geometric parameters of canonical left-handed parallel and antiparallel coiled coils, respectively. The superhelical radius R_0 for H1-ACTR–H1-NCBD is 5.49 Å, a value that is in the upper range of values previously observed for helical dimers, whereas for H1-NCBD–H2-NCBD it is more tight with R_0 equal to 4.98 Å, a value that is close to the most common superhelical radius of 4.85 Å in dimeric coiled coils (1). The other parameters such as superhelical frequency (ω_0) and pitch angle (α) for these two helix pairs (Table S15) approach the most common average values (ω_0 −3.6 °/residue and α −12 °/residue) (1). The helical frequencies ω_1 that characterize the angular rotation of the helices around their local axes with each residue are 101.8 and 101.9 °/residue, respectively, and are also close to the canonical coiled-coil value of 102.8 °/residue. The helical axial shift ΔZ_{off} defined as the distance between the most inward-facing points on the helical curves of the two helices is 0.8 Å for parallel H1-NCBD–H1-ACTR interface and -2.47 Å for antiparallel H1-NCBD–H2-NCBD helix pair, which is in agreement with more coaligned inter-helix side-chain interactions for parallel and interdigitated contacts for antiparallel coiled coils.

The other helix-helix interactions are however less optimal and diverge significantly from the statistically most common values observed for a large number of crystal structures in PDB. For instance, the interhelical crossings in H2-NCBD–H2-ACTR, H3-NCBD–H3-ACTR and H3-NCBD–H1-ACTR are right-handed, which is rather rare for helix-helix interactions (1). The superhelical radii R_0 are in the 5.45-6.20 Å range, which indicate that the helix interfaces are not tightly packed. The superhelical frequency ω_0 and pitch angle α also deviate significantly from canonical values. The helical frequencies ω_1 for right-handed helix-helix interactions are attenuated as expected in comparison to the canonical left-handed value (2).

To characterize the interactions between the respective helices we applied SOCKET software (3) in order to identify stabilizing knob-into-hole interactions (Figure S18d). The packing between H1-ACTR–H1-NCBD is stabilized by three well-defined knobs-into-holes, while H1-NCBD–H2-NCBD is held together by two complementary knob-into-hole contacts. Less optimal packing was observed between H2-NCBD–H2-ACTR and H3-NCBD–H3-ACTR with only one knob-into-hole contact each, however, both deviating from ideal geometry, where a typical knob residue is centered from four side residues of the hole. The two helices H2-ACTR and H3-NCBD do not have knobs-into-holes, instead they interact via the salt-bridge requiring more space at the helix interface and which also explains why the superhelical radius R_0 6.20 Å is the highest among other helix pairs. The packing between helices H3-NCBD and H1-ACTR is particularly poor with no knobs-into-holes present despite the large and generally hydrophobic interface. Overall, the analysis of crystal structure reveals that the best complementary interactions are between helices H1-ACTR–H1-NCBD and H1-NCBD–H2-NCBD. Despite being physically and chemically reasonable, the other helix-helix contacts are found to be less optimal when compared to ideal geometries. By providing quantitative metrics for helix-helix contacts our analysis corroborates and extends the results of Ala-scanning mutagenesis and thermodynamics study that concluded that the binding interface in the AD1-ACTR/NCBD complex is energetically non-optimal or "frustrated" (4).

Supplementary Materials and Methods

1. Chemical synthesis of peptides and protein domains

Reagents: Solvents, chemicals and reagents were purchased from commercial sources. Fmoc-α-*L*-amino acids and resins for solid-phase peptide synthesis were purchased from Aapptec, Bachem or Iris Biotech, diisopropylethylamine (DIEA) and piperidine from Sigma-Aldrich, trifluoroacetic acid (Biograde) from Halocarbon. Fmoc-protected α-methylated *L*-amino acids were purchased from OKeanos Tech. (China), Iris Biotech and Bachem. The coupling reagents O-(7-azabenzotriazol-1-yl)-N,N,N',N′-tetramethyluronium hexafluorophosphate (HATU), O-(benzotriazol-1-yl)-N,N,N',N'-tetramethyluronium hexafluorophosphate (HBTU), N,N'-diisopropylcarbodiimide (DIC) and ethyl cyano(hydroxyimino)acetate (OxymaPure) were obtained from Iris Biotech. Fmoc-Lys(Biotin), Fmoc-NH-$(PEG)_3$-COOH and Fmoc-NH-$(PEG)_5$-COOH were purchased from Iris Biotech, and 5-(iodoacetamido)fluorescein from Santa Cruz biotechnology.

Peptide synthesis: The peptide-$^{\alpha}$thioesters and cysteinyl-peptides were synthesized according to the previously described methods of SPPS and conjugated via native chemical ligation as reported (5-8). In this work, in addition to two-segment ligation approach, protein domains were synthesized on solid phase in full length (47 residues) using microwave-assisted automated synthesis. The procedures for this approach are detailed below.

Polypeptides corresponding to [1040-1086]-fragment of the ACTR (numbering as in *Nature* **415**, 549-553 (2002), which corresponds to [1045-1091]-fragment of sequence Q9Y6Q9 (NCOA3_HUMAN) in UniProtKB) and [2066-2112]-fragment of CBP (CREB-binding protein, UniProtKB - P45481 (CBP_MOUSE)) were assembled using a Liberty Blue microwave-assisted automatic synthesizer (CEM Corporation, USA) on either 0.05, 0.1 or 0.2 mmol scale. Variants of the [1040-1086]-fragment of the ACTR containing α-methylated amino acids were synthesized analogously. The following protocol describes a synthesis on 0.1 mmol scale using Fmoc-Lys(Boc)-Wang polystyrene resin, 100-200 mesh with 0.47 mmol/g loading. To perform standard microwave-assisted coupling reactions the coupling reagent DIC (1 mL, 0.5 M), the activator OxymaPure (0.5 mL, 1 M) and the amino acid (2.5 mL, 0.2 M) were added to the resin and the suspension was treated at 90 °C for 2 min (170 W for 15 s, 30 W for 110 s). For some of the amino acids special conditions were used to achieve complete coupling. For Arg as well as for β-branched amino acids the coupling under standard microwave conditions was performed twice. The coupling of His was performed twice at 50 °C for 10 min (0 W 120 s, 35 W 480 s). The coupling of α-

methylated amino acids (0.2 M solution) was performed at 90 °C for 4 min. Fmoc-deprotections were performed by adding 20% (v/v) 4-methylpiperidine (3 mL) to the resin and treating the suspension for 1 min at 90 °C (155 W 15 s, 32 W 50 s).

The peptides with sequences *(H)*-DERALLDQLHTLLSN-*(NH_2)* and *(H)*-DERALLDQLHT-meLeu-LSN-*(NH_2)* (meLeu = α-methyl-*L*-leucine) corresponding to [1045-1059]-fragment of ACTR were also assembled by a microwave-assisted SPPS using Fmoc-Rink-Amide-AM polystyrene resin with 0.71 mmol/g loading. Shorter peptides corresponding to the LXXLL motif of AD1-ACTR with two flanking additional amino acids, *(H)*-QLHTLLS-*(NH_2)* and *(H)*-QLHT-meLeu-LS-*(NH_2)* were prepared in the same manner.

Biotinylated peptides needed for surface plasmon resonance (SPR) measurements were synthesized on a 0.05 mmol scale using Rink-Amide ChemMatrix resin (0.49 mmol/g loading). First, Fmoc-Lys(Biotin) was coupled to the resin followed by Fmoc-NH-$(PEG)_3$-COOH (Iris Biotech, art. no.: PEG4370, chemical structure depicted below) and subsequently three glycine residues. Then, the actual sequence of the corresponding AD1-ACTR variant was assembled.

Fluoresceine-labeled AD1-ACTR peptides: Cys-$(PEG)_5$-[1040-1086] peptides were synthetized using microwave-assisted peptide synthesis as described above. In these constructs the N-terminal cysteine is separated from the peptide sequence using a $(PEG)_5$ linker. After purification on a Jupiter C4 column (same method as other AD1-ACTR, see below) Cys-$(PEG)_5$-(WT)AD1-ACTR and Cys-$(PEG)_5$-[1055meLeu;1076meLeu]AD1-ACTR were labeled using the thiol reactive 5-(iodoacetamido)fluorescein. To do so, two solutions were prepared. First, 2 mg of peptide (1 eq, 0.37 μmole) were dissolved in 300 μL of 100 mM $NaHCO_3$, 5 mM TCEP at pH 7.5. Then, protected from light, 1 mg of 5-(iodoacetamido)fluorescein (5 eq) were dissolved in 300 μL of anhydrous DMF. The two solutions were mixed and allowed to react for 10 min at room temperature. The reaction mixture was further purified on a Jupiter C4 column (same method as other AD1-ACTR, see below) and pure fractions were combined and lyophilized furnishing a green-yellowish powder (1.3 mg, 59%). The structure of the dye and spacer are shown below:

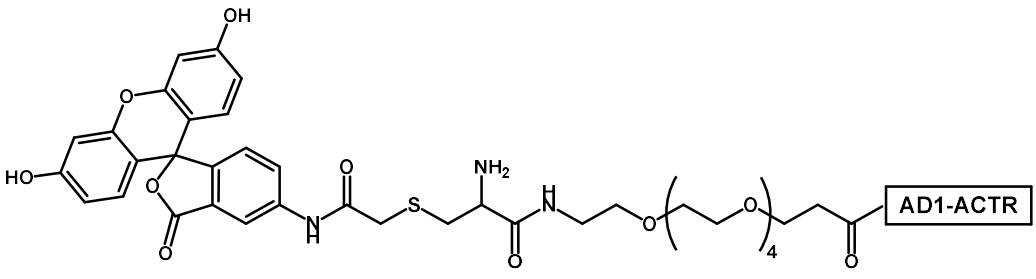

Analytical HPLC: Analytical reversed phase HPLC of all peptides and proteins was performed on a Dionex Ultimate 3000 (Thermo Fisher) equipped with a UV detector, a column heater set to 40 °C and an autosampler. Analyzes were performed on a Kinetex EVO C18 column (Phenomenex, particle size 2.6 µm, pore size 100 Å, dimensions 50 × 2.1 mm^2) or a Kinetex XB C18 column (Phenomenex, particle size 2.6 µm, pore size 100 Å, dimensions 50 × 2.1 mm^2) at a flow rate of 1 mL/min and a gradient of 2-50% of eluent B (0.08% TFA in acetonitrile) in eluent A (0.1% TFA in H_2O) within 4 min.

Preparative HPLC: Preparative reversed phase HPLC was performed on a Shimadzu instrument equipped with a CBM-20A communication module, a SPD-M20A UV detector, a SIL-10AP autosampler and a FRC-10A fraction collector.

Wild type AD1-ACTR and its α-methylated variants were injected onto a Jupiter C4 column (Phenomenex, particle size 10 µm, pore size 300 Å, dimensions 250 × 21 mm^2) at a flow rate of 10 mL/min and a gradient of 10-46% of eluent B (0.08% TFA in acetonitrile) in eluent A (0.1% TFA in H_2O) within 70 min. After purification, pure fractions were identified by analytical HPLC and LC/MS, combined and lyophilized.

NCBD protein was purified two times on a Jupiter C4 column (Phenomenex, particle size 10 µm, pore size 300 Å, dimensions 250 × 21 mm^2) at a flow rate of 10 mL/min and a gradient of 10-40% of eluent B (0.08% TFA in acetonitrile) in eluent A (0.1% TFA in H_2O) within 85 min. After purification, pure fractions were identified by analytical HPLC and LC/MS, combined and lyophilized.

Peptides *(H)*-DERALLDQLHTLLSN-*(NH_2)* and *(H)*-DERALLDQLHT-meLeu-LSN-*(NH_2)* (meLeu = α-methyl-*L*-leucine) and shorter LXXLL motif containing peptides (see above) were purified on a C18 column (Phenomenex, particle size 10 µm, pore size 300 Å, dimensions 250 × 21.00 mm^2) at a flow rate of 10 mL/min and a gradient of 5-30 % of eluent B (0.08% TFA in acetonitrile) in eluent A (0.1% TFA in H_2O) within 40 min. After purification, pure fractions were identified by analytical HPLC and LC/MS, combined and lyophilized.

Mass-spectrometry: Peptide masses were determined using a LC/MS instrument containing a Thermo Scientific Accela UHPLC (Hypers II GOLD column, 1.9 µm, 50 × 2.1 mm^2) integrated with a Thermo Scientific LCQ Fleet ion trap. Deconvolution of experimental data was performed using the Zscore algorithm with the help of MagTran 1.03 software. Tables S1 and S2 provide the list of sequences of the peptides studied in this work and the corresponding mass-spectrometry data.

2. Protein expression

Maltose binding protein (MBP)-NCBD construct was over-expressed in *E. coli* BL21(DE3) overnight at 16 °C. The construct was purified by amylose affinity chromatography in buffer A (50 mM Tris pH 8, 400 mM NaCl, 1 mM DTT). In order to remove soluble oligomers, the purified sample was ultracentrifuged overnight at 40,000 RPM in a swing SW41 rotor (Beckman) at 4 °C. Then the resulting MBP-NCBD sample was concentrated and loaded onto a Superdex 200 pg HiLoad 26/60 gel filtration column (GE Healthcare) equilibrated in buffer A. The sample eluted as a monomer.

The full length CREB-binding protein (CBP) hsCBP (1-2442 aa) cloned into pDEST10 plasmid with N-terminal His-tag and C-terminal Flag and Myc-tag was a kind gift of Dr. P. Tompa (Flanders Institute for Biotechnology, Belgium). The protein was expressed in Sf21 insect cells for 48 h. To avoid the intracellular proteolytic degradation, 1 tablet of Roche cOmplete EDTA free protease inhibitor dissolved in ultrapure sterile water was added to the expression culture after 24 h of culture. The purification of the protein was performed as described in Bekesi et al. (9) with small modifications. The cell pellet of 1 L expression culture was resuspended in 50 mM Tris pH 7.5, 300 mM NaCl, 2 mM $MgCl_2$, 5 % glycerol, 1 mM DTT, 5 µg/ml DNase I, 5 µg/ml RNase A. The cell suspension was homogenized in Dounce homogenizer, sonicated (2 min, 40% amplitude, 0.5 cycle, in ice) and homogenized. The lysate was ultracentrifuged for 1 h at 125 000 g and the supernatant was filtered with 0.45 µM pore-size filter. The purification was performed in 3 steps: a Ni-affinity using Ni-cOmplete resin (Roche), a Flag affinity step in batch chromatography followed by a size-exclusion chromatography on Superose 6 Increase column (GE Healthcare Life Sciences) using Akta systems and 50 mM Tris pH 7.5, 300 mM NaCl, 1 mM TCEP buffer. All steps were carried out in presence of the protease inhibitors: Roche cOmplete EDTA free, pepstatin A, bestatin, Pefabloc and E64, 25 µM Pefabloc and 2 µg/ml E64, and performed at 4°C. The SDS PAGE confirmed molecular weight of recombinant CBP:

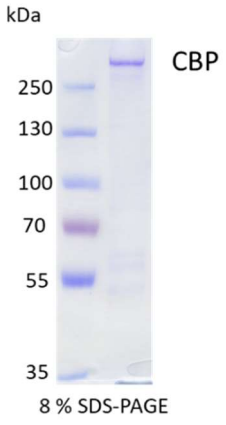

3. Isothermal titration calorimetry (ITC)

Most ITC measurements were performed according to the previously described procedure using an iTC 200 microcalorimeter (GE Healthcare) (5). To analyze and visualize the data NITPIC, SEDPHAT/ITCsy, and GUSSI software were used (10-12). For each AD1-ACTR variant two titrations and two control experiments (i.e., titration of buffer into buffer, and the NCBD into buffer) were performed. The data depicted in Figure S1 (panels 1-36) show only one representative titration with baseline subtracted. The observed positive signal on the right side of the titration curves is due to the slight buffer mismatch and heat of NCBD dilution that were corrected by subtraction of control titrations. For each AD1-ACTR variant the two recorded titration curves were fitted globally. The error estimation for K_D and ΔH values were ±20% and ±5-8%, respectively.

For weak binding AD1-ACTR variants such as [1064mL;1071mL], as well as *(H)*-DERALLDQLHTLLSN-*(NH_2)*, *(H)*-DERALLDQLHT-meLeu-LSN-*(NH_2)* (meLeu = α-methyl-*L*-leucine), *(H)*-QLHTLLS-*(NH_2)* and *(H)*-QLHT-meLeu-LS-*(NH_2)* peptides a PEAK ITC microcalorimeter (Malvern Instruments) was used. To avoid aggregation of NCBD protein at high concentrations, 25-60 μM of NCBD was in a sample cell (titrant) and the corresponding ACTR derived variants were in the syringe (titrators) at 250-600 μM concentrations. The solutions of AD1-ACTR variants were dialyzed for 48 h before measurements against a 10 mM Tris, 50 mM NaCl, 0.05% (w/v) NaN_3 buffer at pH 6.9 and room temperature. The titration parameters were set as following, temperature 31 °C, reference power 10 μcal/s, feedback=high, stirring speed 750 RPM, initial delay 60 s, first injection 0.4 μL in 0.8 s and the remaining 19 injections were 2 μL in 4 s with 120 s of spacing. The initial fitting was performed using the analysis software from Malvern with subtraction of three control experiments (*i.e.,* titration of buffer into buffer, buffer into NCBD solution and the ACTR variants into buffer) and a correction of concentration taking into account precise concentration measurements by analytical HPLC using calibration curve at OD 220 nm. For [1064mL;1071mL]AD1-ACTR analogue previously used fitting protocol was applied to report the thermodynamic parameters listed in Table S3. The inversion of the analytes and method of fitting are not significantly affecting the thermodynamics parameters: the control titrations of the WT AD1-ACTR and [1055mL]AD1-ACTR variants were performed using these settings resulting in similar K_D values of 0.208 μM and 0.072 μM compared to values of 0.204 μM (5) and 0.075 μM (Table S3), obtained by the first method.

4. Circular dichroism (CD)

CD spectra were recorded using a J-1500 (Jasco) spectrophotometer. All samples were prepared in a quartz cuvette (thickness of 1 mm and a volume of 300 µL). For every measurement protein or protein complexes were dissolved in a buffered solution (20 mM phosphate, pH 7.4) at a concentration of 25 µM. For data collection the following parameters were set: scan range 185-280 nm, band width 1.00 nm, scanning speed 100 nm/min, data pitch 0.1 nm. Every CD curve was obtained by averaging of 5 scans and subtracting the background signal. The data are depicted in Figure S3.

The thermal stability of complexes of several AD1-ACTR variants with NCBD (concentration of complex 50 µM) was evaluated by monitoring the ellipticity at 222 nm as a function of temperature from 20 to 90 °C. Rate of heating / cooling was 1 °C/min. The thermal denaturation was found to be highly reversible. The thermal denaturation curves are depicted in Figure S5 and the apparent melting temperatures are listed in Table S4.

For free AD1-ACTR protein variants, the ratio of ellipticities ($\theta_{222}/\theta_{199}$) was calculated in order to compare their helical contents (Figure S4a) (13). For their complexes with NCBD, the other ratio ($\theta_{222}/\theta_{208}$) was derived (Figure S4b), which may serve as a readout of helix-helix interactions (14). All obtained values are summarized in Tables S5 and S6, respectively.

5. NMR measurements

All NMR spectra were recorded on a 700 MHz Bruker spectrometer equipped with TCI cryo-probe at 304 K in 3 mm NMR tubes. The proton frequencies were referenced using DSS (2,2-dimethyl-2-silapentane-5-sufonate) as external reference and carbon frequencies were referenced using the indirect method (15). Proteins samples were obtained by dissolving the appropriate amount of each protein in 200 µL 90 % H_2O, 10 % D_2O, 20 mM sodium phosphate, 0.05 % NaN_3 buffer at pH 7.2. The exact concentrations were measured by analytical HPLC using a calibration curve and adjusted to 1.4 mM. For NMR experiments in D_2O, 200 µL of the samples described above were lyophilized for at least 48 h. The resulting powder was then re-dissolved in 200 µL of pure D_2O just before the experiment.

The ^{1}H-^{13}C HSQC spectra were recorded using the gradient-selected coherence transfer pulse-sequence of the Bruker standard library. A resolution of 2 and 12 Hz in the ^{1}H and ^{13}C dimensions, respectively, were used with relaxation delays set to 1.2 s for a total experimental time of

approximately 3.5 h. 60 kHz Chirp pulses of 500 μs and a B_1-field of 8 kHz were used for ^{13}C resonance inversion.

The measurements of the ^{13}C R_1 and R_2 relaxation rates were performed using refocused ^{1}H-^{13}C HSQC type experiments incorporating ^{13}C relaxation time (16). For the R_1 relaxation experiment proton decoupling was applied with 180 degree pulses every 2.5 ms. The following T_1 delays were used: 10, 50, 100, 200, 300, 400, 600, 800 ms. Additional points (50, 500 ms) were recorded for wild type and [1055meLeu]AD1-ACTR variant samples to estimate the experimental uncertainty on peak volumes. For the R_2 relaxation, a CPMG pulse sequence was used during the carbon relaxation time with 300 μs half-echo delay and a B_1-field of 10 kHz. The T_2 delays were 35, 70, 140, 176, 211, 246, 317, 387 ms. Additional points (105, 211 ms) were recorded for wild-type and [1055mL]AD1-ACTR variant to estimate the experimental uncertainty on peak volumes. The relaxation delay was set to 2.5 s and total acquisition time was approximately 25 hours for each set of relaxation experiments.

The ^{1}H homonuclear TOCSY and NOESY experiments were recorded using 4096 and 600 points in the direct and indirect dimensions, respectively. The spectral width was set to 7.8 kHz and the relaxation delay to 2 s. The mixing times were 80 ms and 500 ms for the TOCSY and the NOESY, respectively. A B_1-field of 9 kHz was used for the TOCSY spin-lock. ^{1}H-^{13}C HSQC-TOCSY were recorded with a resolution of 4 and 24 Hz for the ^{1}H and ^{13}C dimensions, respectively, a relaxation time of 1.2 s and a TOCSY mixing time of 80 ms (B_1-field of 9 kHz) for a total experiment time of 14 h. The ^{1}H-^{13}C HMBC experiment was recorded with carrier frequency centered on the carbonyl resonances (174 ppm) to correlate the carbonyl with the adjacent Hα proton frequencies using the gradient-selected coherence transfer pulse-sequence of the Bruker standard library. The delay for long-range magnetization transfer was set to 89.3 ms ($^{2}J_{CO\text{-}H\alpha}$ 5.6 Hz). The resolution were 4 Hz and 7 Hz for the proton and carbon dimensions, respectively. The relaxation time was set to 2 s for a total measurement time of 32 h.

Spin systems were manually identified using ^{1}H-^{1}H TOCSY (80 ms mixing time) and the sequential assignment was based on the inter-residue correlations identified in the ^{1}H-^{1}H NOESY (500 ms mixing time). Cα carbon assignments were obtained using high-resolution ^{1}H-^{13}C HSQC experiment. Ambiguities in the ^{1}H-^{13}C HSQC were solved using ^{1}H-^{13}C HSQC-TOCSY (80 ms mixing time) experiment. In two cases (N1058 and N1078) HMBC experiment was used to resolve the ambiguities of the assignment. When the WT AD1-ACTR protein was fully assigned, the chemical shifts being mostly the same, except for some residues, were used to assign the signals of [1055meLeu] and [1055meLeu;1076meLeu] AD1-ACTR analogues.

Data processing was performed using TopSpin software 2.1. All spectral analysis including frequency assignments and relaxation rate measurements were performed using ccpNmr (version 2.4.2) (17). For relaxation measurements, time dependent evolutions of the peak intensities were fitted using a single exponential model and the estimate of the uncertainty of the fitted parameters was obtained using the covariance method implemented in ccpNmr.

Chemical shifts for wild-type AD1-ACTR, [1055meLeu]AD1-ACTR and [1055meLeu;1076meLeu]AD1-ACTR analogues are listed in Tables S7-S9. POTENCI program (18) was used to create a neighbor-corrected list of the random coil chemical shifts of the wild-type AD1-ACTR sequence including the effect of temperature, pH and ionic strength to be subtracted from the experimental chemical shifts. Relaxation rates R_1 and R_2 and experimental uncertainties are tabulated in Tables S10 and S11.

6. Crystallization, data collection and structure refinement

The NCBD-ACTR complexes were reconstituted by mixing MBP-NCBD construct and synthetic wild-type AD1-ACTR, [1055meLeu] or [1055meLeu;1076meLeu] in a 1:1 stoichiometric ratio in buffer B (10 mM Tris pH 8, 100 mM NaCl, 1 mM DTT, 5 mM Maltose) and concentrated to 85 mg/mL prior to crystallization. Crystallization conditions were screened using commercially available kits (Qiagen, Hampton Research, Emerald Biosystems) by the sitting-drop vapor-diffusion method in 96-well MRC 2-drop plates (SWISSCI), using a Mosquito robot (TTP Labtech). After 3 weeks a crystal grew for a complex of MBP-NCBD with [1055meLeu;1076meLeu] variant in a drop made from 200 nL of protein solution at 85 mg/mL and 100 nL of reservoir solution containing 20% polyethylene glycol 6000, 100 mM Tris pH 8 and 10 mM $ZnCl_2$. The crystals were flash-cooled in a cryoprotectant solution containing 30% ethylene glycol and stored in liquid nitrogen.

X-ray diffraction data were collected up to a resolution of 2.28Å at the Synchrotron Swiss Light Source (SLS) (Switzerland) on the X06DA beamline and processed with the program XDS (19). The crystal structure was solved by molecular replacement with a high resolution crystal structure of MBP (PDB entry 5H7Q) (20) using Phaser (21) and structure refinement was carried out with PHENIX (22). Building of the unnatural meLeu residues were achieved using eLBOW (23). TLS refinement was applied during the refinement (24). The crystallographic parameters and the statistics of data collection and refinement are shown in Table S12.

7. Molecular dynamics (MD) simulations

Molecular dynamics simulations were carried out with the GROMOS biomolecular simulation package (25) (www.gromos.net) and the GROMOS force-field parameter set 54A7 (26,27). The initial coordinates for AD1-ACTR/NCBD, [1055meLeu]AD1-ACTR/NCBD and [1055meLeu;1076meLeu]AD1-ACTR/NCBD complexes were derived from the solution NMR structure of the ACTR-NCBD complex (PDB ID 1KBH, model 1) and sequence has been matched to the experimentally studied sequence from this work. In the NCBD sequence methionine 2098 was replaced by norleucine. Each complex was solvated in approximately 8400 simple point charge (SPC) water molecules (28). Rectangular periodic boundary conditions were used and 26 Na^+ and 24 Cl^- ions were added to each simulation box to neutralize the negative charge and to mimic the ionic strength of 0.15 M. The dimensions of the box were determined by a minimum solute-wall distance of 1.2 nm and a minimum solute-solvent atom-atom distance of 0.23 nm. In order to relax unfavorable contacts between atoms of the solute and the solvent, the systems were relaxed by performing a steepest-descent energy minimization with harmonic positional restraints on all solute atoms (force constant 2.5×10^4 kJ mol^{-1} nm^{-2}), followed by an equilibration period of 1 ns in which the strength of the positional restraints was gradually released from 2.5×10^4 to 0.0 kJ mol^{-1} nm^{-2}, and the temperature was raised from 60 to 300 K. Initial velocities for the MD simulations were taken from a Maxwell–Boltzmann distribution. Solvent and solute were weakly coupled to separate temperature baths (29) with a relaxation time of 0.1 ps. After equilibration, the systems were also coupled to a pressure bath (29) with a relaxation time of 0.5 ps and an isothermal compressibility of 0.4575×10^{-3} $(kJmol^{-1}nm^{-3})^{-1}$. Bond lengths of the solute and the geometry of the solvent molecules were constrained using the SHAKE algorithm (30) with a relative geometric tolerance of 10^{-4}, so the leapfrog integration time step could be set to 2 fs. The non-bonded van der Waals and electrostatic interactions were calculated using a triple-range cutoff scheme. Nonbonded interactions were truncated at a distance of 1.4 nm and recalculated every time step in the range 0.0-0.8 nm and every five time steps in the range 0.8-1.4 nm. The long-range electrostatic interactions beyond the outer cutoff of 1.4 nm were represented by a reaction field (31) with a relative dielectric permittivity of 61 for water (32). The motion of the center of mass was removed every 2 ps. The simulations were carried out for 200 ns at a constant pressure of 1 atm and a constant temperature of 300 K.

The coordinate trajectories were saved at 1 ps intervals and were analyzed using the GROMOS++ set of programs (33). The first 50 ns of every simulation were considered as equilibration time and were omitted from the analysis. Atom-positional root-mean-square deviation (RMSD) and atom-positional root-mean-square fluctuations (RMSF) were calculated for the backbone atoms N, C, O and Cα using the energy-minimized initial structure as a reference. Conformational clustering

analysis was performed with the approach of Daura et al. (34) using as a criterion a backbone atom-positional RMSD of less than 0.2 nm.

8. Biomolecular interaction analysis by Surface Plasmon Resonance (SPR)

The SPR measurements were performed on a Biacore T200 instrument (GE Healthcare - Biacore). Kinetics of NCBD binding to WT AD1-ACTR as well as to [1055meLeu;1076meLeu]AD1-ACTR, [1076meLeu]AD1-ACTR and [1055meLeu]AD1-ACTR variants were measured at five different temperatures (20, 22, 25, 27 and 31 °C). The buffer consisted of 10 mM HEPES, 500 mM NaCl and 0.005% (v/v) 10% P20 surfactant (GE Healthcare) at pH 7.5. The capture of biotinylated peptides on the chip was performed with the Biotin CAPture kit, Series S (GE Healthcare-Biacore). The oligo-streptavidin diluted 5 times in the running buffer was injected on all 4 channels at flow rate 2 µL/min for 300 sec. The first channel was always kept as a reference for subtraction of non-specific binding of NCBD to the chip surface. On the remaining 3 channels biotinylated AD1-ACTR variants at a concentration of 100 nM were injected at a flow rate of 20 µL/min for 10 sec yielding around 25 to 35 RU. For regeneration between each sensogram, a solution of 6 M guanidine-HCl, 250 mM NaOH was injected into all channels at 5 µL/min for 60 sec. The parameters for the binding measurement were set as follows: temperature varied from 20 to 31 °C, initial delay 60 sec, injection of NCBD 120 sec at 50 µL/min, dissociation 120 sec. NCBD solutions were prepared with a two-fold cascade dilution with a range of concentrations from 1 µM to 1.95 nM (10 concentrations).

Data analysis was performed using BiaEvaluation 3.2 software (GE Healthcare). After subtraction of the background signal obtained from the reference channel and the buffer signal, the curves were fitted assuming a simple 1:1 binding isotherm model. More advanced “two state” kinetic model involving a conformational change did not improve the fitting. The apparent dissociation constants (K_D), as well as association and dissociation kinetics (k_{on} and k_{off}) obtained upon fitting the data are provided in Table S16.

Since the kinetics reaches the limitations of the SPR method, steady-state analysis was made to obtain dissociation constants and the corresponding experimental uncertainties (Figure S20) (35). The steady-state binding (R_{eq}) was derived by averaging the signals at equilibrium during the association phase. Subsequently, steady-state analysis using in-house Python scripts was performed by fitting the average signal R_{eq} as a function of analyte concentration, assuming a simple 1:1 interaction binding isotherm model, and leading to 3 fitted parameters: the minimal signal (R_{min}), the maximum capacity of the surface (R_{max}) and the affinity (K_D). A Monte Carlo approach was further used in order to estimate the values and uncertainties of the 3 fitted

parameters (Table S17). This method consists of reproducing the fit using 1000 datasets in which noise fluctuations were introduced based on the experimental uncertainty, and then the mean and the standard deviation of the fitted parameters were calculated.

The SPR measurements with full length 270 kDa CBP were also performed using Biotin CAPture kit, Series S (GE Healthcare-Biacore) on a Biacore T200 instrument (GE Healthcare - Biacore). The running buffer was 50 mM Tris, pH 7.5, 300 mM NaCl, 1 mM TCEP, 0.01% P20 supplemented with Roche Complete EDTA free protease inhibitor and the running temperature was set to 10 °C. First, the biotin capture reagent was immobilized on the chip surface followed by the immobilization of the biotinylated ACTR variants (WT, [1055mL;1076mL]AD1-ACTR and [1064mL;1071mL]AD1-ACTR) as ligands. Interactions of the hCBP full length protein with the WT or AD1-ACTR analogues were analyzed in the manner of dose response using twofold dilution series of hCBP ranging from 380 to 0.75 nM. The association and dissociation phases were 100 s each and the analyte flow rate 40 µl/min. For regeneration, a solution of 6 M guanidine-HCl, 250 mM NaOH was injected into all channels at 5 µL/min for 60 sec. After subtracting the reference and buffer signal, the data were fit to a steady state binding model to define the apparent K_D.

Equilibrium signals were extracted from experimental SPR data for both systems and subsequently fitted with a 1:1 binding model. Since the data recorded for WT ACTR / hCBP interaction are so far from saturation for the highest concentrations, the fitting has been done in two steps: a first one by fitting the equilibrium data for the ACTR doubly methylated variant, leading, among others, to the maximum capacity R_{max} value; then a second step in which this previous R_{max} value has been used as a forced parameter into the fit of the wild-type AD1-ACTR data, assuming that the saturation level is the same for both the wild type and the doubly methylated analogue (Figure S21).

9. Fluorescence polarization (FP) measurements

The fluorescein labeled AD1-ACTR (WT and [1055meLeu;1076meLeu] variant) was diluted at 5 nM in the assay buffer (25 mM Hepes pH 7.5, 150 mM NaCl, 1 mM TCEP, 0.05% Tween-20) and mixed with increasing concentration of hCBP (0.03-470 nM). The triplicates of the mixtures were transferred into 384 well black microplate (PS, F-bottom; Greiner Bio-one) and let incubate for 10 min at 25 °C in the dark. The FP was recorded by PHERAstar Plus (BMG LABTECH) at 25 °C, using excitation and emission filters of 485 and 520 nm, respectively. Graphpad Prism 8 software was used to calculate the dissociation constant (K_D) by fitting a curve with the one site binding model (Figure S22).

10. Pull down experiments

The MCF7 cells (6.6 x 10^6 cell/ sample) were resuspend and lysed in the following buffer: 50 mM Tris pH 8.0, 75 mM NaCl, 75 mM KCl, 10 % glycerol, 0.1 % NP-40, 2 mM TCEP, supplemented with protease inhibitors. The total cell extract was treated with biotin conjugated [1055meLeu;1076meLeu]AD1-ACTR or the corresponding wild type peptide in 5 μM final concentration for 1 h at + 4 °C, then the cell extract was centrifuged for 1 h at 20 000 *g*. The soluble fraction was incubated with Strep-Tactin Sepharose resin (IBA Lifescience) for 2 h. As control, the soluble extract without peptide treatment was incubated with the Strep-Tactin Sepharose resin. After washing the resin with lysis buffer, the elution was performed by SDS-PAGE loading solution. The eluted sample was analyzed by silver stained 8% SDS-PAGE and also by Western-blot using primary antibody against the hCBP (1CB2F3, IGBMC Antibody platform). In addition, label free quantitative MS analysis using Thermo Scientific Orbitrap Elite hybrid mass-spectrometer was performed. The preliminary data showed the increased abundance of CBP for [1055meLeu;1076meLeu]AD1-ACTR variant than for wild type sample with the statistical significance (fold change: 2.24; -logP 3.92, based on 3 technical replicates).

Supplementary Tables

Table S1. Amino acid sequences of the variants of AD1-ACTR studied in this work[#].

	Protein	Sequence
1	wild type (WT) AD1-ACTR	EGQSDERALLDQLHTLLSNTDATGLEEIDRALGIPELVNQGQALEPK
2	[S1043M;D1050E;T1054Q]*	EGQMDERALLEQLHQLLSNTDATGLEEIDRALGIPELVNQGQALEPK
3	[A1047G]*	EGQSDERGLLDQLHTLLSNTDATGLEEIDRALGIPELVNQGQALEPK
4	[1047mA]**	EGQSDERALLDQLHTLLSNTDATGLEEIDRALGIPELVNQGQALEPK
5	[1048mL]	EGQSDERALLDQLHTLLSNTDATGLEEIDRALGIPELVNQGQALEPK
6	[1049mL]	EGQSDERALLDQLHTLLSNTDATGLEEIDRALGIPELVNQGQALEPK
7	[1050mD]**	EGQSDERALLDQLHTLLSNTDATGLEEIDRALGIPELVNQGQALEPK
8	[1052mL]	EGQSDERALLDQLHTLLSNTDATGLEEIDRALGIPELVNQGQALEPK
9	[1055mL]	EGQSDERALLDQLHTLLSNTDATGLEEIDRALGIPELVNQGQALEPK
10	[1056mL]	EGQSDERALLDQLHTLLSNTDATGLEEIDRALGIPELVNQGQALEPK
11	[1061mA]**	EGQSDERALLDQLHTLLSNTDATGLEEIDRALGIPELVNQGQALEPK
12	[1064mL]	EGQSDERALLDQLHTLLSNTDATGLEEIDRALGIPELVNQGQALEPK
13	[1071mL]**	EGQSDERALLDQLHTLLSNTDATGLEEIDRALGIPELVNQGQALEPK
14	[1072mA]	EGQSDERALLDQLHTLLSNTDATGLEEIDRALGIPELVNQGQALEPK
15	[1076mL]**	EGQSDERALLDQLHTLLSNTDATGLEEIDRALGIPELVNQGQALEPK
16	[1077mV]	EGQSDERALLDQLHTLLSNTDATGLEEIDRALGIPELVNQGQALEPK
17	[1080mA]	EGQSDERALLDQLHTLLSNTDATGLEEIDRALGIPELVNQGQALEPK
18	[1082mA]	EGQSDERALLDQLHTLLSNTDATGLEEIDRALGIPELVNQGQALEPK
19	[1083mL]**	EGQSDERALLDQLHTLLSNTDATGLEEIDRALGIPELVNQGQALEPK
20	[1085mP]**	EGQSDERALLDQLHTLLSNTDATGLEEIDRALGIPELVNQGQALEPK
21	[1047mA;1071mL]**	EGQSDERALLDQLHTLLSNTDATGLEEIDRALGIPELVNQGQALEPK
22	[1047mA;1072mA]	EGQSDERALLDQLHTLLSNTDATGLEEIDRALGIPELVNQGQALEPK
23	[1047mA;1076mL]**	EGQSDERALLDQLHTLLSNTDATGLEEIDRALGIPELVNQGQALEPK
24	[1047mA;1077mV]	EGQSDERALLDQLHTLLSNTDATGLEEIDRALGIPELVNQGQALEPK
25	[1047mA;1083mL]**	EGQSDERALLDQLHTLLSNTDATGLEEIDRALGIPELVNQGQALEPK
26	[1048mL;1076mL]	EGQSDERALLDQLHTLLSNTDATGLEEIDRALGIPELVNQGQALEPK
27	[1048mL;1077mV]	EGQSDERALLDQLHTLLSNTDATGLEEIDRALGIPELVNQGQALEPK
28	[1048mL;1083mL]	EGQSDERALLDQLHTLLSNTDATGLEEIDRALGIPELVNQGQALEPK
29	[1050mD;1071mL]	EGQSDERALLDQLHTLLSNTDATGLEEIDRALGIPELVNQGQALEPK
30	[1050mD;1072mA]	EGQSDERALLDQLHTLLSNTDATGLEEIDRALGIPELVNQGQALEPK
31	[1050mD; 1076mL]	EGQSDERALLDQLHTLLSNTDATGLEEIDRALGIPELVNQGQALEPK
32	[1050mD;1077mV]	EGQSDERALLDQLHTLLSNTDATGLEEIDRALGIPELVNQGQALEPK
33	[1050mD;1083mL]**	EGQSDERALLDQLHTLLSNTDATGLEEIDRALGIPELVNQGQALEPK
34	[1055mL;1076mL]	EGQSDERALLDQLHTLLSNTDATGLEEIDRALGIPELVNQGQALEPK
35	[1061mA;1071mL]	EGQSDERALLDQLHTLLSNTDATGLEEIDRALGIPELVNQGQALEPK
36	[1061mA;1076mL]**	EGQSDERALLDQLHTLLSNTDATGLEEIDRALGIPELVNQGQALEPK
37	[1061mA;1077mV]	EGQSDERALLDQLHTLLSNTDATGLEEIDRALGIPELVNQGQALEPK
38	[1061mA;1083mL]**	EGQSDERALLDQLHTLLSNTDATGLEEIDRALGIPELVNQGQALEPK
39	[1064mL;1071mL]	EGQSDERALLDQLHTLLSNTDATGLEEIDRALGIPELVNQGQALEPK
40	[1064mL;1076mL]	EGQSDERALLDQLHTLLSNTDATGLEEIDRALGIPELVNQGQALEPK
41	[1064mL;1077mV]	EGQSDERALLDQLHTLLSNTDATGLEEIDRALGIPELVNQGQALEPK
42	[1064mL;1083mL]	EGQSDERALLDQLHTLLSNTDATGLEEIDRALGIPELVNQGQALEPK
43	[1047mA;1055mL;1061mA]	EGQSDERALLDQLHTLLSNTDATGLEEIDRALGIPELVNQGQALEPK
44	[1055mL;1076mL;1083mL]	EGQSDERALLDQLHTLLSNTDATGLEEIDRALGIPELVNQGQALEPK
45	[1047mA;1050mD;1061mA;1076mL]	EGQSDERALLDQLHTLLSNTDATGLEEIDRALGIPELVNQGQALEPK
46	[1047mA;1055mL;1061mA;1076mL]	EGQSDERALLDQLHTLLSNTDATGLEEIDRALGIPELVNQGQALEPK
47	[1047mA;1055mL;1076mL;1083mL]	EGQSDERALLDQLHTLLSNTDATGLEEIDRALGIPELVNQGQALEPK
48	[1047mA;1061mA;1076mL;1083mL]	EGQSDERALLDQLHTLLSNTDATGLEEIDRALGIPELVNQGQALEPK
49	[1047mA;1055mL;1061mA;1076mL;1083mL]	EGQSDERALLDQLHTLLSNTDATGLEEIDRALGIPELVNQGQALEPK
50	[1047mA;1055mL;1061mA;1076mL;1083mL;1085mP]	EGQSDERALLDQLHTLLSNTDATGLEEIDRALGIPELVNQGQALEPK
51	NCBD	SALQDLLRTLKSPSSPQQQQQVLNILKSNPQLJAAFIKQRTAKYVAN***

Residues in red are α-methylated;

* These sequences correspond to protein variants with canonical amino acids incorporated to modify the helix propensity: Ješmantavičius et al. *Angew. Chem. Int. Ed.* **2014**, *53*, 1548-1551. We synthesized these protein variants and included them in our study to compare their properties with α-methylated analogues;

** These variants were reported in our previous communication: Schmidtgall et al. *Chem. Commun.* **2017**, *53*, 7369-7372;

*** J = *Nle* = norleucine in the NCBD sequence replaces Met being nearly isosteric to the native residue and resistant to oxidation.

Table S2. Characterization of synthesized proteins by mass-spectrometry**.

Protein	Measured mass [Da]	Calculated mass [Da]
[S1043M;D1050E;T1054Q]	5184.9	5184.8
[A1047G]	5085.1	5085.6
[1048mL]	5113.7	5113.6
[1049mL]	5113.6	5113.6
[1052mL]	5113.6	5113.6
[1055mL]	5113.6	5113.6
[1056mL]	5113.6	5113.6
[1064mL]	5112.6	5113.6
[1072mA]	5128.3	5127.6
[1077mV]	5114.6	5113.6
[1080mA]	5127.9	5127.6
[1082mA]	5113.8	5113.6
[1047mA;1072mA]	5142.2	5141.6
[1047mA;1077mV]	5128.0	5127.6
[1048mL;1076mL]	5127.6	5127.6
[1048mL;1077mV]	5127.6	5127.6
[1048mL;1083mL]	5127.6	5127.6
[1050mD;1071mL]	5127.5	5127.6
[1050mD;1072mA]	5141.4	5141.6
[1050mD; 1076mL]	5127.5	5127.6
[1050mD;1077mV]	5126.6	5127.6
[1055mL;1076mL]	5127.6	5127.6
[1061mA;1071mL]	5128.8	5127.6
[1061mA;1077mV]	5127.9	5127.6
[1064mL;1071mL]	5127.6	5127.6
[1064mL;1076mL]	5127.1	5127.6
[1064mL;1077mV]	5127.9	5127.6
[1064mL;1083mL]	5128.3	5127.6
[1047mA;1055mL;1061mA]	5141.6	5141.6
[1055mL;1076mL;1083mL]	5141.0	5141.6
[1047mA;1050mD;1061mA;1076mL]	5155.7	5155.7
[1047mA;1055mL;1061mA;1076mL]	5155.0	5155.7
[1047mA;1055mL;1076mL;1083mL]	5155.7	5155.7
[1047mA;1061mA;1076mL;1083mL]	5155.5	5155.7
[1047mA;1055mL;1061mA;1076mL;1083mL]	5169.7	5169.7
[1047mA;1055mL;1061mA;1076mL;1083mL;1085mP]	5183.7	5183.7
WT-AD1-ACTR-GGG-$(PEG)_3$-K(Biotin)-amide*	5826.5	5827.5
[1055mL]AD1-ACTR-GGG-$(PEG)_3$-K(Biotin)-amide*	5841.3	5841.5
[1076mL]AD1-ACTR-GGG-$(PEG)_3$-K(Biotin)-amide*	5841.7	5841.5
[1055mL;1076mL]AD1-ACTR-GGG-$(PEG)_3$-K(Biotin)-amide*	5854.9	5855.5
[1064mL;1071mL]AD1-ACTR-GGG-$(PEG)_3$-K(Biotin)-amide*	5854.2	5855.5
Fluo-$(PEG)_5$-WT-AD1-ACTR*	5879.3	5880.5
Fluo-$(PEG)_5$-[1055meLeu;1076meLeu]-AD1-ACTR*	5907.3	5908.5

* The exact chemical structure for 'Fluo-$(PEG)_5$' is provided on p.5;

** For HPLC traces see Figure S25, purity for all samples was equal or exceeded 95%. Analytical ESI-MS characterization of the variants marked with two asterisks (**) in Table S1 is not listed here and reported in our previous communication: Schmidtgall et al. *Chem. Commun.* **2017**, *53*, 7369-7372.

Table S3. Thermodynamic parameters of binding of AD1-ACTR variants to NCBD obtained by isothermal titration calorimetry (ITC)*,#. The error estimation for K_D and ΔH values are ± 20 % and ± 5-8 %, respectively.

	Protein	K_D [μM]	ΔG [kcal mol^{-1}]	ΔH [kcal mol^{-1}]	-TΔS [kcal mol^{-1}]
1	wild type (WT) AD1-ACTR**	0.206	-9.30	-12.7	3.40
2	[S1043M;D1050E;T1054Q]	0.188	-9.36	-13.7	4.29
3	[A1047G]	0.844	-8.45	-13.8	5.33
4	[1047mA]**	0.145	-9.51	-11.8	2.29
5	[1048mL]	0.281	-9.12	-12.2	3.04
6	[1049mL]	0.806	-8.48	-14.8	6.32
7	[1050mD]**	0.800	-8.48	-11.7	3.22
8	[1052mL]	0.634	-8.63	-12.1	3.52
9	[1055mL]	0.075	-9.91	-18.7	8.78
10	[1056mL]	2.60	-7.77	-9.07	1.30
11	[1061mA]**	0.327	-9.02	-13.6	4.58
12	[1064mL]	1.34	-8.17	-12.6	4.43
13	[1071mL]**	7.11	-7.16	-5.58	-1.58
14	[1072mA]	0.144	-9.52	-11.8	2.30
15	[1076mL]**	0.206	-9.30	-15.0	5.70
16	[1077mV]	0.347	-8.99	-20.5	11.5
17	[1080mA]	0.496	-8.77	-19.4	10.7
18	[1082mA]	0.518	-8.75	-18.3	9.58
19	[1083mL]**	0.520	-8.74	-13.1	4.36
20	[1085mP]**	0.487	-8.78	-14.8	6.02
21	[1047mA;1071mL]**	5.11	-7.36	-5.18	-2.18
22	[1047mA;1072mA]	0.569	-8.69	-15.2	6.51
23	[1047mA;1076mL]**	0.055	-10.1	-13.2	3.10
24	[1047mA;1077mV]	0.311	-9.06	-18.9	9.88
25	[1047mA;1083mL]**	0.166	-9.43	-11.5	2.07
26	[1048mL;1076mL]	0.301	-9.08	-15.9	6.79
27	[1048mL;1077mV]	0.483	-8.79	-14.4	5.59
28	[1048mL;1083mL]	0.788	-8.49	-13.4	4.97
29	[1050mD; 1071mL]	4.99	-7.37	-4.20	-3.18
30	[1050mD;1072mA]	0.798	-8.49	-14.3	5.86
31	[1050mD; 1076mL]	0.659	-8.60	-17.1	8.46
32	[1050mD;1077mV]	0.595	-8.66	-16.5	7.81
33	[1050mD;1083mL]**	0.614	-8.64	-11.7	3.06
34	[1055mL;1076mL]	0.042	-10.3	-20.4	10.1
35	[1061mA;1071mL]	3.37	-7.62	-6.50	-1.12
36	[1061mA;1076mL]**	0.180	-9.38	-16.3	6.92
37	[1061mA;1077mV]	0.236	-9.22	-19.2	9.96
38	[1061mA;1083mL]**	0.277	-9.12	-15.3	6.18
39	[1064mL;1071mL]	6.05	-7.26	-2.20	-5.06
40	[1064mL;1076mL]	0.796	-8.49	-15.4	6.94
41	[1064mL;1077mV]	0.829	-8.46	-15.2	6.69
42	[1064mL;1083mL]	1.60	-8.07	-13.3	5.20
43	[1047mA;1055mL;1061mA]	0.177	-9.40	-20.2	10.8
44	[1055mL;1076mL;1083mL]	0.042	-10.3	-20.3	10.0
45	[1047mA;1050mD;1061mA;1076mL]	0.221	-9.20	-18.1	8.91
46	[1047mA;1055mL;1061mA;1076mL]	0.136	-9.56	-21.6	12.0
47	[1047mA;1055mL;1076mL;1083mL]	0.298	-9.07	-16.8	7.71
48	[1047mA;1061mA;1076mL;1083mL]	0.155	-9.48	-18.6	9.16
49	[1047mA;1055mL;1061mA;1076mL;1083mL]	0.090	-9.80	-21.8	12.0
50	[1047mA;1055mL;1061mA;1076mL;1083mL; 1085mP]	0.108	-9.70	-20.5	10.8

* The ITC data for 13 analogues marked with two asterisks (**) were published in our previous communication: Schmidtgall et al. *Chem. Commun.* **2017**, *53*, 7369-7372;

The respective values of ΔH and ΔS for all α-methylated variants can be fitted with a linear regression (ΔH = *a* + *b* × ΔS), where the slope *b* or "compensation temperature" is 340 ± 7 K.

Table S4. Apparent melting points of AD1-ACTR/NCBD complexes (CD-monitored).

AD1-ACTR variant complexed with NCBD	T_m [°C]
WT	69
[1071mL]	50
[1047mA;1071mL]	50
[A1047G]	67
[1050mD]	67
[1056mL]	66
[1047mA;1076mL]	73
[S1043M;D1050E;T1054Q]	74
[1055mL]	>85
[1055mL;1076mL]	>85
[1047mA;1061mA;1076mL;1083mL]	>85
[1047mA;1055mL;1061mA;1076mL;1083mL]	>85
[1047mA;1055mL;1061mA;1076mL;1083mL;1086mP]	>85

Table S5. Ratios of ellipticities in CD spectra of AD1-ACTR variants.

	Protein	$\theta_{222}/\theta_{199}$
1	WT AD1-ACTR	0.23
2	[S1043M;D1050E;T1054Q]	0.33
3	[A1047G]	0.20
4	[1047mA]**	0.23
5	[1048mL]	0.30
6	[1049mL]	0.28
7	[1050mD]**	0.26
8	[1052mL]	0.31
9	[1055mL]	0.44
10	[1056mL]	0.26
11	[1061mA]**	0.24
12	[1064mL]	0.25
13	[1071mL]**	0.24
14	[1072mA]	0.26
15	[1076mL]**	0.27
16	[1077mV]	0.29
17	[1080mA]	0.24
18	[1082mA]	0.25
19	[1083mL]**	0.26
20	[1085mP]**	0.25
21	[1047mA;1071mL]**	0.26
22	[1047mA;1072mA]	0.24
23	[1047mA;1076mL]**	0.28
24	[1047mA;1077mV]	0.29
25	[1047mA;1083mL]**	0.25
26	[1048mL;1076mL]	0.34
27	[1048mL;1077mV]	0.37
28	[1048mL;1083mL]	0.28
29	[1050mD; 1071mL]	0.21
30	[1050mD;1072mA]	0.23
31	[1050mD; 1076mL]	0.23
32	[1050mD;1077mV]	0.24
33	[1050mD;1083mL]**	0.27
34	[1055mL;1076mL]	0.40
35	[1061mA;1071mL]	0.25
36	[1061mA;1076mL]**	0.31
37	[1061mA;1077mV]	0.30
38	[1061mA;1083mL]**	0.25
39	[1064mL;1071mL]	0.26
40	[1064mL;1076mL]	0.28
41	[1064mL;1077mV]	0.33
42	[1064mL;1083mL]	0.23
43	[1047mA;1055mL;1061mA]	0.48
44	[1055mL;1076mL;1083mL]	0.50
45	[1047mA;1050mD;1061mA;1076mL]	0.29
46	[1047mA;1055mL;1061mA; 1076mL]	0.57
47	[1047mA;1055mL;1076mL;1083mL]	0.63
48	[1047mA;1061mA;1076mL;1083mL]	0.29
49	[1047mA;1055mL;1061mA;1076mL;1083mL]	0.61
50	[1047mA;1055mL;1061mA;1076mL;1083mL;1085mP]	0.75

** The CD spectra for these analogues were previously published in our preceding communication: Schmidtgall et al. *Chem. Commun.* **2017**, *53*, 7369-7372.

Table S6. Ratios of ellipticities in CD spectra of AD1-ACTR variants complexes with NCBD.

	Protein complex	$\theta_{222}/\theta_{208}$
1	WT AD1-ACTR / NCBD	0.949
2	[S1043M;D1050E;T1054Q] / NCBD	0.948
3	[A1047G] / NCBD	0.924
4	[1047mA] / NCBD**	0.964
5	[1048mL] / NCBD	0.953
6	[1049mL] / NCBD	0.944
7	[1050mD] / NCBD**	0.934
8	[1052mL] / NCBD	0.941
9	[1055mL] / NCBD	0.960
10	[1056mL] / NCBD	0.922
11	[1061mA] / NCBD**	0.949
12	[1064mL] / NCBD	0.935
13	[1071mL] / NCBD**	0.889
14	[1072mA] / NCBD	0.939
15	[1076mL] / NCBD**	1.00
16	[1077mV] / NCBD	0.932
17	[1080mA] / NCBD	0.968
18	[1082mA] / NCBD	0.963
19	[1083mL] / NCBD**	0.968
20	[1085mP] / NCBD**	0.975
21	[1047mA;1071mL] / NCBD**	0.893
22	[1047mA;1072mA] / NCBD	0.959
23	[1047mA;1076mL] / NCBD**	1.02
24	[1047mA;1077mV] / NCBD	0.987
25	[1047mA;1083mL] / NCBD**	0.924
26	[1048mL;1076mL] / NCBD	0.974
27	[1048mL;1077mV] / NCBD	0.977
28	[1048mL;1083mL] / NCBD	0.943
29	[1050mD; 1071mL] / NCBD	0.944
30	[1050mD;1072mA] / NCBD	0.943
31	[1050mD; 1076mL] / NCBD	0.979
32	[1050mD;1077mV] / NCBD	0.981
33	[1050mD;1083mL] / NCBD**	0.980
34	[1055mL;1076mL] / NCBD	0.949
35	[1061mA;1071mL] / NCBD	0.900
36	[1061mA;1076mL] / NCBD**	0.989
37	[1061mA;1077mV] / NCBD	0.993
38	[1061mA;1083mL] / NCBD**	0.981
39	[1064mL;1071mL] / NCBD	0.882
40	[1064mL;1076mL] / NCBD	0.973
41	[1064mL;1077mV] / NCBD	0.953
42	[1064mL;1083mL] / NCBD	0.938
43	[1047mA;1055mL;1061mA] / NCBD	0.973
44	[1055mL;1076mL;1083mL] / NCBD	1.02
45	[1047mA;1050mD;1061mA;1076mL] / NCBD	1.01
46	[1047mA;1055mL;1061mA; 1076mL] / NCBD	0.996
47	[1047mA;1055mL;1076mL;1083mL] / NCBD	0.965
48	[1047mA;1061mA;1076mL;1083mL] / NCBD	0.986
49	[1047mA;1055mL;1061mA;1076mL;1083mL] / NCBD	0.990
50	[1047mA;1055mL;1061mA;1076mL;1083mL;1085mP] / NCBD	0.994

** The CD spectra for these analogues were previously published in our preceding communication: Schmidtgall et al. *Chem. Commun.* **2017**, *53*, 7369-7372.

Table S7. Chemical shifts (ppm) for wild type [1040-1086]-fragment of AD1-ACTR measured on a 700 MHz spectrometer used to calculate secondary chemical shifts.

Residue number	Residue type	Hα	Cα	Cβ
1040	E	not determined	not determined	not determined
1041	G	4.008	45.136	not present
1042	Q	4.415	55.818	29.566
1043	S	4.441	58.257	63.699
1044	D	4.611	54.425	41.175
1045	E	4.188	57.569	29.878
1046	R	4.205	56.889	30.325
1047	A	4.249	53.193	18.778
1048	L	4.262	55.807	not assigned
1049	L	4.230	56.089	not assigned
1050	D	4.537	55.082	40.978
1051	Q	4.275	56.359	29.160
1052	L	4.251	55.927	not assigned
1053	H	4.573	57.182	30.926
1054	T	4.227	62.600	69.496
1055	L	4.363	55.206	not assigned
1056	L	4.363	55.240	not assigned
1057	S	4.447	58.437	63.746
1058	N	4.803	53.316	38.898
1059	T	4.341	61.985	69.592
1060	D	4.615	54.391	41.134
1061	A	4.381	52.635	19.113
1062	T	4.295	62.508	69.849
1063	G	3.980	45.452	not present
1064	L	4.340	54.830	not assigned
1065	E	4.244	57.036	30.158
1066	E	4.264	56.773	30.150
1067	I	4.100	61.515	38.933
1068	D	4.563	54.650	41.001
1069	R	4.233	56.581	30.527
1070	A	4.274	52.797	18.824
1071	L	4.300	55.270	not assigned
1072	G	3.880	45.108	not present
1073	I	4.443	58.970	38.389
1074	P	4.374	63.692	32.081
1075	E	4.211	56.942	30.196
1076	L	4.344	55.247	not assigned
1077	V	4.077	62.512	32.748
1078	N	4.692	53.267	38.769
1079	Q	4.305	56.228	29.229
1080	G	3.944	45.391	not present
1081	Q	4.324	55.657	29.646
1082	A	4.313	52.366	19.063
1083	L	4.336	55.593	not assigned
1084	E	4.580	54.229	29.933
1085	P	4.413	63.335	31.919
1086	K	4.169	57.434	33.957

Table S8. Chemical shifts (ppm) for [1055meLeu] variant of [1040-1086]-fragment of AD1-ACTR measured on a 700 MHz spectrometer used to calculate secondary chemical shifts.

Residue number	Residue type	Hα	Cα	Cβ
1040	E	not determined	not determined	not determined
1041	G	4.042	45.134	not present
1042	Q	4.408	55.897	29.548
1043	S	4.442	58.500	63.6830
1044	D	4.609	54.442	41.172
1045	E	4.165	57.827	29.870
1046	R	4.181	57.143	30.2490
1047	A	4.245	53.484	18.660
1048	L	4.225	56.209	not assigned
1049	L	4.195	56.332	not assigned
1050	D	4.524	55.631	40.899
1051	Q	4.181	56.383	28.904
1052	L	4.186	56.372	not assigned
1053	H	4.483	58.010	30.642
1054	T	4.062	64.236	69.290
1055	mL (meLeu)	n/a	n/a	α-CH_3 (C: 23.79 ppm; H 1.501 ppm), Leu side chain not assigned
1056	L	4.195	56.391	not assigned
1057	S	4.381	59.288	63.586
1058	N	4.834	53.341	39.066
1059	T	4.359	62.149	69.749
1060	D	4.617	54.388	41.116
1061	A	4.368	52.709	19.131
1062	T	4.283	62.625	69.805
1063	G	3.979	45.498	not present
1064	L	4.400	54.823	not assigned
1065	E	4.229	57.167	30.144
1066	E	4.257	56.834	30.096
1067	I	4.085	61.599	38.890
1068	D	4.552	54.748	41.000
1069	R	4.224	56.624	30.508
1070	A	4.269	52.845	18.843
1071	L	4.296	55.278	not assigned
1072	G	3.868	45.112	not present
1073	I	4.432	59.036	38.355
1074	P	4.369	63.746	32.068
1075	E	4.205	57.003	30.185
1076	L	4.355	55.258	not assigned
1077	V	4.072	62.530	32.741
1078	N	4.690	53.280	38.716
1079	Q	4.302	56.257	29.222
1080	G	3.943	45.396	not present
1081	Q	4.322	55.679	29.633
1082	A	4.311	52.376	19.078
1083	L	4.333	55.298	not assigned
1084	E	4.578	54.238	29.933
1085	P	4.412	63.325	31.925
1086	K	4.167	57.419	33.957

Table S9. Chemical shifts (ppm) for [1055meLeu;1076meLeu] variant of [1040-1086]-fragment of AD1-ACTR measured on a 700 MHz spectrometer used to calculate secondary chemical shifts.

Residue number	Residue type	Hα	Cα	Cβ
1040	E	not determined	not determined	not determined
1041	G	4.029	45.138	not present
1042	Q	4.414	55.848	29.561
1043	S	4.445	58.469	63.703
1044	D	4.612	54.437	41.158
1045	E	4.164	57.857	29.856
1046	R	4.178	57.160	30.239
1047	A	4.244	53.514	18.641
1048	L	4.223	56.303	not assigned
1049	L	4.184	56.433	not assigned
1050	D	4.522	55.732	40.867
1051	Q	4.173	56.432	28.905
1052	L	4.181	56.434	not assigned
1053	H	4.466	58.159	30.675
1054	T	4.045	64.419	69.241
1055	mL (meLeu)	n/a	n/a	α-CH_3 (C: 23.68 ppm; H: 1.500 pm), Leu side chain not assigned
1056	L	4.177	56.436	not assigned
1057	S	4.380	59.356	63.580
1058	N	4.838	53.321	39.102
1059	T	4.361	62.150	69.740
1060	D	4.619	54.381	41.114
1061	A	4.362	52.768	19.112
1062	T	4.280	62.671	69.787
1063	G	3.978	45.503	not present
1064	L	4.334	54.843	not assigned
1065	E	4.224	57.241	30.110
1066	E	4.253	56.884	30.111
1067	I	4.077	61.677	38.868
1068	D	4.548	54.802	41.018
1069	R	4.217	56.689	30.498
1070	A	4.269	52.905	18.831
1071	L	4.300	55.302	not assigned
1072	G	3.880	45.149	not present
1073	I	4.408	59.205	38.289
1074	P	4.397	63.589	32.083
1075	E	4.133	57.820	29.891
1076	mL (meLeu)	n/a	n/a	α-CH_3 (C: 24.54 ppm; H: 1.444 ppm), Leu side chain not assigned
1077	V	3.928	63.806	32.180
1078	N	4.704	53.641	38.847
1079	Q	4.307	56.411	29.133
1080	G	3.956	45.506	not present
1081	Q	4.327	55.685	29.600
1082	A	4.315	52.357	19.093
1083	L	4.329	55.363	not assigned
1084	E	4.578	54.226	29.935
1085	P	4.411	63.330	31.929
1086	K	4.169	57.430	33.962

Table S10. The $^{13}C\alpha$ spin-lattice R_1 relaxation rates (s^{-1}) for wild type AD1-ACTR, [1055meLeu] and [1055meLeu;1076meLeu] variants.

	WT AD1-ACTR		[1055meLeu]		[1055meLeu;1076meLeu]	
Residue	R_1	uncertainty	R_1	uncertainty	R_1	uncertainty
1040	N/A	N/A	N/A	N/A	N/A	N/A
1041	N/A	N/A	N/A	N/A	N/A	N/A
1042	2.29	1.15	2.40	1.56	2.53	1.15
1043	2.22	0.832	2.23	0.647	2.44	1.44
1044	2.38	0.882	2.30	0.836	2.49	1.80
1045	2.50	1.41	2.11	0.864	1.96	1.02
1046	2.49	1.76	2.56	1.36	2.17	1.01
1047	2.35	0.772	2.27	0.579	2.42	1.27
1048	2.55	0.870	1.65	0.405	1.90	0.80
1049	2.47	1.04	2.40	0.953	2.17	1.29
1050	2.25	0.839	2.45	1.43	2.44	1.45
1051	2.48	0.887	1.94	1.21	2.37	1.49
1052	2.26	1.13	2.37	0.507	2.00	1.17
1053	2.31	0.579	2.22	1.15	2.71	0.853
1054	2.36	0.777	2.41	1.05	2.50	1.47
1055	2.26	1.61	N/A	N/A	N/A	N/A
1056	2.40	1.59	2.40	0.953	2.10	1.04
1057	2.32	1.16	2.21	1.06	2.18	1.23
1058	2.33	0.871	2.18	1.06	2.28	1.60
1059	2.41	1.12	2.12	1.46	2.53	1.40
1060	2.46	0.842	2.32	1.04	2.30	1.21
1061	2.14	1.01	2.29	0.894	2.18	1.14
1062	2.25	1.04	2.08	0.875	2.14	1.57
1063	N/A	N/A	N/A	N/A	N/A	N/A
1064	2.51	1.08	2.38	0.880	2.71	1.13
1065	2.46	0.762	2.25	0.488	2.24	1.13
1066	2.37	1.51	2.43	0.624	2.42	1.03
1067	2.40	1.48	2.11	0.787	2.24	0.947
1068	2.36	1.45	2.31	1.09	2.64	0.569
1069	2.31	0.881	2.22	0.743	2.54	0.995
1070	2.35	0.893	2.00	1.19	2.02	1.14
1071	2.41	0.628	2.26	0.894	1.89	0.713
1072	N/A	N/A	N/A	N/A	N/A	N/A
1073	2.61	0.858	2.45	1.28	2.36	1.21
1074	2.45	0.703	2.37	0.683	2.30	1.01
1075	2.37	1.37	2.00	0.837	2.54	0.988
1076	2.39	1.02	2.20	0.789	N/A	N/A
1077	2.50	1.05	2.50	1.11	2.36	1.05
1078	2.67	1.10	2.51	0.875	2.25	2.22
1079	2.23	1.15	2.15	0.842	2.37	0.789
1080	N/A	N/A	N/A	N/A	N/A	N/A
1081	2.45	1.16	2.45	0.768	2.55	0.615
1082	2.33	1.10	2.50	1.17	2.07	1.10
1083	2.54	1.02	2.44	0.887	2.10	0.832
1084	2.58	0.988	2.63	0.973	2.61	0.784
1085	2.37	1.63	2.38	0.476	2.25	0.704
1086	1.97	0.971	1.96	1.02	1.86	1.28

Table S11. The $^{13}C\alpha$ spin-spin R_2 relaxation rates (s^{-1}) for wild type AD1-ACTR, [1055meLeu] and [1055meLeu;1076meLeu] variants.

	WT AD1-ACTR		[1055meLeu]		[1055meLeu;1076meLeu]	
Residue	R_2	uncertainty	R_2	uncertainty	R_2	uncertainty
1040	N/A	N/A	N/A	N/A	N/A	N/A
1041	N/A	N/A	N/A	N/A	N/A	N/A
1042	3.25	1.04	3.92	0.937	4.09	0.708
1043	4.33	0.694	4.43	1.29	5.48	1.11
1044	5.28	1.10	5.56	1.27	5.98	1.31
1045	5.76	0.864	6.67	1.10	8.66	0.923
1046	5.66	0.772	8.78	1.18	6.48	0.451
1047	5.49	1.39	8.21	0.871	8.61	0.701
1048	5.23	0.805	7.31	0.932	11.0	0.984
1049	6.24	1.16	8.66	0.668	10.5	0.515
1050	6.00	0.405	13.2	1.36	16.0	0.853
1051	6.87	0.970	9.44	1.17	9.45	1.27
1052	6.58	1.45	11.0	0.958	10.2	1.01
1053	6.85	0.744	10.6	0.967	14.3	0.801
1054	6.14	0.834	14.0	0.831	24.9	0.689
1055	5.17	0.615	N/A	N/A	N/A	N/A
1056	6.31	0.917	8.66	0.668	9.73	1.17
1057	4.37	1.12	9.41	0.507	9.83	1.26
1058	5.10	0.745	6.70	0.671	7.23	0.748
1059	5.39	0.990	5.99	1.20	7.45	1.05
1060	4.87	0.598	5.48	0.922	5.62	1.35
1061	4.75	0.696	4.50	1.20	6.55	1.16
1062	4.70	0.844	5.59	1.30	6.89	1.01
1063	N/A	N/A	N/A	N/A	N/A	N/A
1064	4.18	0.900	4.10	1.07	4.45	0.672
1065	6.20	1.01	9.62	1.02	10.5	0.976
1066	7.51	1.25	7.02	1.15	8.00	0.974
1067	6.59	0.843	6.92	0.380	9.04	0.999
1068	6.28	1.46	7.90	0.520	8.18	0.926
1069	5.58	0.920	8.06	1.43	8.71	0.649
1070	5.21	0.710	7.00	1.22	6.70	0.791
1071	5.37	0.968	5.51	1.52	5.46	0.880
1072	N/A	N/A	N/A	N/A	N/A	N/A
1073	8.42	0.860	7.77	0.999	13.0	0.524
1074	5.64	0.396	6.73	1.05	8.32	0.842
1075	6.98	0.868	6.58	1.05	8.06	0.549
1076	6.01	0.802	6.15	1.57	N/A	N/A
1077	4.54	0.439	4.74	0.835	7.28	1.08
1078	4.67	1.22	5.26	0.795	6.50	0.965
1079	4.87	0.716	5.48	0.918	6.02	1.12
1080	N/A	N/A	N/A	N/A	N/A	N/A
1081	4.59	0.900	4.18	0.888	4.90	1.43
1082	3.50	1.14	3.26	0.775	4.24	0.729
1083	5.32	0.637	5.51	1.016	7.31	1.11
1084	3.91	0.687	4.05	0.828	4.00	0.579
1085	2.83	1.08	3.12	1.01	3.10	0.574
1086	2.55	0.853	2.73	0.557	2.76	1.069

Table S12. Crystallographic data collection and refinement statistics for the complex of NCBD with [1055meLeu;1076meLeu]AD1-ACTR variant (values in parentheses are for the highest resolution shell).

Data collection	
X-ray source	Swiss Light Source (PXIII beamline)
Wavelength	1.00003 Å
Resolution range	41.72 - 2.28 Å (2.362 - 2.28 Å)
Space group	*C* 2
Unit cell	*a* = 103.18 Å, *b* = 42.46 Å, *c* = 113.79 Å, α = γ = 90°, β = 101.125°
Total reflections	73662 (7372)
Unique reflections	21924 (2175)
Multiplicity	3.4 (3.4)
Completeness	97.23 % (96.97 %)
Mean I/sigma(I)	9.58 (1.94)
Wilson B-factor	33.76 Å^2
R-merge	0.09578 (0.6837)
CC1/2	0.995 (0.745)
Refinement	
Reflections used in refinement	21873 (2173)
Reflections used for R-free	1100 (107)
R-work	0.2264 (0.2965)
R-free	0.2712 (0.3260)
Number of non-hydrogen atoms	3765
macromolecules	3578
ligands	29
solvent	158
Protein residues	466
RMS(bonds)	0.006
RMS(angles)	1.13
Ramachandran favored	97.36 %
Ramachandran allowed	2.64 %
Ramachandran outliers	0 %
Rotamer outliers	2.72 %
Clash score	7.93
Average B-factor	50.92 Å^2
macromolecules	51.33 Å^2
ligands	36.86 Å^2
solvent	44.35 Å^2
Number of TLS groups	8

Table S13. Hydrogen bond analysis: the increase in occurrences of intermolecular hydrogen bonds between AD1-ACTR and NCBD for the [1055meLeu]AD1-ACTR and [1055meLeu;1076meLeu]AD1-ACTR analogues indicates the increase in stabilizing interactions between the two proteins and agrees with enhanced binding affinities observed for NCBD binding. The differences in the hydrogen bonding patterns between activation domain of ACTR and NCBD for different complexes indicate structural differences between the three complexes. Listed are hydrogen bonds that occur for at least 20% of the time in at least one of the three complexes. Shaded in gray are hydrogen bonds that occur in at least two complexes (10 out of 40). First 50 ns were excluded from the analysis.

Hydrogen Bond	Occurrence (%)		
	WT AD1-ACTR / NCBD	[1055mL] AD1-ACTR / NCBD	[1055mL;1076mL] AD1-ACTR / NCBD
ACTR:Glu1066 NH – NCBD:Ser2077 O	0.0	69.7	0.0
NCBD:Ser2077 NH – ACTR:Leu1064 O	0.0	65.9	0.0
NCBD:Gln2086 NH – ACTR:Glu1065 OE1	0.0	65.5	0.0
NCBD:Gln2085 NE2HE22 – ACTR:Glu1065 OE2	0.0	63.6	0.0
NCBD:Lys2076 NH - ACTR:Gly1063 O	0.0	60.8	0.0
NCBD:Leu2088 NH – ACTR:Glu1065 OE2	0.0	58.3	0.0
NCBD:Val2087 NH – ACTR:Glu1065 OE2	0.0	55.3	0.0
NCBD:Ser2079 NH – ACTR:Glu1065 OE2	13.9	0.0	49.9
NCBD:Gln2104 NH – ACTR:Asp1068 OD1	0.0	0.0	48.9
NCBD:Ser2079 NH – ACTR:Glu1065 OE1	10.8	0.0	48.4
NCBD:Ser2079 OGHG – ACTR:Glu1065 OE1	5.1	4.6	44.6
NCBD:Ser2079 OGHG – ACTR:Glu1065 OE2	2.5	3.1	44.4
NCBD:Lys2103 NH – ACTR:Asp1068 OD1	0.0	0.0	43.7
NCBD:Val2087 NH – ACTR:Glu1065 OE1	0.0	43.6	0.0
NCBD:Gln2085 NE2HE21 – ACTR:Glu1066 O	0.0	41.6	0.0
NCBD:Gln2085 NE2HE22 – ACTR:Glu1065 OE1	0.0	39.7	0.0
NCBD:Gln2104 NH – ACTR:Asp1068 OD2	0.0	0.0	38.8
NCBD:Ser2080 NH - ACTR:Glu1065 OE2	38.2	3.2	19.1
NCBD:Lys2103 NH – ACTR:Asp1068 OD2	0.0	0.0	36.1
NCBD:Ser2080 OGHG - ACTR:Glu1065 OE2	36.1	1.5	16.9
NCBD:Gln2086 NE2HE22 – ACTR:Glu1065 OE1	0.0	35.4	0.0
NCBD:Arg2105 NH - ACTR:Asp1068 OD1	0.0	0.0	34.9
NCBD:Arg2105 NH - ACTR:Asp1068 OD2	0.0	0.0	34.9
ACTR:Leu1064 NH – NCBD:Leu2091 O	34.4	0.0	0.0
NCBD:Ser2079 NH – ACTR:Glu1066 OE2	0.0	34.2	0.0
ACTR:Leu25 NH – NCBD:Leu2075 O	0.0	0.0	33.7
NCBD:Ser2080 NH – ACTR:Glu1065 OE1	33.5	19.7	15.1
NCBD:Arg2105 NEHE – ACTR:Asp1068 O	0.0	0.0	32.9
ACTR:Gly24 NH – NCBD:Leu2075 O	0.0	0.0	31.4
NCBD:Ser2080 OGHG – ACTR:Glu1065 OE1	29.4	2.0	15.5
NCBD:Ser2079 NH – ACTR:Glu1066 OE1	0.0	29.3	0.0
NCBD:Asn2089 ND2HD22 – ACTR:Thr1054 O	28.0	0.0	0.0
NCBD:Ser2079 OGHG – ACTR:Glu1066 OE2	0.0	24.5	0.0
NCBD:Gln2086 NH – ACTR:Glu1065 OE2	0.0	24.2	0.0
NCBD:Leu2068 NH – ACTR:Asn1058 O	21.9	0.0	0.0
NCBD:Ser2079 OGHG – ACTR:Glu1066 OE1	0.0	21.9	0.0
NCBD:Thr2106 OG1HG1 - ACTR:Glu1084 OE2	21.6	0.0	0.0
NCBD:Tyr2109 OHHH – ACTR:Asp1068 OD2	0.0	20.6	1.2
NCBD:Tyr2109 OHHH – ACTR:Asp1068 OD1	0.0	20.2	3.2
NCBD:Thr2106 NH – ACTR:Glu1084 OE2	20.0	0.0	0.0

Table S14. Salt-bridge analysis: the differences in occurrences of intermolecular and intramolecular salt bridges between AD1-ACTR and NCBD for the three complexes agree with the results of the hydrogen bond analysis and indicate structural differences at the ACTR/NCBD interface of the complexes. First 50 ns are excluded from the analysis.

Intermolecular salt bridges:

Salt Bridge	Occurrence (%)		
	WT AD1-ACTR / NCBD	[1055mL] AD1-ACTR / NCBD	[1055mL;1076mL] AD1-ACTR / NCBD
ACTR:Glu1045 OE1 – NCBD:Arg2073 NH2	30.9	7.2	0.2
ACTR:Glu1045 OE2 – NCBD:Arg2073 NH2	30.6	7.5	0.2
ACTR:Asp1060 OD2 – NCBD:Lys2092 NZ	24.3	0.0	0.0
ACTR:Glu1045 OE1 – NCBD:Arg2073 NH1	23.1	3.8	0.2
ACTR:Asp1060 OD1 – NCBD:Lys2092 NZ	23.1	0.0	0.0
ACTR:Glu1045 OE2 – NCBD:Arg2073 NH1	22.0	3.9	0.2
ACTR:Glu1066 OE1 – NCBD:Lys2076 NZ	13.7	8.9	0.0
ACTR:Glu1066 OE2 – NCBD:Lys2076 NZ	12.5	8.8	0.0
ACTR:Glu1084 OE1 – NCBD:Lys2108 NZ	10.7	0.0	0.0
ACTR:Asp1060 OD1 – NCBD:Arg2105 NH2	0.0	29.5	0.0
ACTR:Asp1060 OD2 – NCBD:Arg2105 NH2	0.0	29.2	0.0
ACTR:Asp1060 OD1 – NCBD:Arg2105 NH1	0.0	12.5	0.0
ACTR:Asp1060 OD2 – NCBD:Arg2105 NH1	0.0	13.0	0.0
ACTR:Asp1068 OD1 – NCBD:Arg2105 NH2	1.6	27.3	14.5
ACTR:Asp1068 OD2 – NCBD:Arg2105 NH2	1.8	26.9	15.5
ACTR:Asp1068 OD1 – NCBD:Arg2105 NH1	1.3	21.5	12.8
ACTR:Asp1068 OD2 – NCBD:Arg2105 NH1	1.3	20.7	12.8
ACTR:Asp1060 OD1 – NCBD:Lys2076 NZ	0.0	1.5	29.9
ACTR:Asp1060 OD2 – NCBD:Lys2076 NZ	0.0	1.3	29.5
ACTR:Glu1075 OE2 – NCBD:Lys2092 NZ	0.0	1.8	23.1
ACTR:Glu1075 OE1 – NCBD:Lys2092 NZ	0.0	1.6	21.7
ACTR:Glu1066 OE1 – NCBD:Lys2103 NZ	6.2	0.0	12.3
ACTR:Glu1066 OE2 – NCBD:Lys2103 NZ	6.7	0.0	11.9

Intramolecular salt bridges:

Salt Bridge	Occurrence (%)		
	WT AD1-ACTR / NCBD	[1055mL] AD1-ACTR / NCBD	[1055mL;1076mL] AD1-ACTR / NCBD
ASP1050 OD2 - HIS1053 NE2	19.4	27.3	3.0
ASP1050 OD1 - HIS1053 NE2	18.7	29.7	3.0
Glu1084 OE2 – LYS1086 NZ	16.7	28.3	19.8
Glu1084 OE1 – LYS1086 NZ	15.6	18.0	19.8
ASP1060 OD2 – LYS1086 NZ	12.1	0.3	0.0
ASP1060 OD1 – LYS1086 NZ	11.8	0.5	0.0
GLU1066 OE1 – ARG1069 NH2	10.1	18.6	33.3
GLU1066 OE2 – ARG1069 NH2	9.6	17.5	34.2
GLU1066 OE1 – ARG1069 NH1	9.0	22.1	37.3
GLU1066 OE2 – ARG1069 NH1	8.6	21.5	37.9
GLU1040 OE1 – ARG1046 NH1	0.0	19.1	3.6
GLU1040 OE2 – ARG1046 NH1	0.0	18.0	3.5
GLU1040 OE2 – ARG1046 NH2	0.0	17.6	3.7
ASP1068 OD2 – ARG1069 NH2	0.1	12.7	1.6
ASP1068 OD1 – ARG1069 NH2	0.1	12.6	3.0
ASP1068 OD2 – ARG1069 NH1	0.2	10.2	0.8
ASP1068 OD1 – ARG1069 NH1	0.1	10.0	2.0
GLU1045 OE1 – ARG1046 NH2	3.7	5.7	15.1
GLU1045 OE2 – ARG1046 NH2	4.2	5.1	14.6
GLU1045 OE1 – ARG1046 NH1	2.3	3.6	12.6
GLU1045 OE2 – ARG1046 NH1	2.6	3.0	11.9

Table S15. The values from the fit of helix-helix packing in the structure of [1055meLeu;1076meLeu]AD1-ACTR/NCBD complex to the generalized Crick parameters (see Figure S18). The secondary structure was assigned by DSSP (https://2struc.cryst.bbk.ac.uk/twostruc) and coordinates of helices were submitted to CCCP server for analysis (https://grigoryanlab.org/cccp/). The Cα RMSD for pairwise helix parametrization are in the 0.41-1.2 Å range which is satisfactory and illustrates that the helix pairwise interactions follow the appropriate geometric restrains validated by the analysis of a large number of helix-helix interaction motifs in PDB (1). The attempts to parametrize the selected helices as three-helical bundles led to much higher RMSDs (> 2 Å). There is an apparent correlation of the quality of helix-helix packing with Cα RMSD of the parametric fit with the lowest values corresponding to the tightest and most complementary interfaces of H1-ACTR–H1-NCBD and H1-NCBD–H2-NCBD helix pairs, whereas the highest Cα RMSD was obtained for the loosest right-handed H3-NCBD–H1-ACTR helix-helix interaction.

Helix pair	**H1-ACTR–H1-NCBD**	**H1-NCBD–H2-NCBD**	**H2-NCBD–H2-ACTR**	**H2-ACTR–H3-NCBD**	**H3-NCBD–H3-ACTR**	**H3-NCBD–H1-ACTR**
Orientation	parallel	antiparallel	parallel	antiparallel	parallel	parallel
Interhelical crossing	left-handed	left-handed	right-handed	left-handed	right-handed	right-handed
R_0 (Å)	5.49	4.98	5.45	6.20	5.52	5.76
R_1 (Å)	2.33	2.32	2.28	2.30	2.24	2.29
ω_0 (°/res)	-4.0	-3.2	6.0	-7.1	7.1	3.0
ω_1 (°/res)	101.8	101.9	93.9	103.6	91.8	96.3
α (°)	-15.0	-10.4	21.9	-31.2	27.2	11.9
ΔZ_{off} (Å)	0.81	-2.47	1.23	-0.68	0.35	0.19
Rise per residue (Å)	1.49	1.52	1.52	1.48	1.50	1.47
Pitch (Å)	128.4	169.9	85.1	64.2	67.515	172.6
Cα RMSD	**0.48 Å**	**0.41 Å**	**0.58 Å**	**0.80 Å**	**0.91 Å**	**1.17 Å**

Table S16. Binding parameters obtained upon fitting the SPR binding of AD1-ACTR variants to NCBD using a 1:1 association model with BiaEvaluation 3.2 software. Values of k_{on} and k_{off} are near the limit of the method, therefore, a steady-state analysis (Table S17) was performed for comparison.

Temperature	AD1-ACTR variant	k_{on} ($M^{-1} \cdot s^{-1}$)	k_{off} (s^{-1})	K_D (nM, from kinetics)	Chi² from kinetics (RU^2)
20°C (293 K)	WT	1.20×10^6	0.286	238	0.25
	[1076mL]	1.28×10^6	0.339	264	0.17
	[1055mL]	1.46×10^6	0.031	21.6	1.0
	[1055mL;1076mL]	2.71×10^6	0.021	7.57	1.1
22°C (295 K)	WT	1.21×10^6	0.356	295	0.20
	[1076mL]	1.35×10^6	0.410	304	0.14
	[1055mL]	1.54×10^6	0.036	23.4	0.88
	[1055mL;1076mL]	2.97×10^6	0.024	8.06	0.96
25°C (298 K)	WT	1.09×10^6	0.406	374	0.17
	[1076mL]	1.07×10^6	0.521	489	0.07
	[1055mL]	1.85×10^6	0.049	26.3	1.2
	[1055mL;1076mL]	3.77×10^6	0.030	7.84	0.69
27°C (300 K)	WT	1.02×10^6	0.454	448	0.19
	[1076mL]	1.07×10^6	0.526	493	0.15
	[1055mL]	1.78×10^6	0.059	33.3	1.2
	[1055mL;1076mL]	3.20×10^6	0.034	10.6	0.76
31°C (304 K)	WT	7.14×10^5	0.602	843	0.15
	[1076mL]	7.72×10^5	0.696	902	0.10
	[1055mL]	1.57×10^6	0.084	53.3	0.53
	[1055mL;1076mL]	3.03×10^6	0.055	18.1	0.60

Table S17. Steady-state analysis of SPR data with a 1:1 binding isotherm model.

Temperature	AD1-ACTR variant	K_D (nM ± uncertainty)	R_{max} (RU ± uncertainty)	R_{min} (RU ± uncertainty)
20 °C (293 K)	**WT**	180 ± 24	1.018 ± 0.041	0.013 ± 0.015
	[1076meLeu]	199 ± 35	0.768 ± 0.041	0.015 ± 0.013
	[1055meLeu]	31.6 ± 0.2	1.147 ± 0.001	0.017 ± 0.001
	[1055meLeu;1076meLeu]	15.3 ± 0.2	1.543 ± 0.002	0.097 ± 0.004
22 °C (295 K)	**WT**	186 ± 25	1.007 ± 0.041	0.000 ± 0.015
	[1076meLeu]	208 ± 39	0.714 ± 0.041	0.013 ± 0.012
	[1055meLeu]	33.2 ± 0.1	1.134 ± 0.001	0.013 ± 0.001
	[1055meLeu;1076meLeu]	15.9 ± 0.2	1.375 ± 0.002	0.085 ± 0.004
25 °C (298 K)	**WT**	233 ± 38	0.973 ± 0.051	0.000 ± 0.015
	[1076meLeu]	268 ± 57	0.635 ± 0.046	0.004 ± 0.012
	[1055meLeu]	35.5 ± 0.3	1.070 ± 0.002	0.018 ± 0.002
	[1055meLeu;1076meLeu]	16.7 ± 0.2	1.114 ± 0.002	0.086 ± 0.003
27 °C (300 K)	**WT**	251 ± 36	1.090 ± 0.053	0.011 ± 0.014
	[1076meLeu]	270 ± 51	0.704 ± 0.046	0.005 ± 0.011
	[1055meLeu]	43.8 ± 0.3	1.320 ± 0.002	0.036 ± 0.002
	[1055meLeu;1076meLeu]	22.1 ± 0.4	1.287 ± 0.003	0.120 ± 0.004
31 °C (304 K)	**WT**	388 ± 63	1.203 ± 0.077	-0.005 ± 0.013
	[1076meLeu]	396 ± 90	0.700 ± 0.064	0.001 ± 0.011
	[1055meLeu]	69.2 ± 0.1	1.526 ± 0.001	0.012 ± 0.000
	[1055meLeu;1076meLeu]	30.2 ± 0.2	1.177 ± 0.001	0.050 ± 0.001

Supplementary Figures

Figure S1. Isothermal titration calorimetry of binding of AD1-ACTR variants to NCBD (consists of 36 panels on p. 33-41).

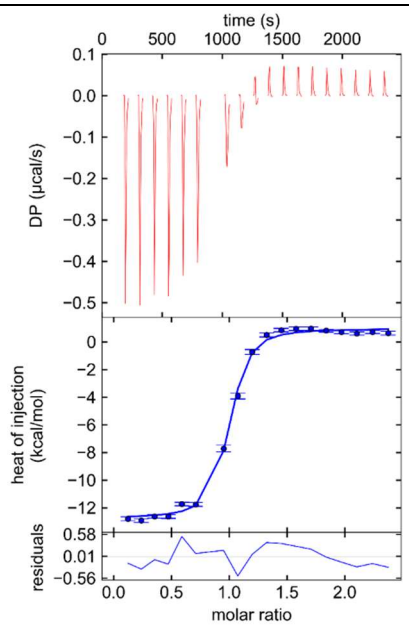

Panel 1: Binding of [S1043M;D1050E;T1054Q] AD1-ACTR to NCBD

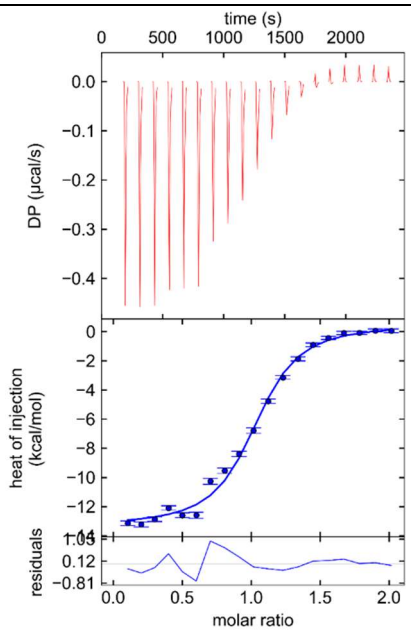

Panel 2: Binding of [A1047G] AD1-ACTR to NCBD

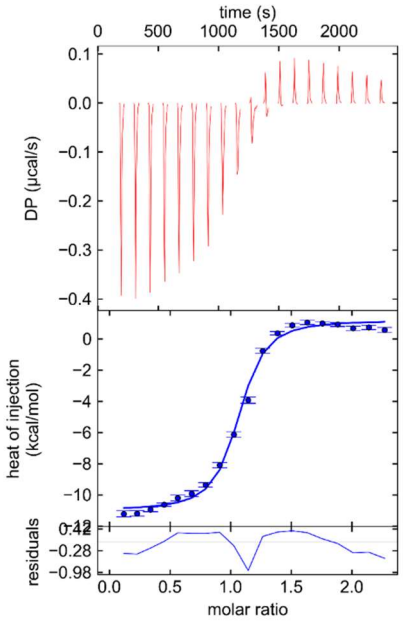

Panel 3: Binding of [1048mL] AD1-ACTR to NCBD

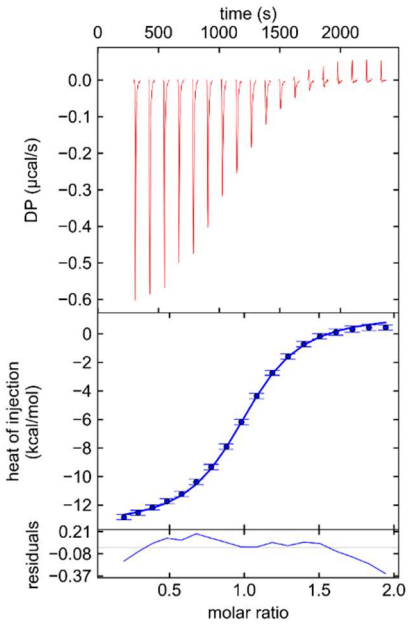

Panel 4: Binding of [1049mL] AD1-ACTR to NCBD

Figure S1. Isothermal titration calorimetry of binding of AD1-ACTR variants to NCBD (continued from p. 33).

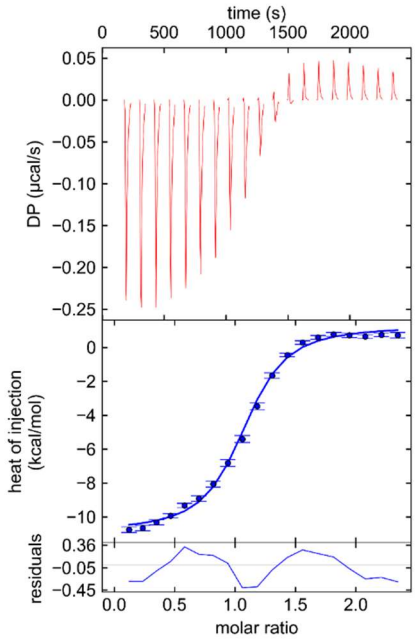

Panel 5: Binding of [1052mL] AD1-ACTR to NCBD

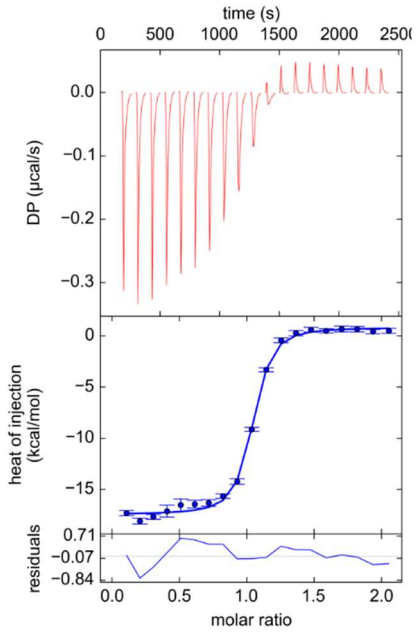

Panel 6: Binding of [1055mL] AD1-ACTR to NCBD

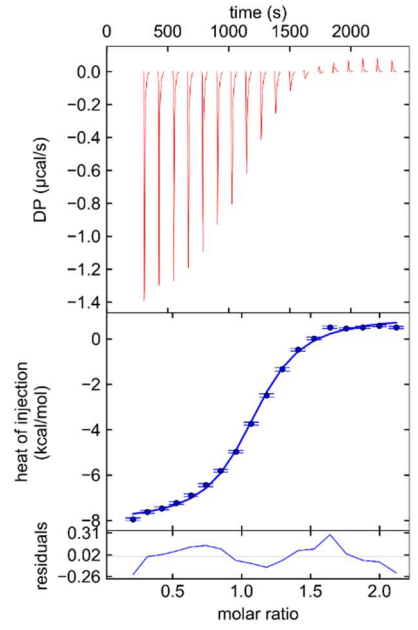

Panel 7: Binding of [1056mL] AD1-ACTR to NCBD

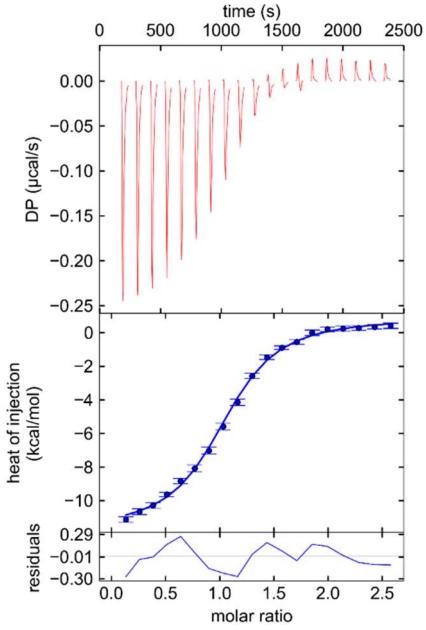

Panel 8: Binding of [1064mL] AD1-ACTR to NCBD

Figure S1. Isothermal titration calorimetry of binding of AD1-ACTR variants to NCBD (continued from p. 34).

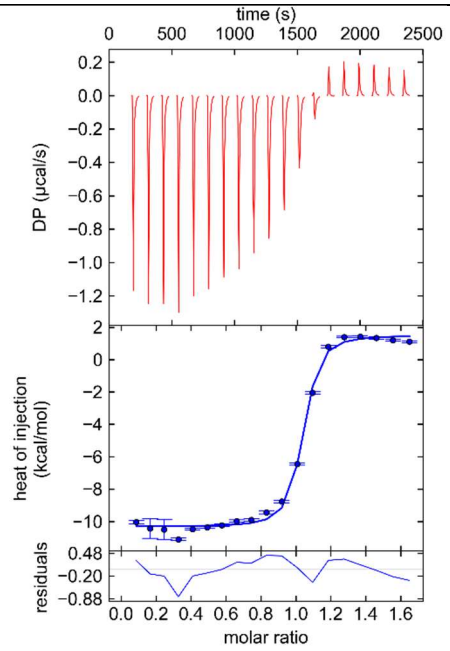

Panel 9: Binding of [1072mA] AD1-ACTR to NCBD

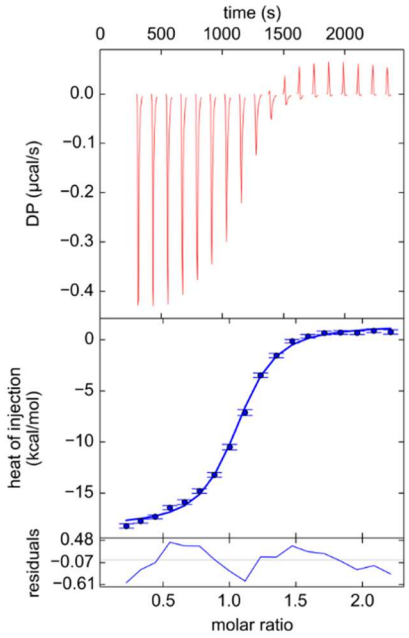

Panel 10: Binding of [1077mL] AD1-ACTR to NCBD

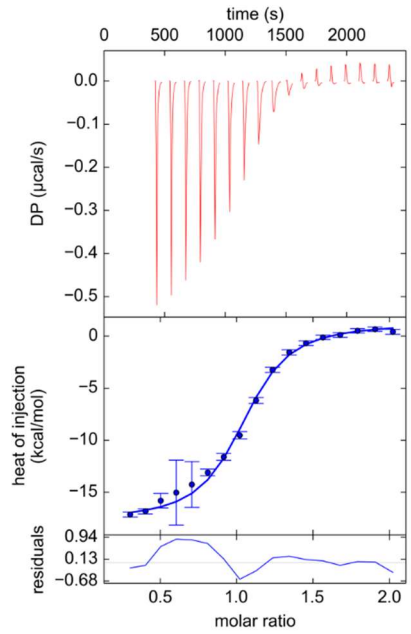

Panel 11: Binding of [1080mA] AD1-ACTR to NCBD

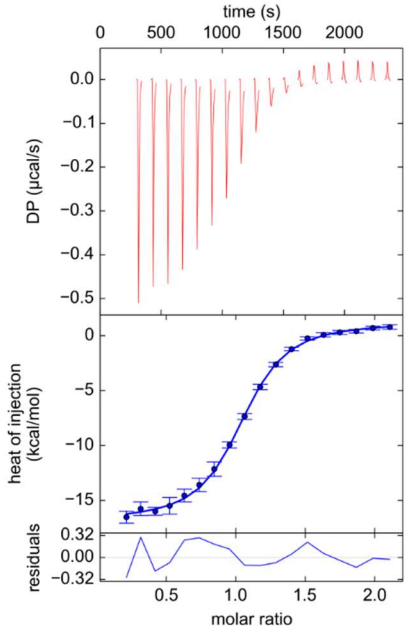

Panel 12: Binding of [1082mA] AD1-ACTR to NCBD

Figure S1. Isothermal titration calorimetry of binding of AD1-ACTR variants to NCBD (continued from p. 35).

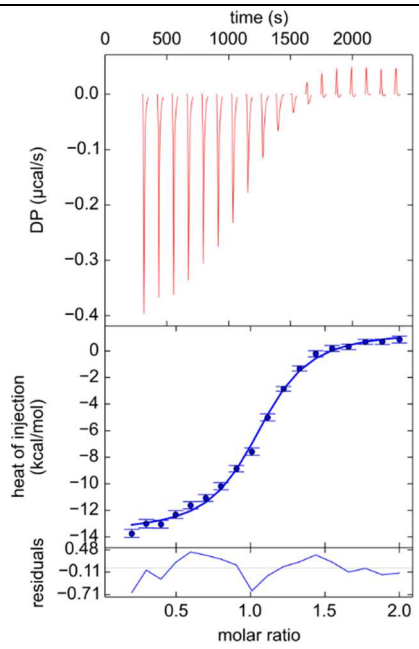

Panel 13: Binding of [1047mA;1072mA] AD1-ACTR to NCBD

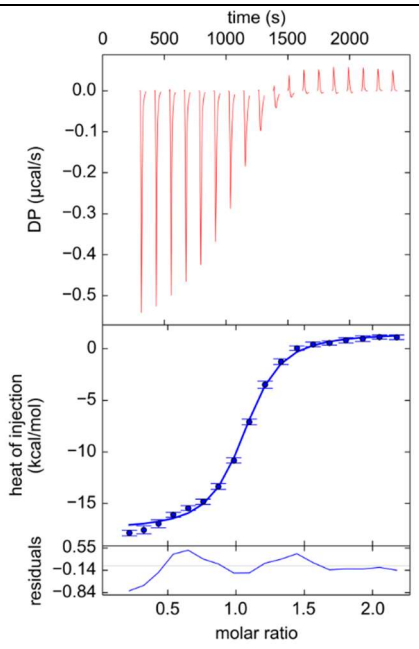

Panel 14: Binding of [1047mA;1077mV] AD1-ACTR to NCBD

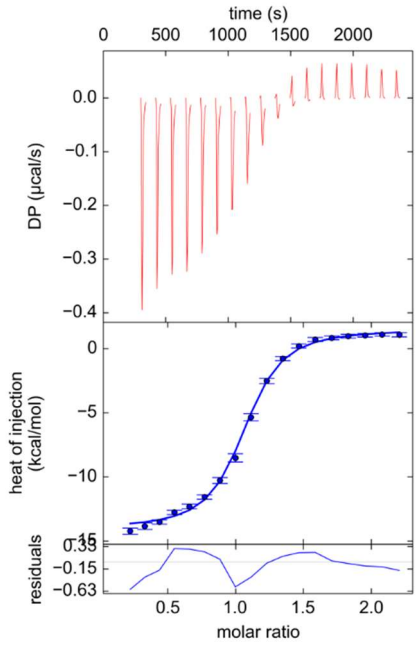

Panel 15: Binding of [1048mL;1076mL] AD1-ACTR to NCBD

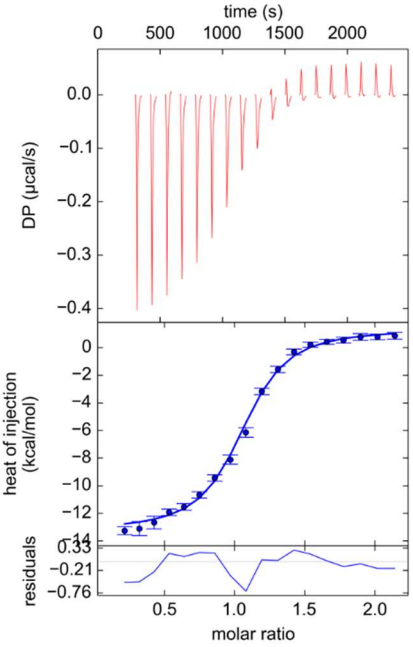

Panel 16: Binding of [1048mL;1077mV] AD1-ACTR to NCBD

Figure S1. Isothermal titration calorimetry of binding of AD1-ACTR variants to NCBD (continued from p. 36).

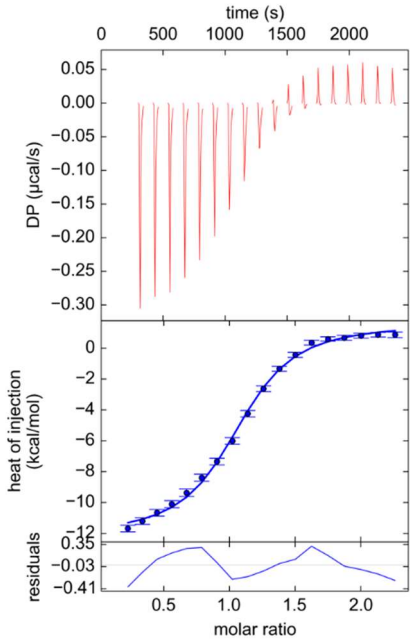

Panel 17: Binding of [1048mL;1083mL] AD1-ACTR to NCBD

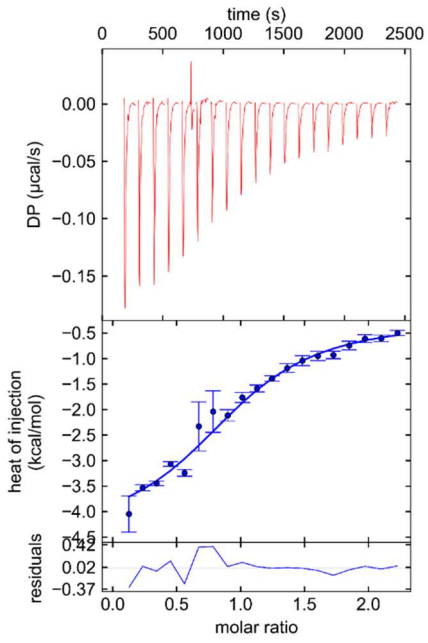

Panel 18: Binding of [1050mD;1071mL] AD1-ACTR to NCBD

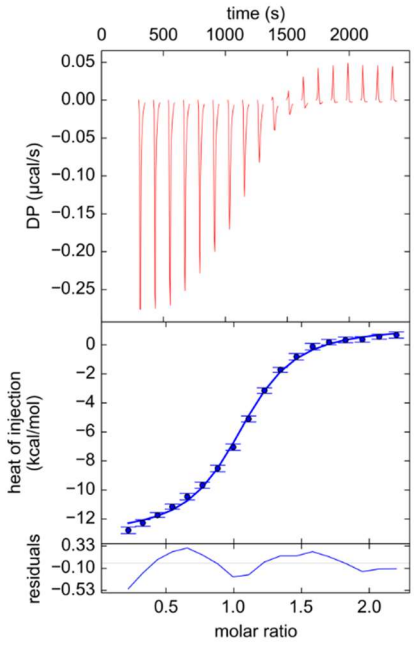

Panel 19: Binding of [1050mD;1072mA] AD1-ACTR to NCBD

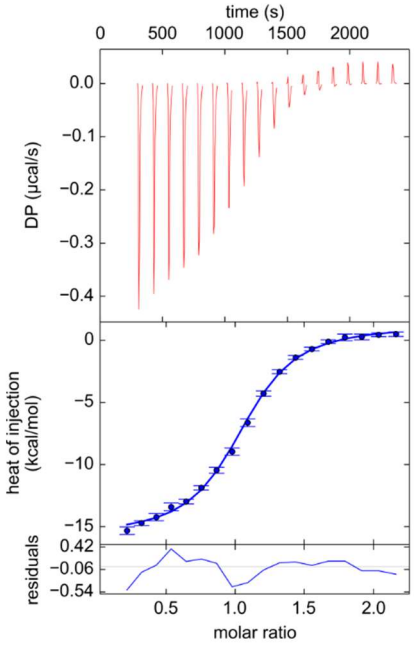

Panel 20: Binding of [1050mD;1076mL] AD1-ACTR to NCBD

Figure S1. Isothermal titration calorimetry of binding of AD1-ACTR variants to NCBD (continued from p. 37).

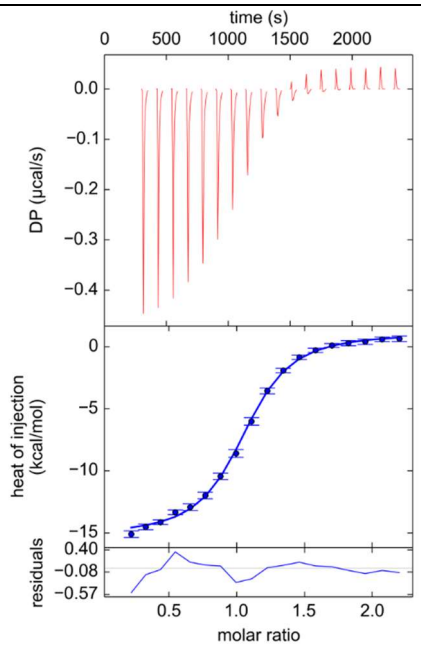

Panel 21: Binding of [1050mD;1077mV] AD1-ACTR to NCBD

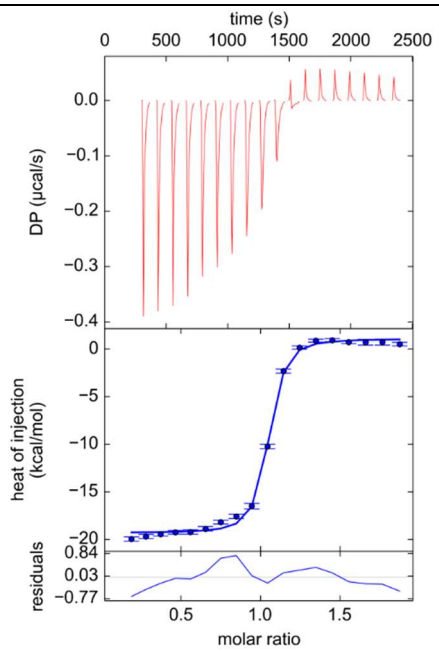

Panel 22: Binding of [1055mA;1076mL] AD1-ACTR to NCBD

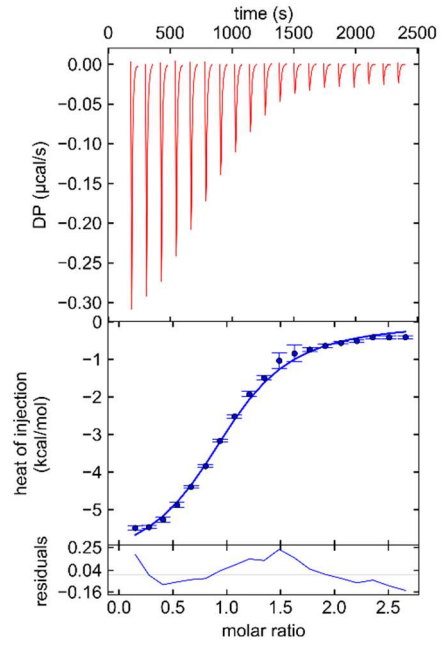

Panel 23: Binding of [1061mA;1071mL] AD1-ACTR to NCBD

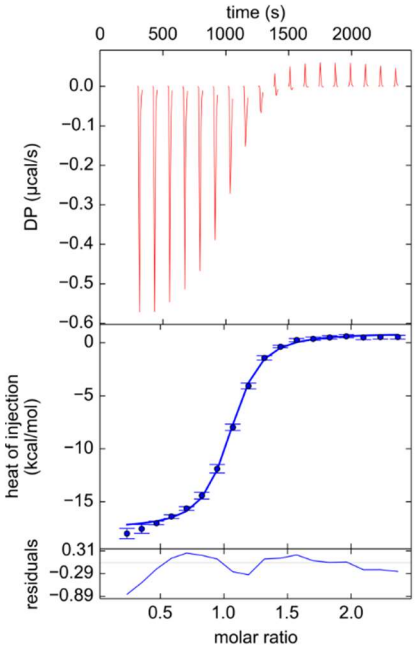

Panel 24: Binding of [1061mA;1077mV] AD1-ACTR to NCBD

Figure S1. Isothermal titration calorimetry of binding of AD1-ACTR variants to NCBD (continued from p. 38).

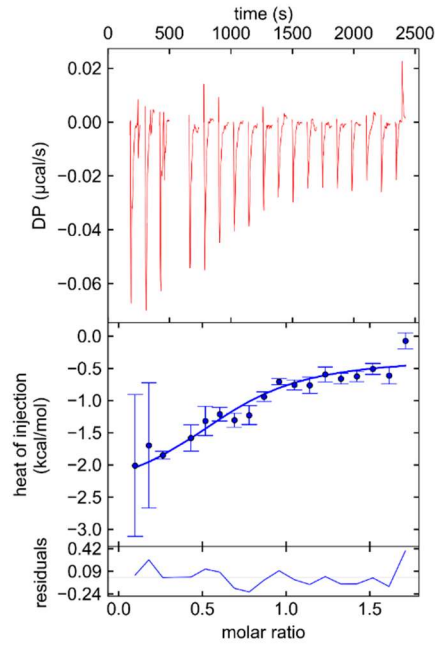

Panel 25: Binding of [1064mL;1071mL] AD1-ACTR to NCBD

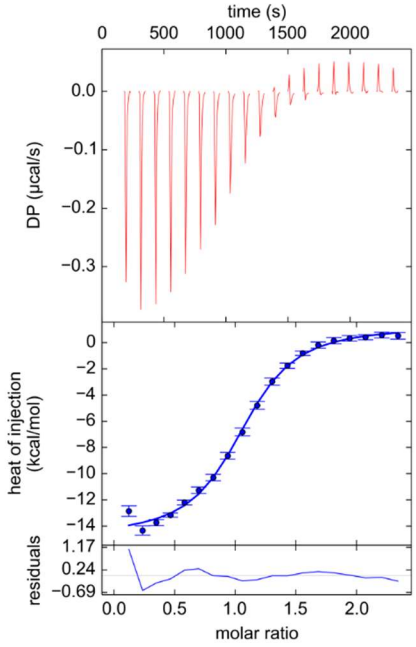

Panel 26: Binding of [1064mL;1076mL] AD1-ACTR to NCBD

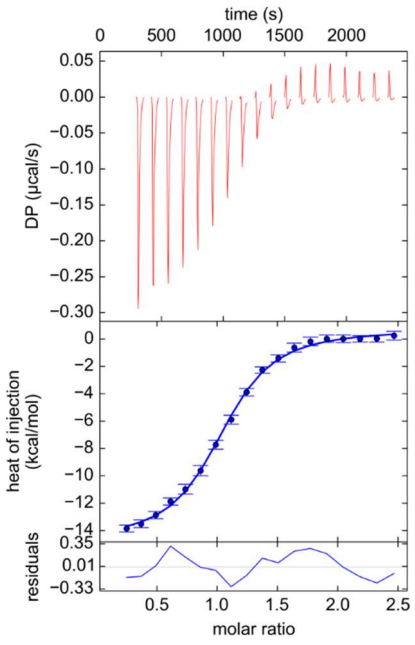

Panel 27: Binding of [1064mL;1077mV] AD1-ACTR to NCBD

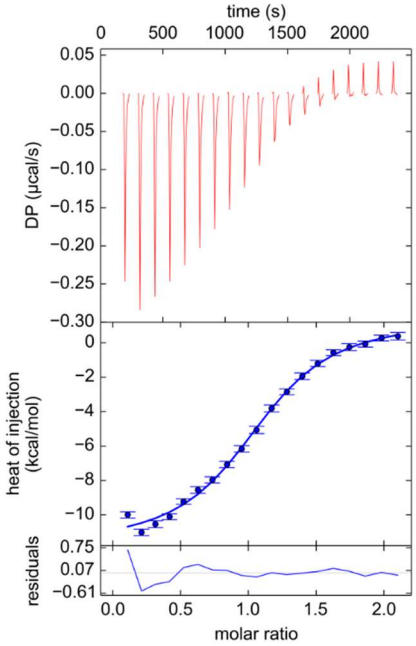

Panel 28: Binding of [1064mL;1083mL] AD1-ACTR to NCBD

Figure S1. Isothermal titration calorimetry of binding of AD1-ACTR variants to NCBD (continued from p. 39).

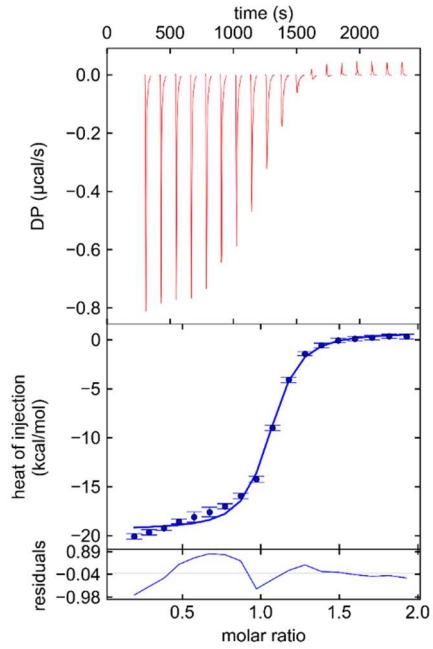

Panel 29: Binding of [1047mA;1055mL;1061mA] AD1-ACTR to NCBD

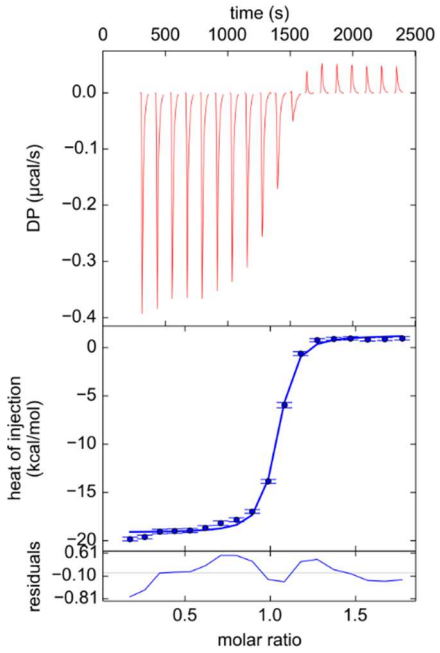

Panel 30: Binding of [1055mL;1076mL;1083mL] AD1-ACTR to NCBD

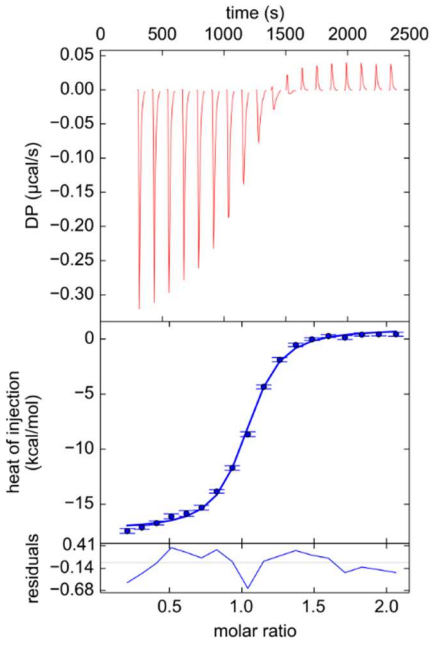

Panel 31: Binding of [1047mA;1050mD;1061mA;1076mL] AD1-ACTR to NCBD

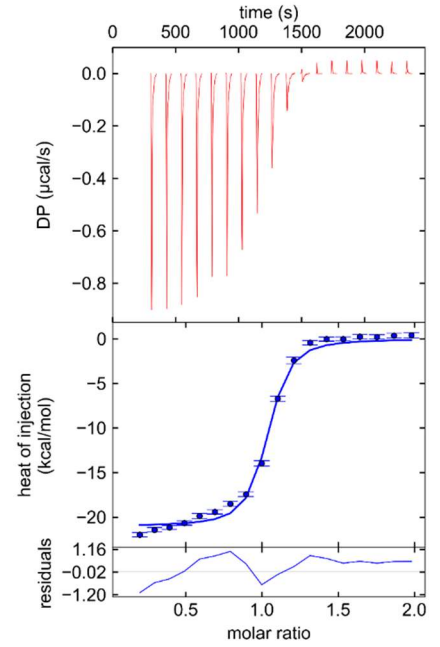

Panel 32: Binding of [1047mA;1055mL;1061mA;1076mL] AD1-ACTR to NCBD

Figure S1. Isothermal titration calorimetry of binding of AD1-ACTR variants to NCBD (continued from p. 40).

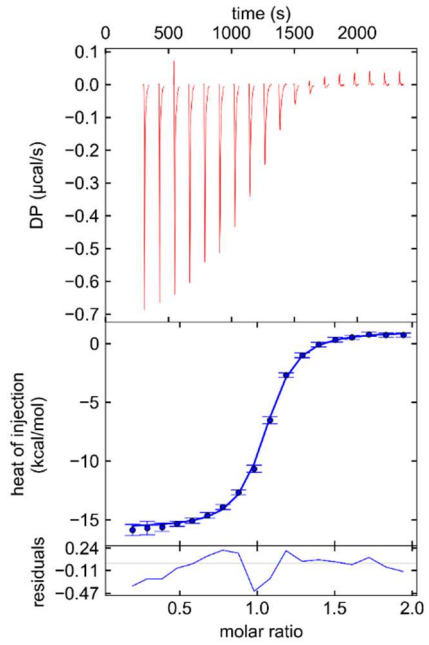

Panel 33: Binding of [1047mA;1055mL;1076mL;1083mL] AD1-ACTR to NCBD

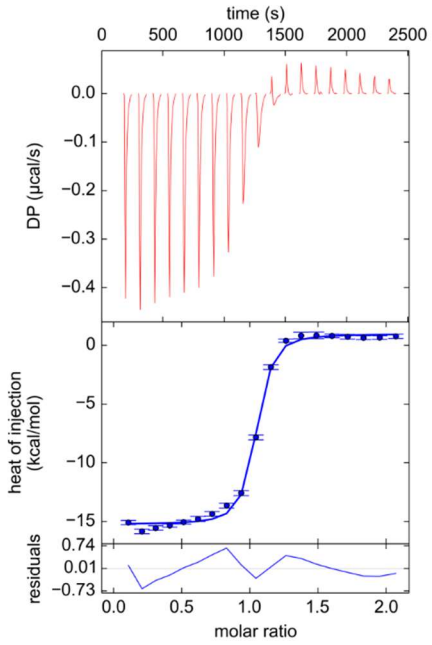

Panel 34: Binding of [1047mA;1061mA;1076mL;1083mL] AD1-ACTR to NCBD

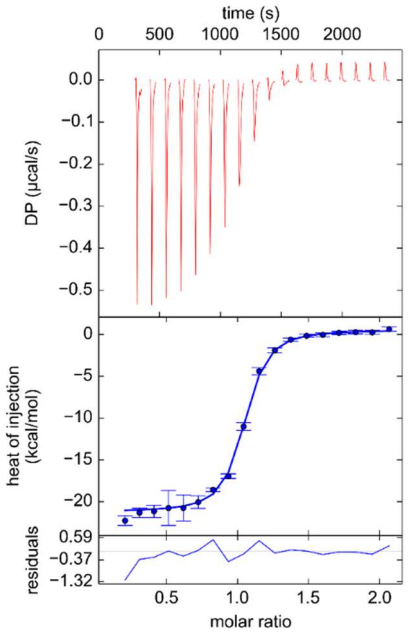

Panel 35: Binding of [1047mA;1055mL;1061mA;1076mL;1083mL] AD1-ACTR to NCBD

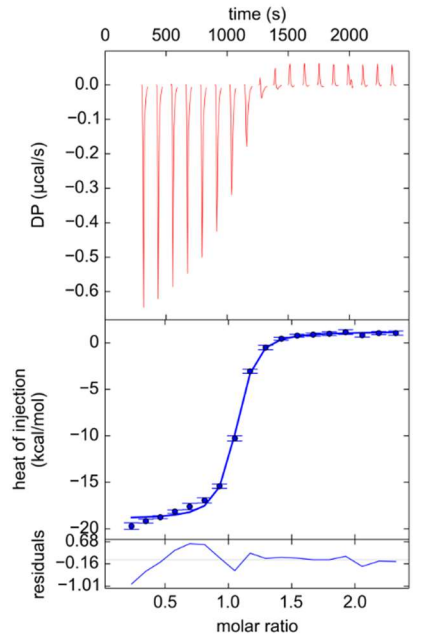

Panel 36: Binding of [1047mA;1055mL;1061mA;1076mL;1083mL;1085mP] AD1-ACTR to NCBD

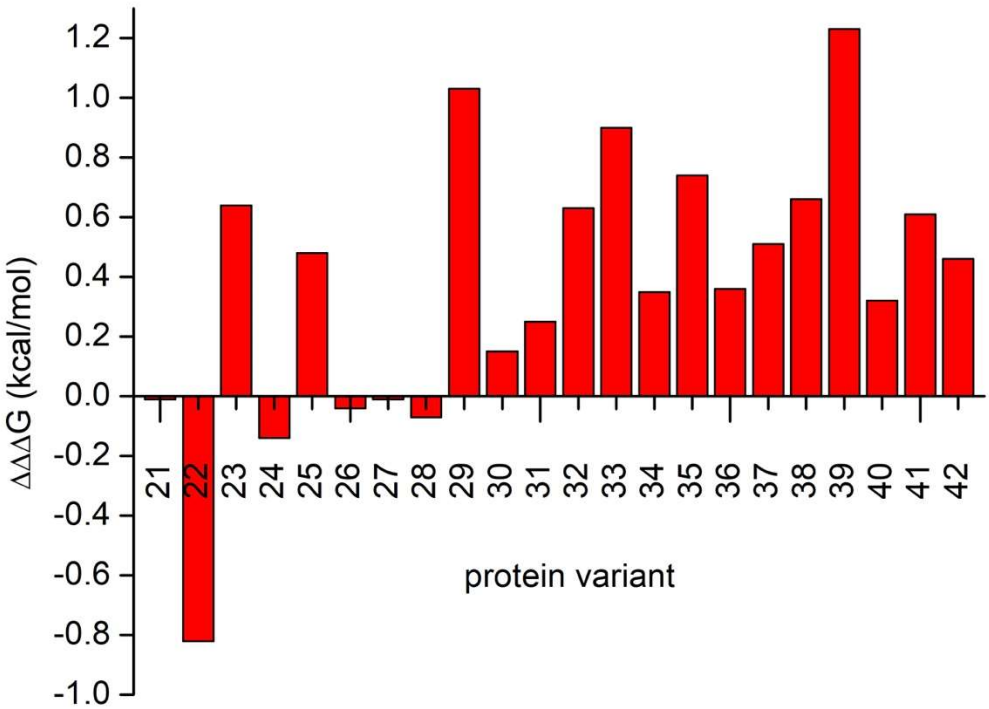

Figure S2. "Double mutant cycle" analysis for Gibbs free energy of complex formation for AD1-ACTR variants with two α-methylations according to relationship: $\Delta\Delta\Delta G = \Delta\Delta G_{variant\text{-}X} + \Delta\Delta G_{variant\text{-}Y} - \Delta\Delta G_{double\text{-}XY}$, where $\Delta\Delta G_{variant}$ is the variation in Gibbs free energy for a singly modified ACTR variant and $\Delta\Delta G_{double\text{-}XY}$ is the variation in Gibbs free energy for the doubly α-methylated protein. The numbering of protein variants is provided in Table S1.

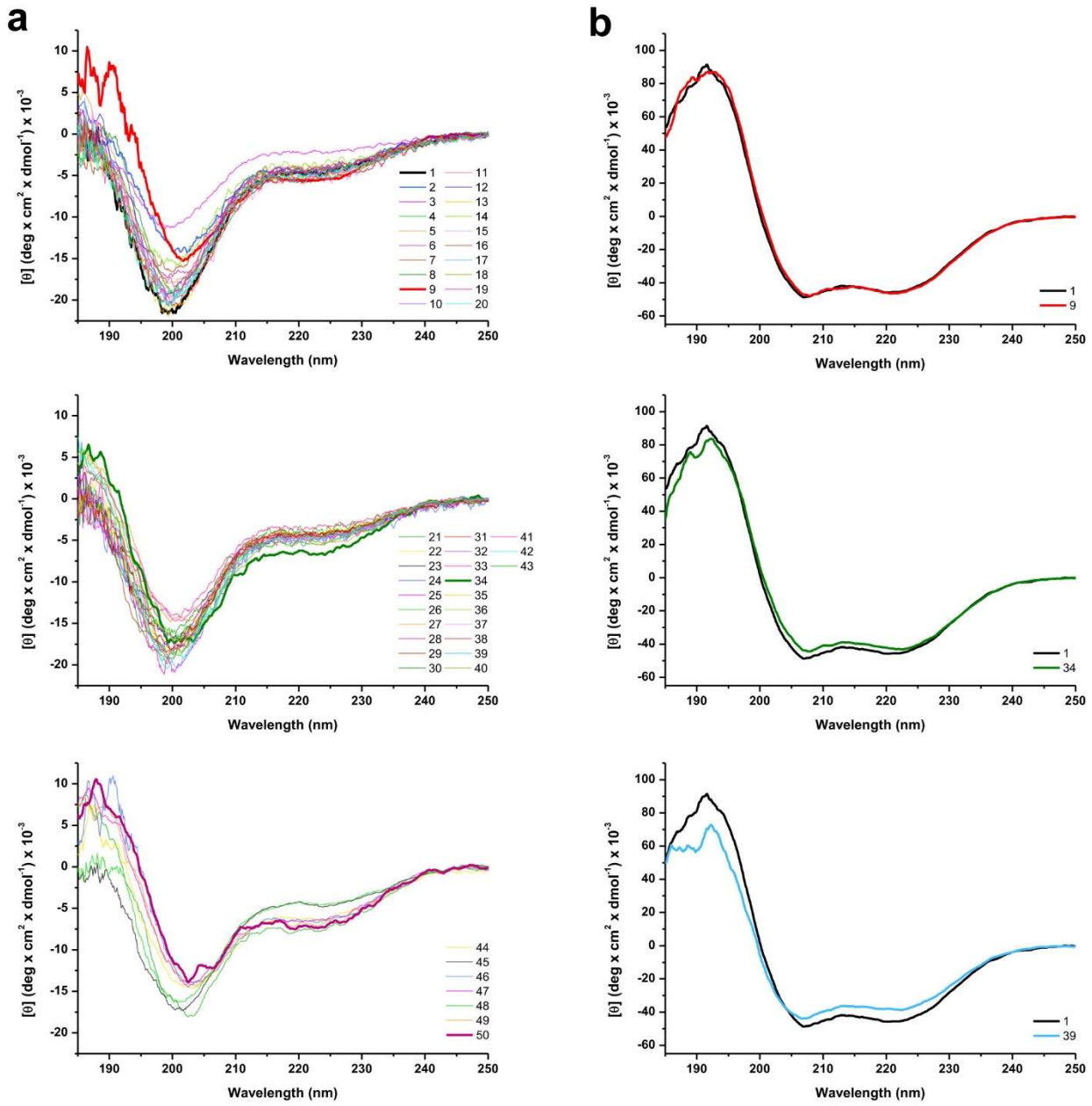

Figure S3. Circular dichroism (CD) spectra of AD1-ACTR variants and their complexes with NCBD. (a) Top panel: two control variants [S1043M;D1050E;T1054Q] (**2**) and [A1047G] (**3**) and protein analogues containing one α-methylated residue overlaid onto spectrum of wild-type (**1**); middle: analogues with two α-methylated amino acids, and bottom: containing multiple α-methylated residues. (b) Representative CD spectra of stabilized [1055mL] (**9**) (top panel), [1055mL;1076mL] (**34**) (middle panel), and destabilized [1064mL;1071mL] (**39**) (bottom panel) variants complexed with NCBD overlaid onto the corresponding spectrum of wild type complex.

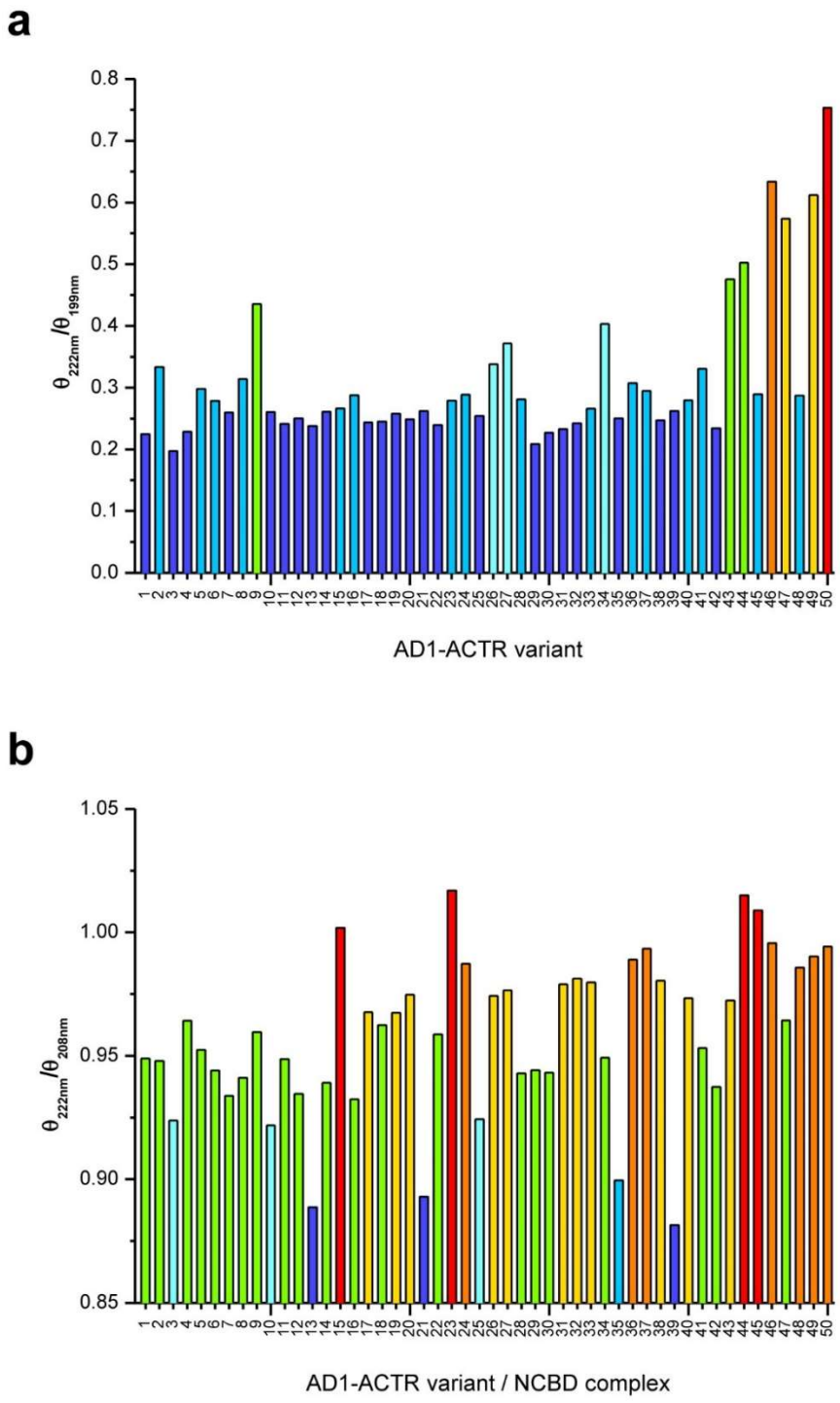

Figure S4. (a) Ellipticity ratio $\theta_{222}/\theta_{199}$ of AD1-ACTR protein variants illustrating different helical content, which increases upon multiple α-methylation. (b) Ellipticity ratio $\theta_{222}/\theta_{208}$ of complexes of AD1-ACTR with NCBD suggesting non-identical secondary/tertiary structure in different complexes. Note especially diminished values for analogues **13**, **21**, **35** and **39**, all containing 1071meLeu residue and the least stable in the library, although there is no straightforward correlation between helicity and stability. Different colors are used to highlight differences in values (blue correspond to lower values, red to higher values).

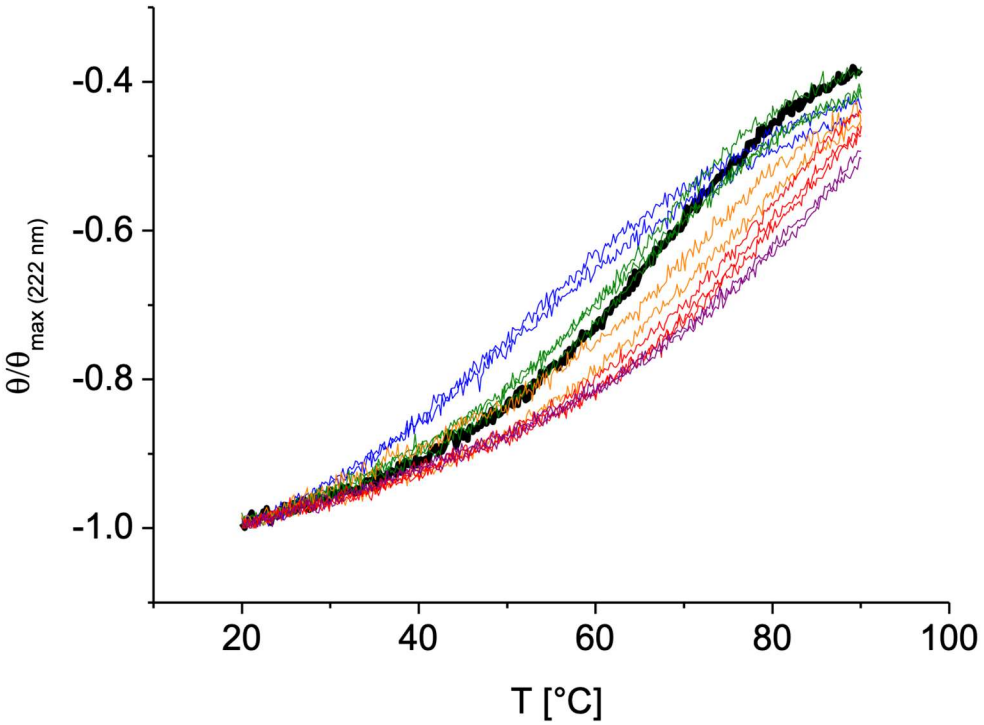

Figure S5. Thermal stability of AD1-ACTR/NCBD complexes evaluated by CD spectroscopy. Ellipticity at 222 nm was monitored as a function of temperature. The signal fully restores upon cooling after heating, i.e., thermal denaturation is reversible. Apparent melting points are provided in Table S4 and are in general agreement with relative order of thermodynamic stabilities (ΔG) of the protein variants obtained by isothermal titration calorimetry (ITC).

a

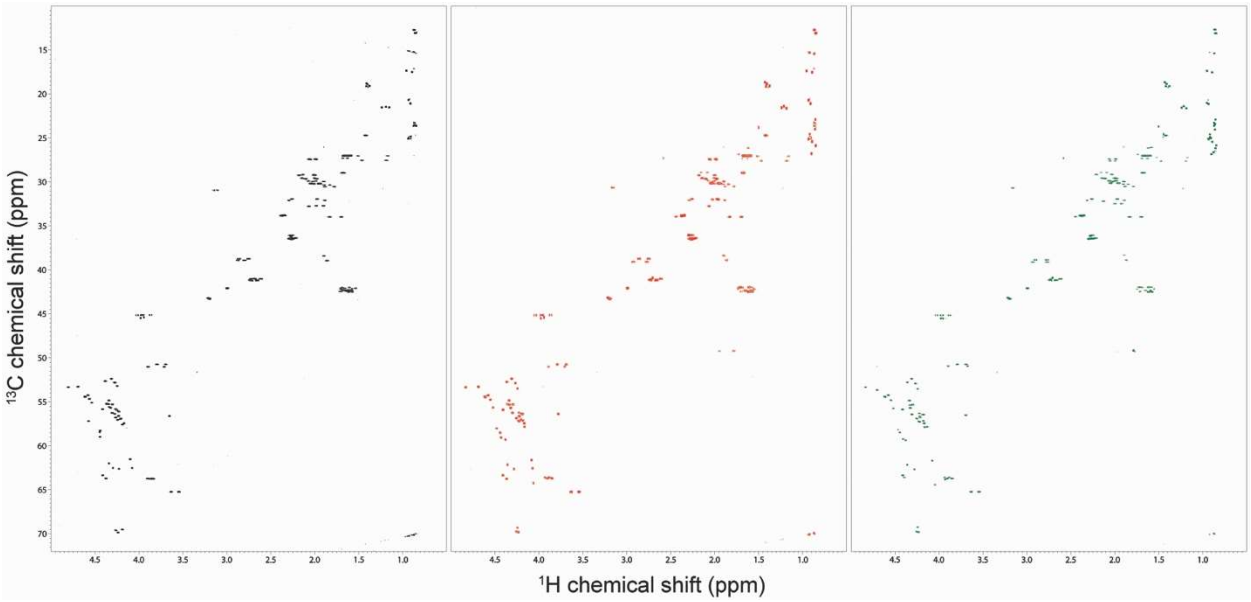

b

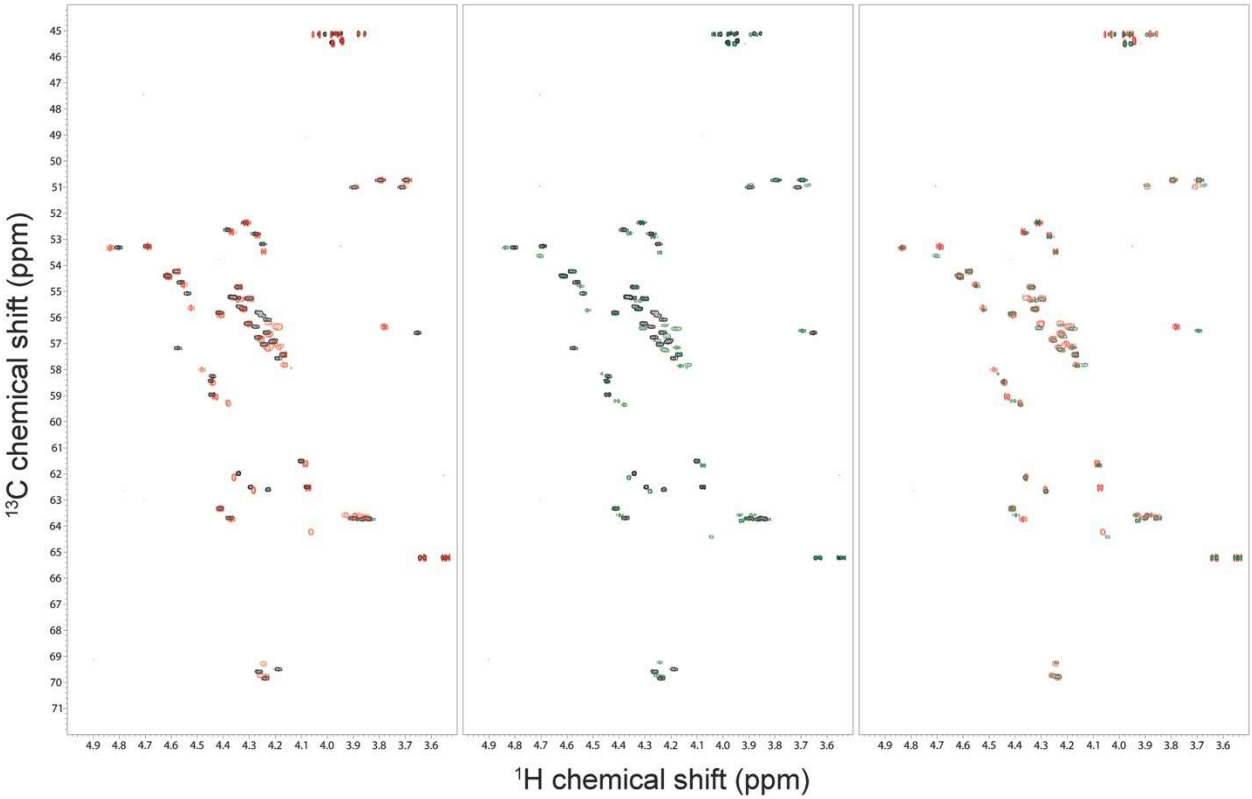

Figure S6. A comparison of ^{13}C-HSQC spectra in D_2O. (a) ^{13}C-HSQC spectra acquired in D_2O for wild type (WT) AD1-ACTR (in black) and two [1055meLeu] (in red) and [1055meLeu;1076meLeu] (in green) variants. (b) Pairwise superposition of the spectral regions corresponding to Cα-Hα correlations with the same color-coding as in (a).

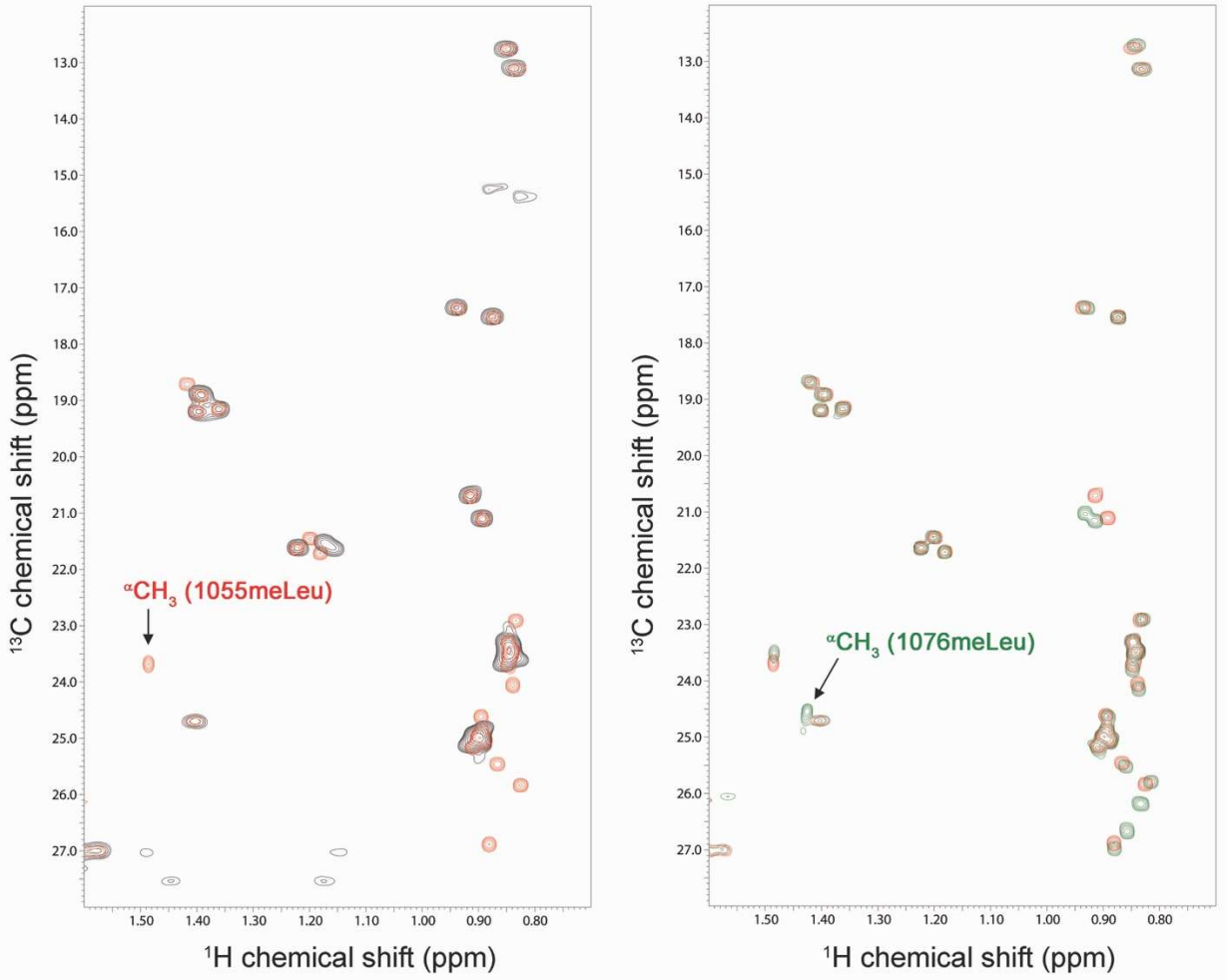

Figure S7. A comparison of ^{13}C-HSQC spectra in D_2O. The excerpts of the ^{13}C-HSQC spectra of WT AD1-ACTR (in black), [1055meLeu] variant (in red) and [1055meLeu;1076meLeu] variant (in green) recorded in D_2O. The spectra are overlaid in a pairwise manner to illustrate the additional peaks for α-methyl groups of residues 1055meLeu and 1076meLeu in the corresponding proteins.

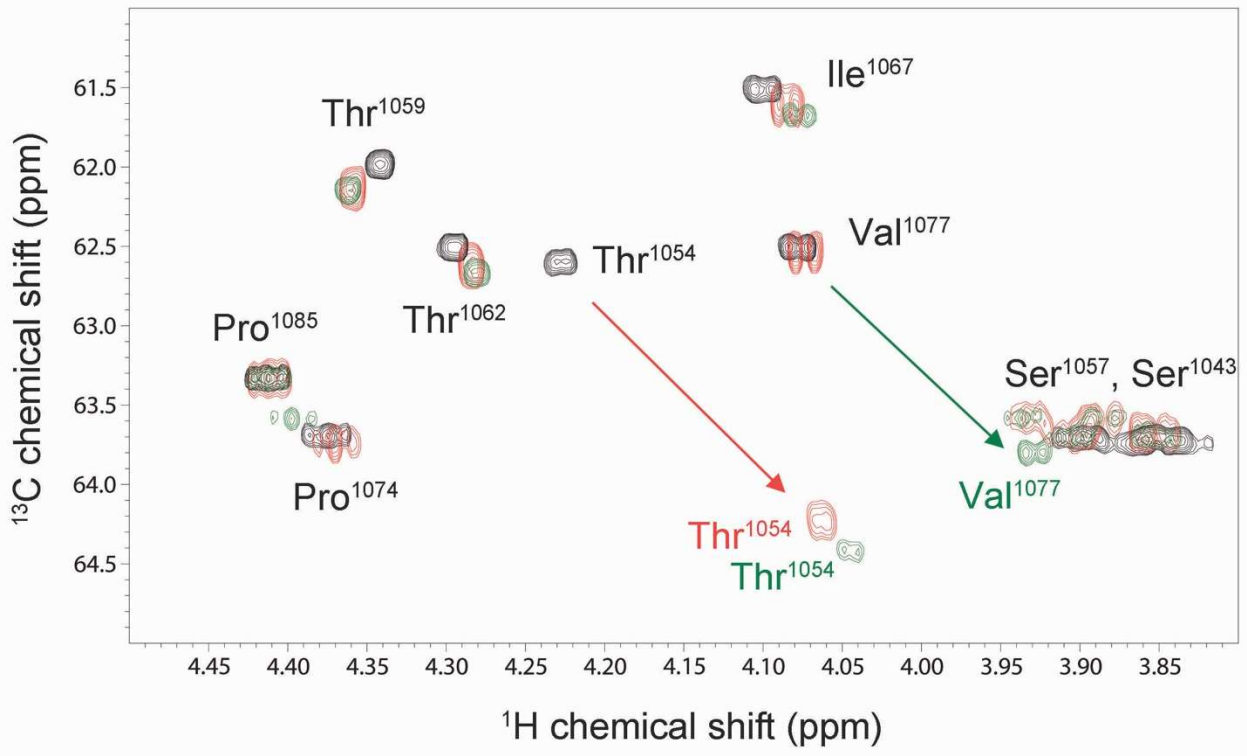

Figure S8. Superposition of the region of ^{13}C-HSQC spectra of WT AD1-ACTR (in black), [1055meLeu] variant (in red) and [1055meLeu;1076meLeu] variant (in green) recorded in D_2O shown to illustrate the changes of chemical shifts for CHα groups for residues Thr1054 and Val1077, which are in close proximity to helix-stabilizing 1055meLeu and 1076meLeu, respectively.

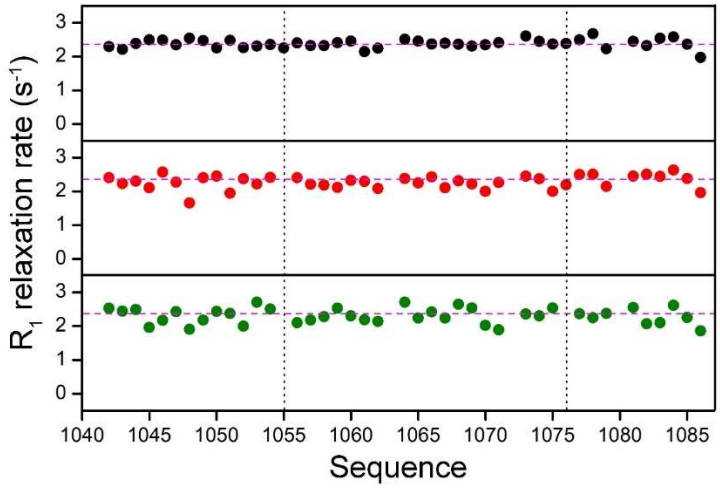

Figure S9. Spin-lattice relaxation rates (R_1) are not perturbed significantly in two studied α-methylated [1055meLeu] (in red) and [1055meLeu;1076meLeu] (in green) variants of AD1-ACTR in comparison to wild type (in black). The vertical dashed lines in black indicate positions for α-methylation (1055 and 1076). The horizontal dashed lines (in magenta) in all three panels indicate the average R_1 value for WT AD1-ACTR. The R_1 values and the experimental uncertainties are listed in Table S10.

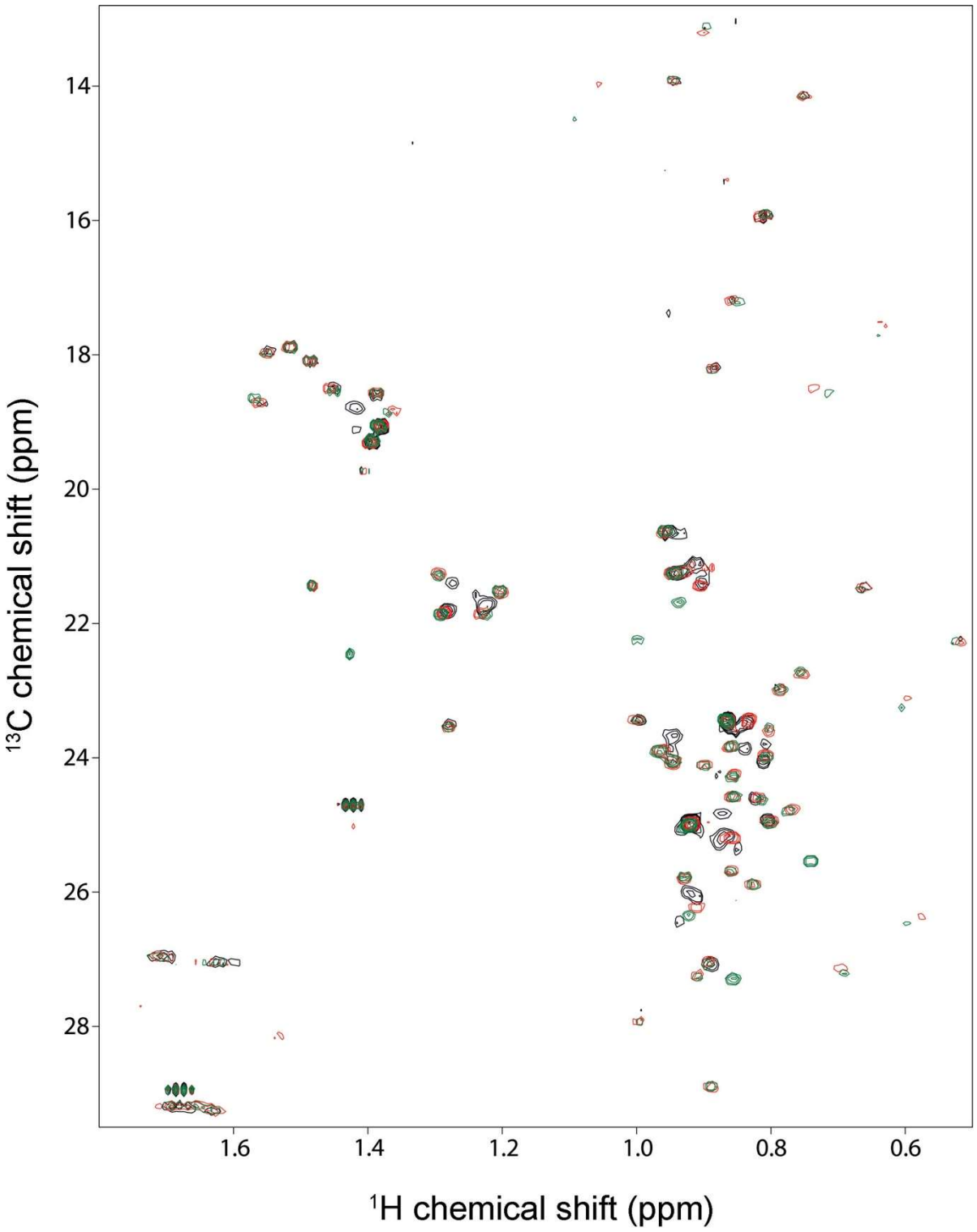

Figure S10. A comparison of methyl regions in the ^{13}C-HSQC spectra of complexes with NCBD. WT AD1-ACTR is depicted in black and two analogues [1055meLeu] and [1055meLeu;1076meLeu] are in red and green, respectively.

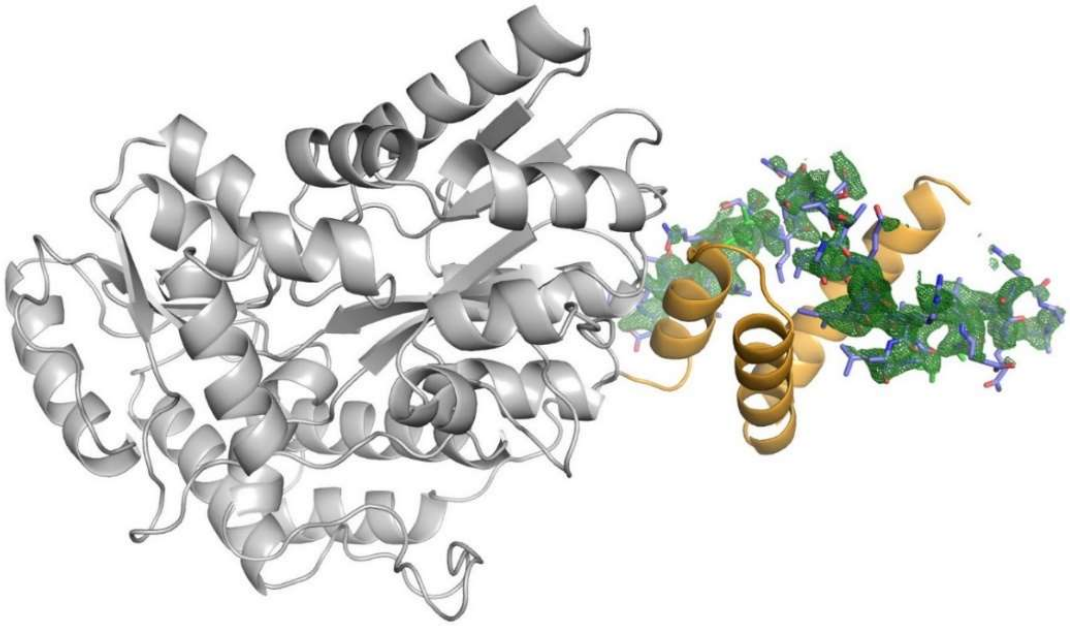

Figure S11. Fo-Fc simulated annealing omit map (contoured at 2σ) calculated for ACTR activation domain.

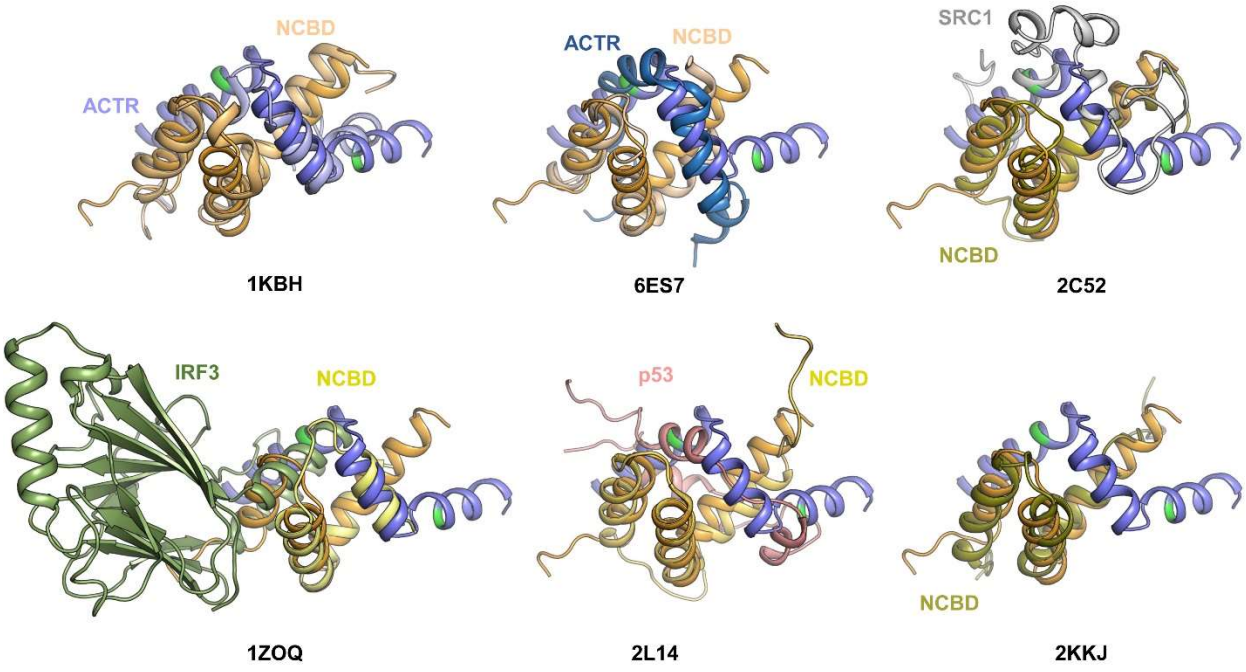

Figure S12. Comparison with the previously reported structures. The X-ray structure of α-methylated [1055meLeu;1076meLeu]AD1-ACTR variant complexed with NCBD of CBP shows similar arrangement of six α-helices with previously solved NMR structure (1KBH) and significant deviations from the other reported structure (6ES7). For comparison, other known structures containing NCBD are superimposed onto new X-ray structure. These include SRC1 isoform of p160 (2C52), complex with IRF3 (1ZOQ), transactivation domain (TAD) of p53 (2L14), and free NCBD (2KKJ).

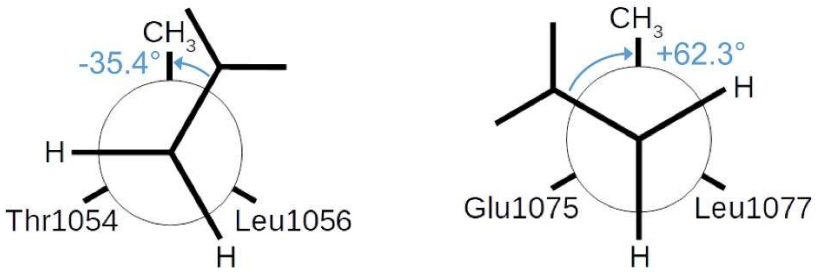

Figure S13. Stereochemical Newman projections for residues 1055meLeu (left) and 1076meLeu (right) in the X-ray structure of [1055meLeu;1076meLeu]AD1-ACTR/NCBD complex. Torsional angles Cγ-Cβ-Cα-Cβ(methyl) are depicted.

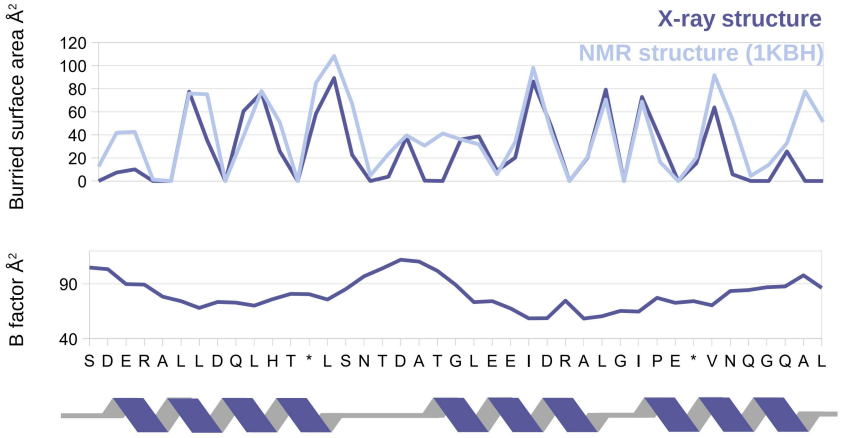

Figure S14. The protein-protein interface is less tight than in the NMR complex (1KBH). The overall buried surface area decreased from 1655 to 1066 Å^2. The trend is similar and the highest difference is between residues 1059-1064 (linker between helix 1 and 2), which shows high flexibility in the crystal and the C-terminal helix which no longer makes close interactions with NCBD. Star (*) indicates α-methyl-Leu residues in the sequence.

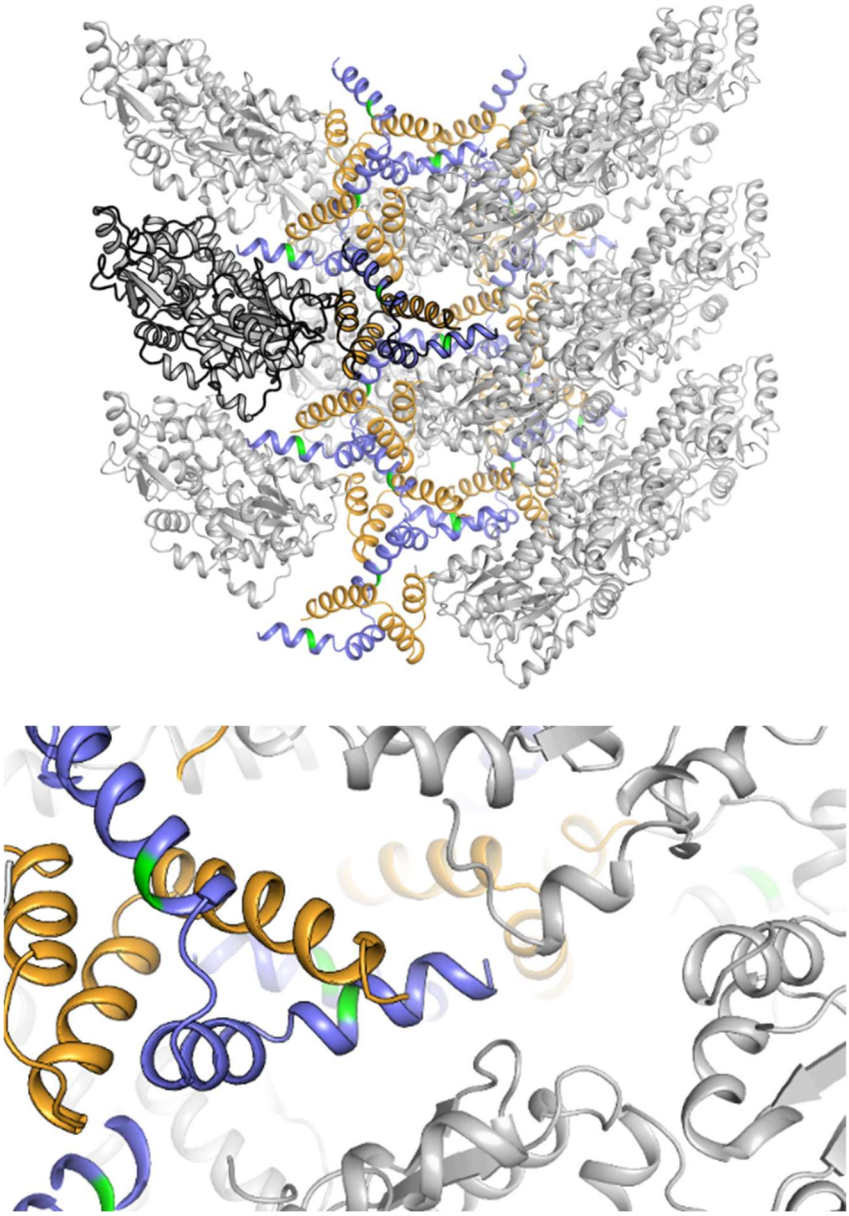

Figure S15. Visualization of molecular interactions in the crystal. Crystal packing does not affect the orientation of α-helices in the [1055meLeu;1076meLeu]AD1-ACTR/NCBD complex.

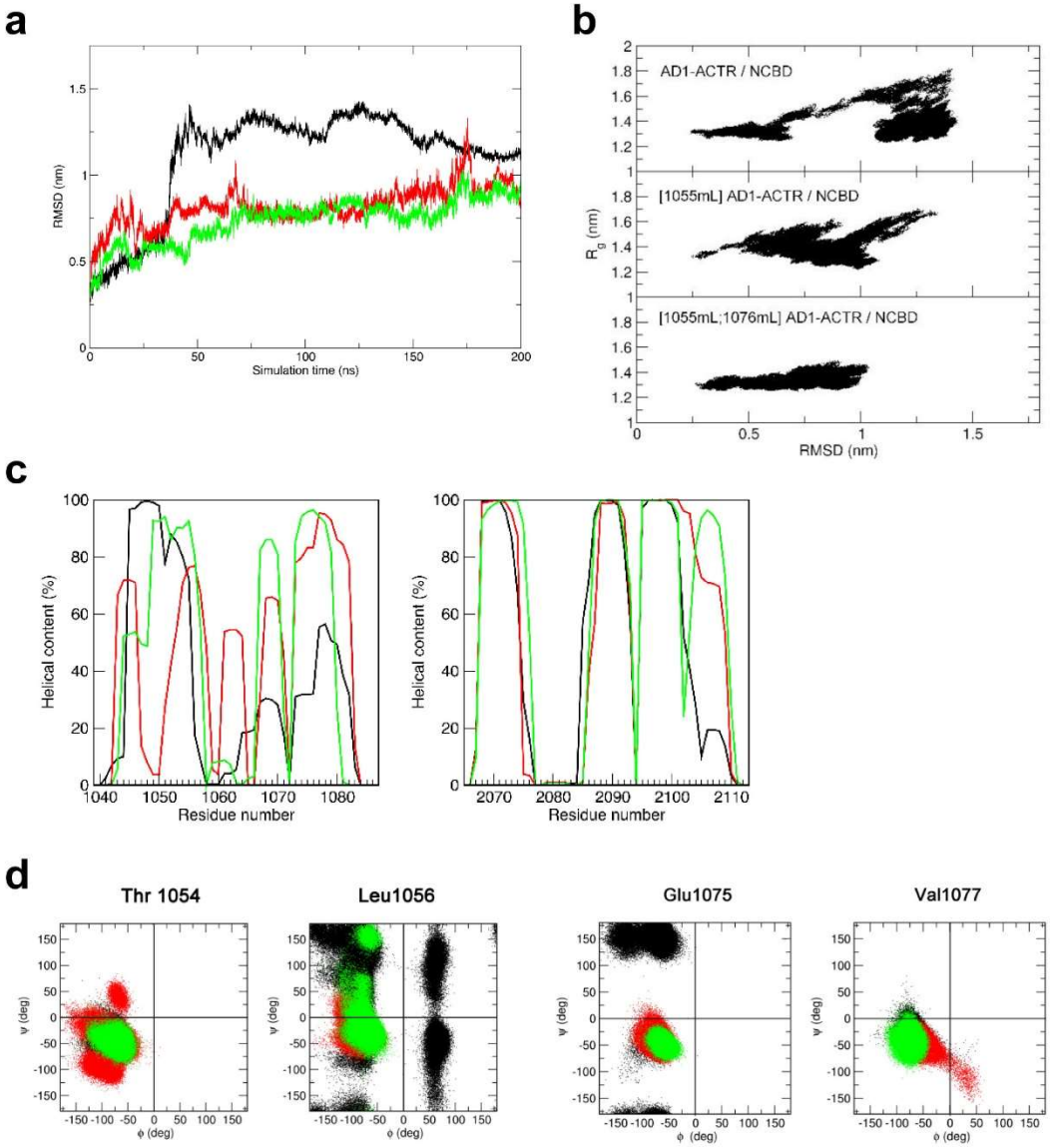

Figure S16. Molecular dynamics (MD) simulations of WT AD1-ACTR/NCBD complex and of the corresponding analogues [1055meLeu] and [1055meLeu;1076meLeu]. (a) Backbone atom-positional root-mean-square deviations (RMSD) of complexes from its initial structure indicate a large structural change around 37 ns. The RMSF analysis, Ramachandran plots, hydrogen bonding and salt-bridge analysis therefore exclude the first 50 ns. Black line: WT complex, red line: [1055meLeu]AD1-ACTR/NCBD complex, green line: [1055meLeu;1076meLeu]AD1-ACTR/NCBD complex. (b) Changes in the radii of gyration of the complexes show that the [1055meLeu;1076meLeu]AD1-ACTR/NCBD complex has the most compact structure. (c) The analysis of helical content per residue shows the overall increase of helicity in the ACTR chain that occurs upon α-methylation of Leu1055 and Leu1076. The pre-organization of ACTR analogues into segments with helical conformations was also observed in CD and NMR experiments on free AD1-ACTR proteins. The secondary structural analysis was performed using the DSSP program as implemented in GROMOS. The helical content per residue was calculated as the sum of the occurrences for 3_{10}-helix, α-helix and π-helix. For this analysis the entire trajectory was used. (d) The conformational distribution of the neighboring residues Thr1054, Leu1056, Glu1075 and Val1077 also gets reduced upon α-methylation of Leu1055 and Leu1076. First 50 ns were omitted from the latter analysis.

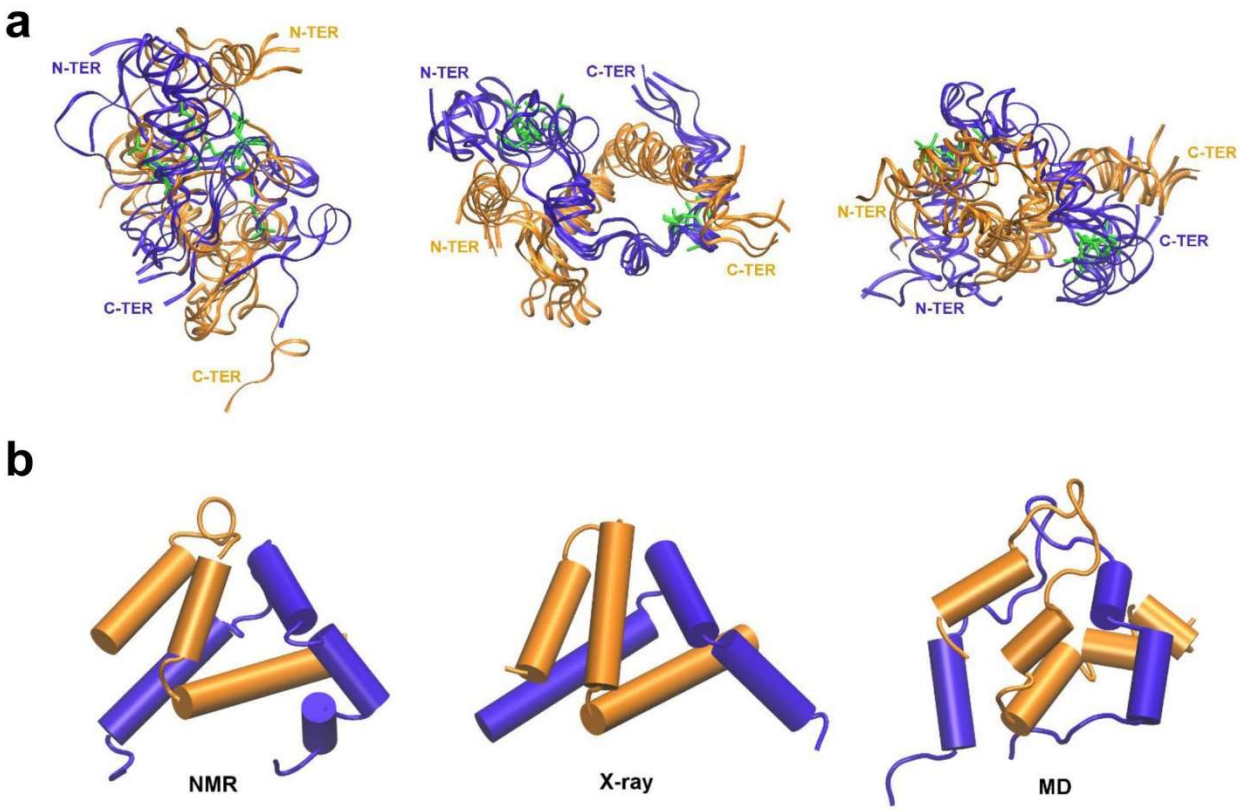

Figure S17. (a) Overlay of five representative conformations (first five central member structures from the conformational clustering) for MD simulation of wild-type AD1-ACTR/NCBD (left), [1055meLeu]AD1-ACTR/NCBD (center) and [1055meLeu;1076meLeu]AD1-ACTR/NCBD (right) complexes. In all plots, chain corresponding to ACTR is colored in purple and for NCBD in orange, while residues 1055 and 1076 are highlighted in green. Evident are the structural differences between the complexes and structural variations within each ensemble. Those are the largest for wild type complex and smallest for [1055meLeu]AD1-ACTR/NCBD complex. (b) Comparison of orientation of helices in the structure of wild-type complex determined by NMR (PDB ID: 1KBH), of the [1055meLeu;1076meLeu]AD1-ACTR/NCBD complex determined by X-ray crystallography in this study (PDB ID: 6SQC) and of the first central member structure from the conformational clustering of the corresponding MD simulation.

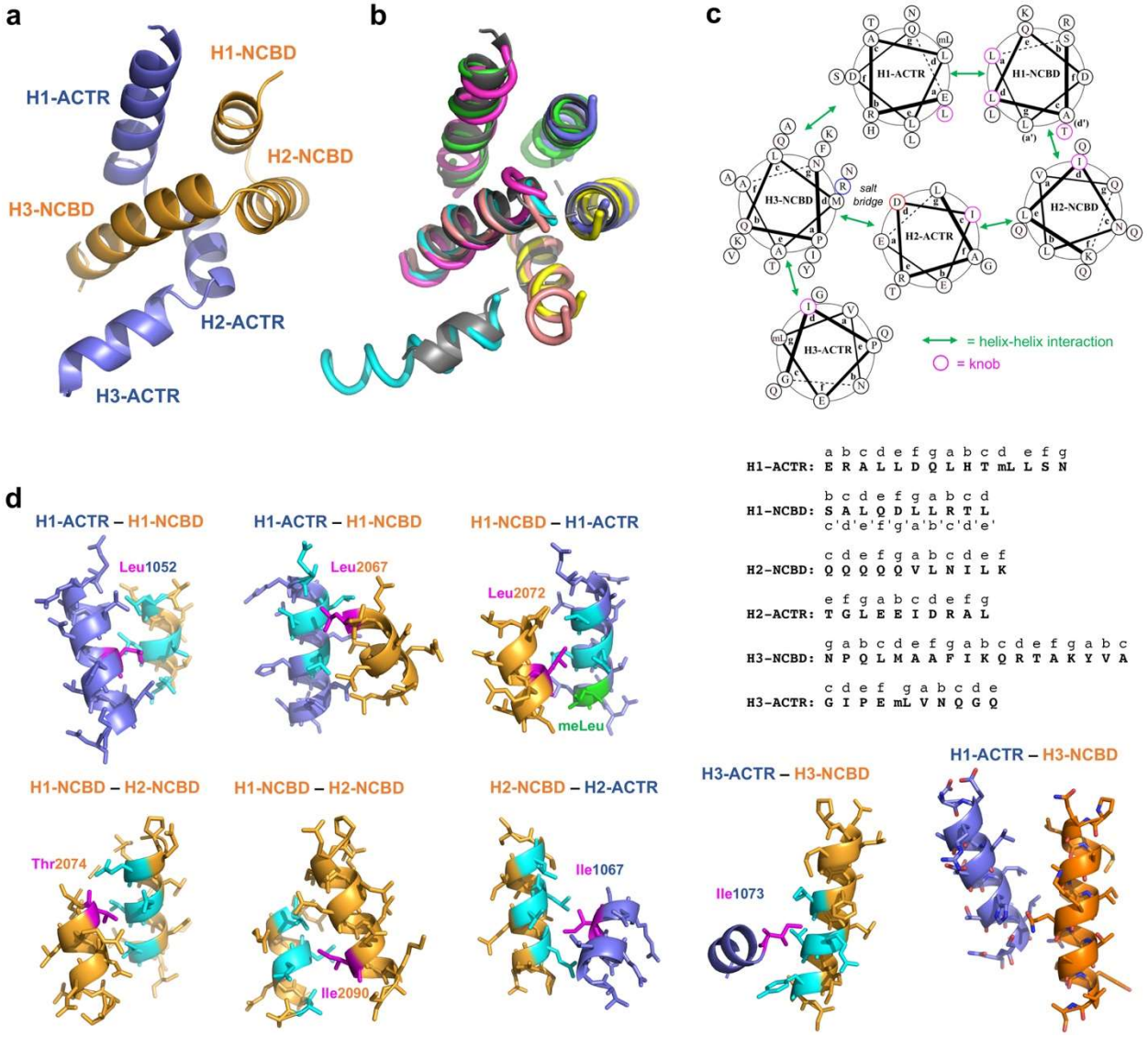

Figure S18. Structural details of the complex of [1055meLeu;1076meLeu]AD1-ACTR/NCBD in the crystal structure 6SQC. (a) Six α-helices form an irregular helix bundle lacking symmetry between helices. (b) The helix-helix interactions can be analyzed pairwise using generalized Crick parameters with the help of CCCP software (https://grigoryanlab.org/cccp/). The pairs of helices represented as tubes in different colors illustrate Cα fits of parametrized helices to the helical segments in the experimental structure (parameters for each fitted pair are in Table S15). (c) Helical diagrams illustrating interactions between helices. Knob-into-hole interactions were identified using SOCKET software (http://coiledcoils.chm.bris.ac.uk/socket/), the knob residues are represented as circles in magenta. The residues Arg2105 and Asp1068 forming the salt-bridge anchoring helix H2-ACTR and H3-NCBD are shown as blue and red circles, respectively. Below are the sequences corresponding to each helix and the heptad registers for the positions in the helix-helix dimers assigned by CCCP. Two alternative registers are provided for H1-NCBD for the coiled coil packing against H1-ACTR (upper register) and H2-NCBD (lower register) signifying multi-faceted helix interactions (36) that can be enabled by LXXLLXXL sequence pattern. Note that the heptad register is applicable for the description of contacts between helices with left-handed crossings and not right-handed (2). (d) The knob-into-hole contacts between different helix pairs are shown as well as poor packing at the H1-ACTR–H3-NCBD interface. Knobs are in magenta and sides of holes are in cyan. The residue IDs are shown for knobs.

Figure S19 (consists of 5 panels on pp. 56-60). Surface plasmon resonance binding data for WT AD1-ACTR, [1055meLeu]AD1-ACTR, [1076meLeu]AD1-ACTR and [1055meLeu;1076meLeu] AD1-ACTR at 20 °C (293 K) (curves in black correspond to fitting to 1:1 association model).

Panel 1:

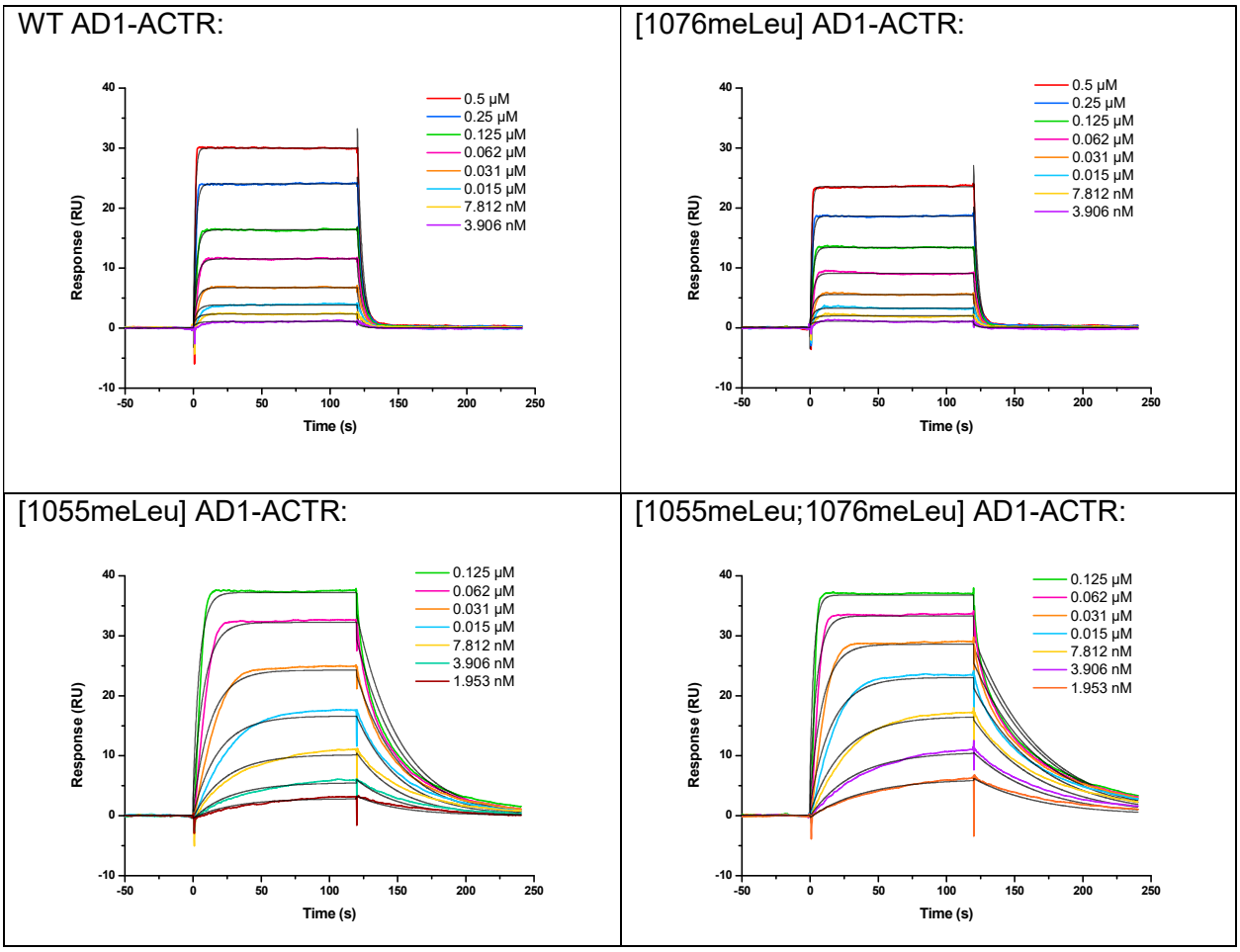

Figure S19 (continued from p. 56). Surface plasmon resonance binding data for WT AD1-ACTR, [1055meLeu]AD1-ACTR, [1076meLeu]AD1-ACTR and [1055meLeu;1076meLeu]AD1-ACTR at 22 °C (295 K) (curves in black correspond to fitting to 1:1 association model).

Panel 2:

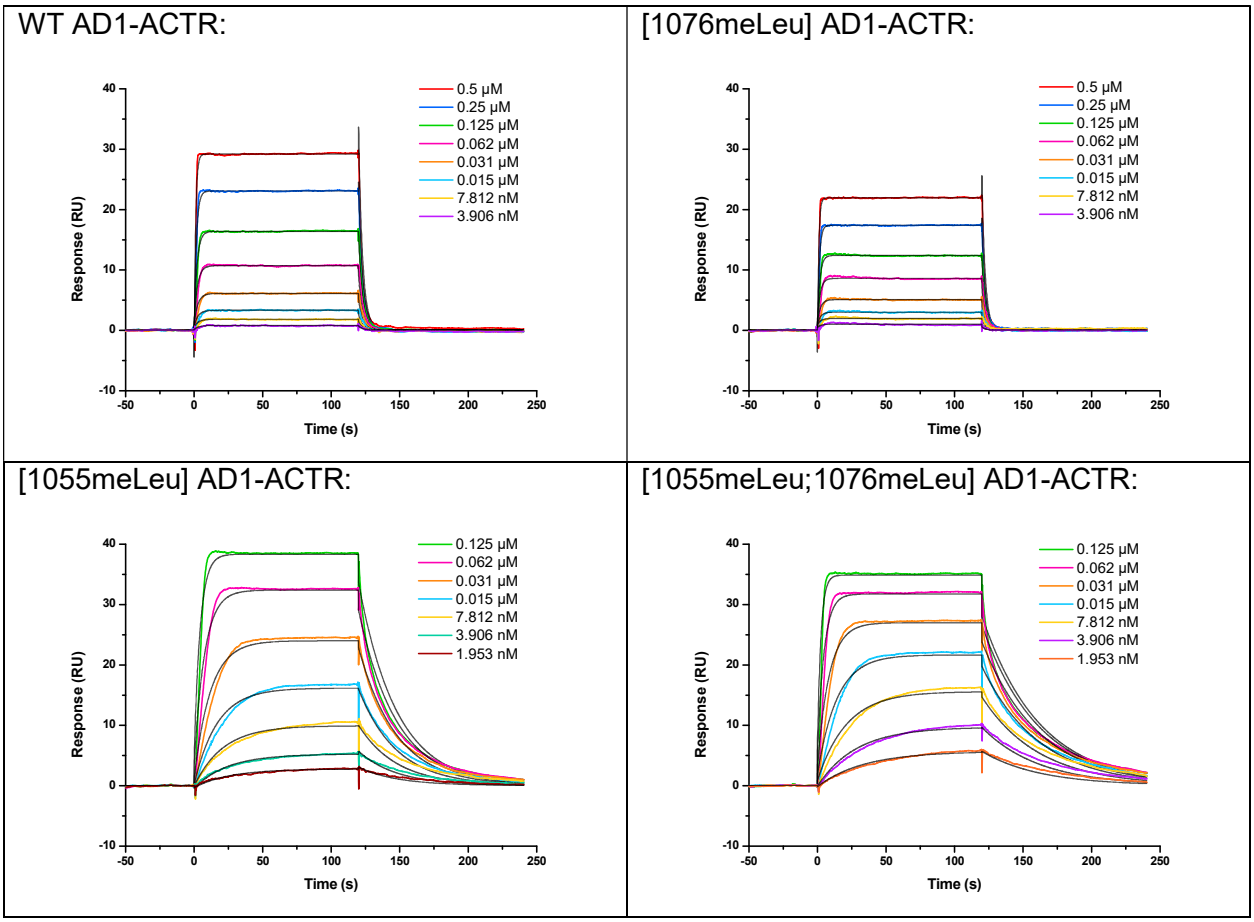

Figure S19 (continued from p. 57). Surface plasmon resonance binding data for WT AD1-ACTR, [1055meLeu]AD1-ACTR, [1076meLeu]AD1-ACTR and [1055meLeu;1076meLeu]AD1-ACTR at 25 °C (298 K) (curves in black correspond to fitting to 1:1 association model).

Panel 3:

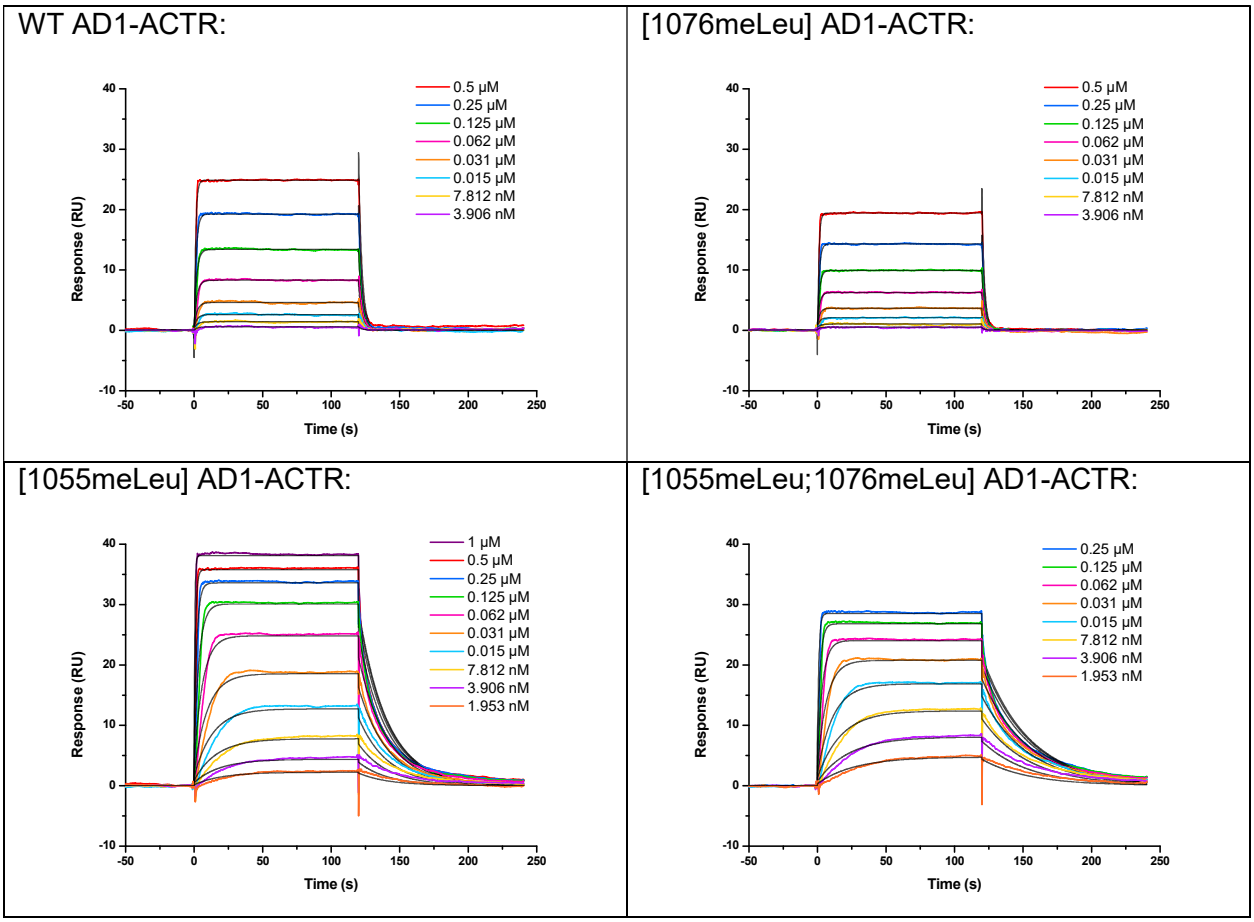

Figure S19 (continued from p. 58). Surface plasmon resonance binding data for WT AD1-ACTR, [1055meLeu]AD1-ACTR, [1076meLeu]AD1-ACTR and [1055meLeu;1076meLeu]AD1-ACTR at 27 °C (300 K) (curves in black correspond to fitting to 1:1 association model).

Panel 4:

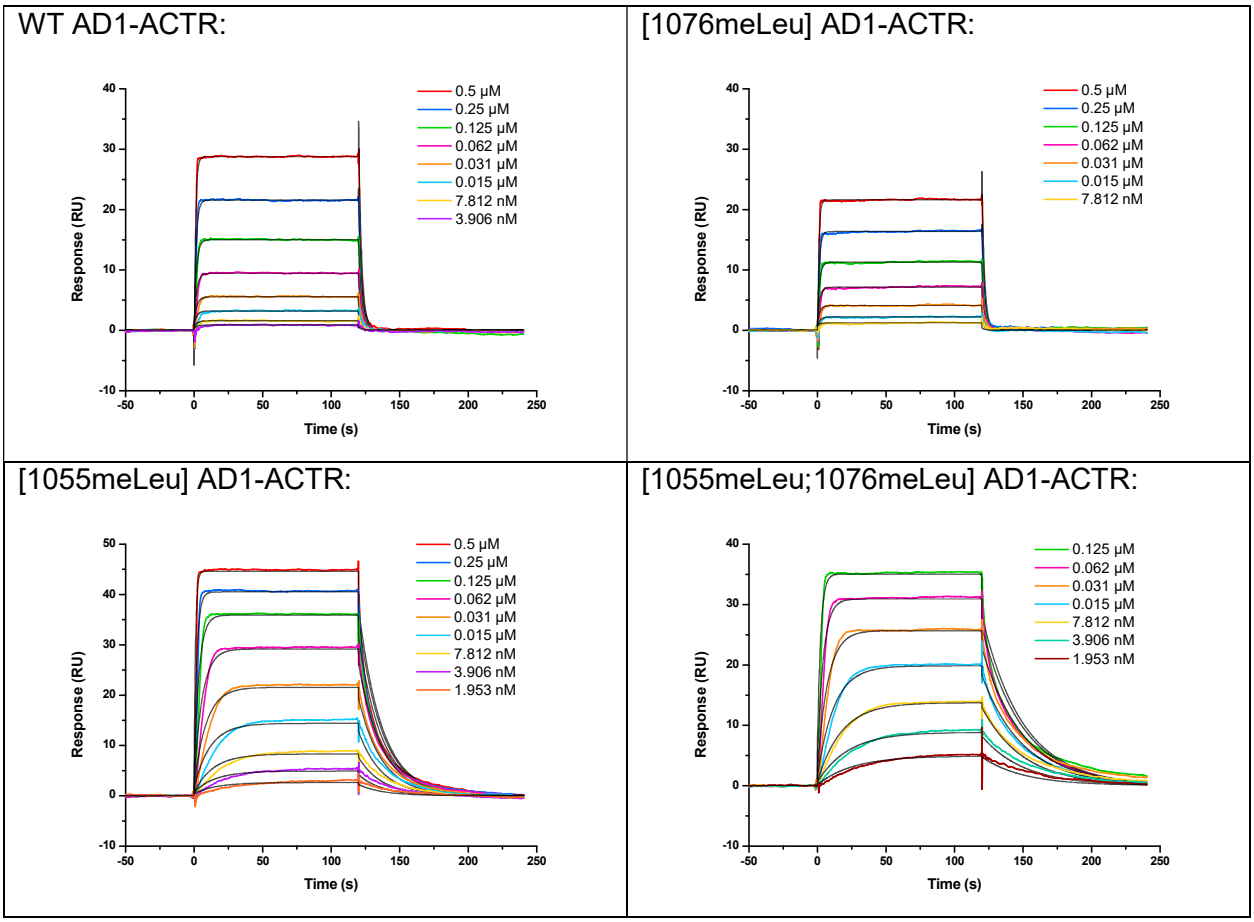

Figure S19 (continued from p. 59). Surface plasmon resonance curves for WT AD1-ACTR, [1055meLeu] AD1-ACTR, [1076meLeu] AD1-ACTR and [1055meLeu;1076meLeu] AD1-ACTR at 31 °C (304 K) (curves in black correspond to fitting to 1:1 association model).

Panel 5:

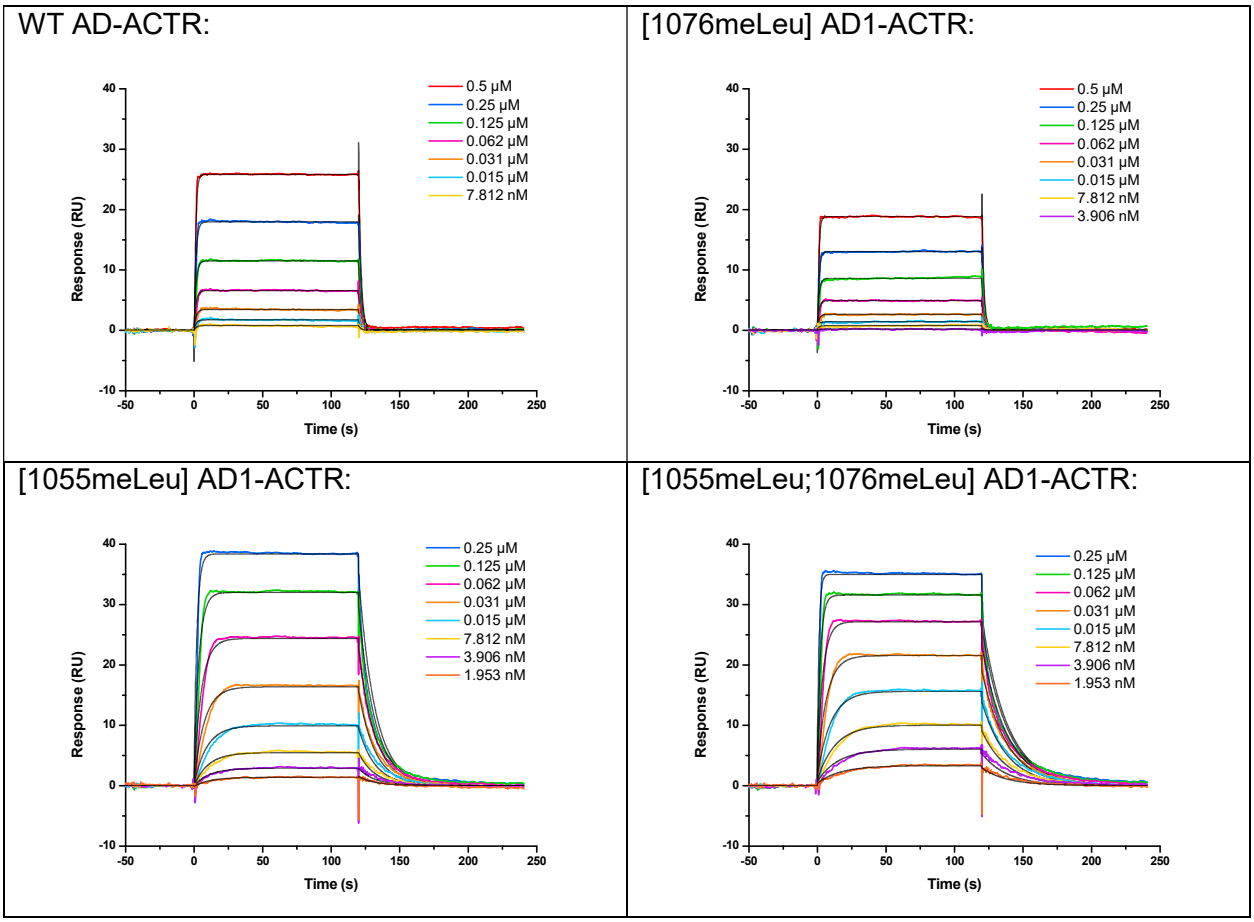

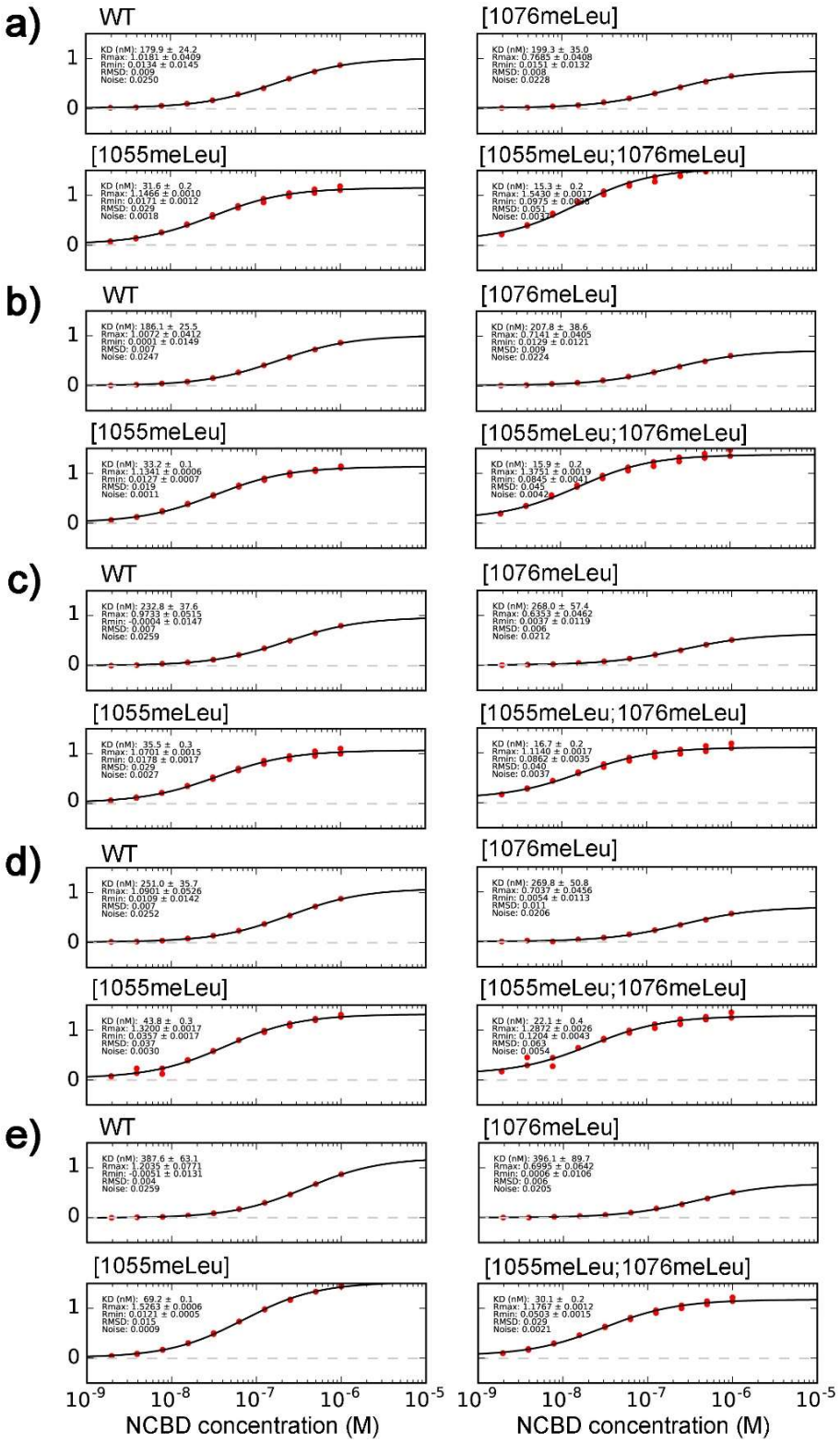

Figure S20. Steady-state analysis of the NCBD binding to four variants of AD1-ACTR (WT, [1076meLeu], [1055meLeu], [1055meLeu;1076meLeu]) at five different temperatures (a) 20 °C, (b) 22 °C, (c) 25 °C, (d) 27 °C and (e) 31 °C. Normalized equilibrium responses (R_{eq}) plotted as a function of NCBD concentration and fitted with a 1:1 binding model (see Table S17 for fitted values).

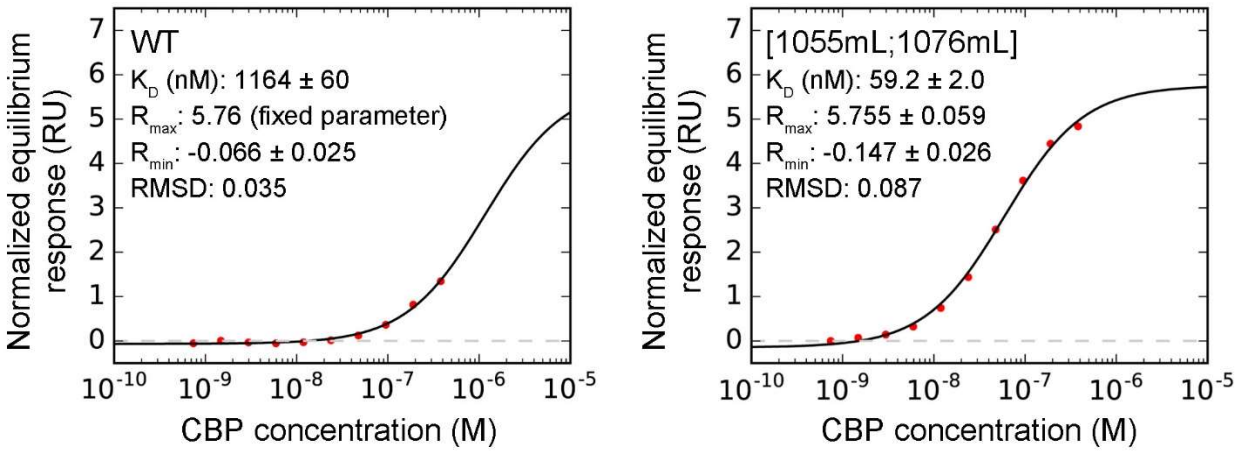

Figure S21. Steady-state analysis of the CBP binding to WT AD1-ACTR and [1055meLeu;1076meLeu] variant at 10 °C. Normalized equilibrium responses (R_{eq}) are plotted as a function of CBP concentration and fitted using a 1:1 binding model (WT: K_D = 1164 ± 60 nM; [1055meLeu;1076meLeu] AD1-ACTR: K_D = 59.2 ± 2.0 nM).

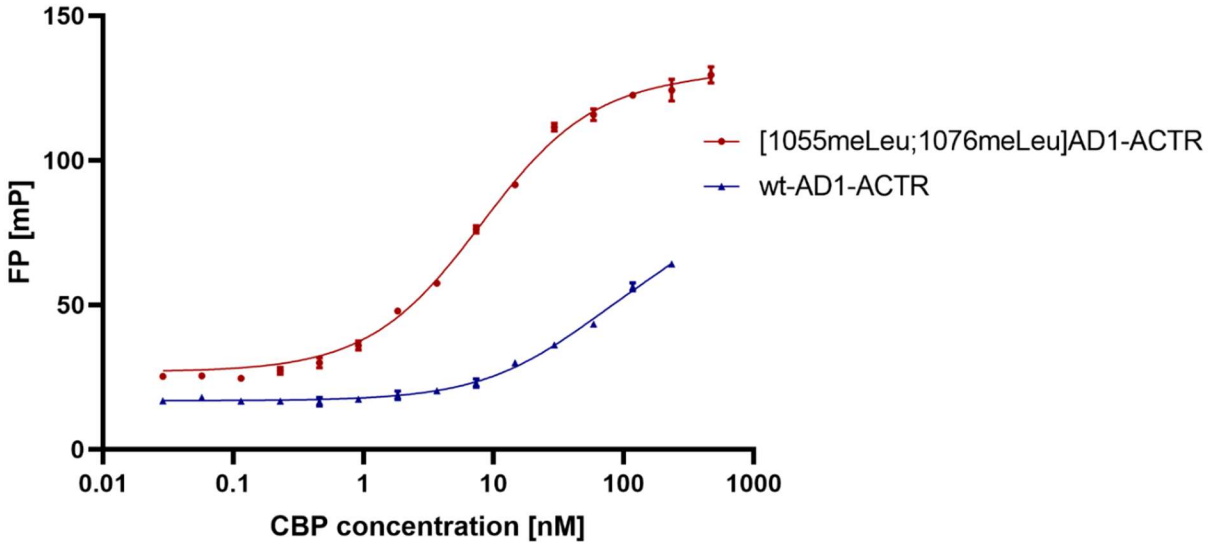

Figure S22. Fluorescent polarization measurements of [1055meLeu;1076meLeu]AD1-ACTR resulted in K_D = 8.1 ± 2.5 nM, whereas for the WT AD1-ACTR K_D could not be calculated accurately because of not reaching the saturation but the affinity is definitively significantly lower. The difference in K_D in the fluorescence polarization and SPR measurements may be explained by distinct conditions (FP: T = 25 °C, buffer: 25 mM Hepes pH 7.5, 150 mM NaCl, 1 mM TCEP, 0.05% Tween-20, protease inhibitors versus SPR: T = 10 °C, buffer: 50 mM Tris pH 7.5, 300 mM NaCl, 1 mM TCEP, 0.01% P20, protease inhibitors). In SPR experiments, higher salt concentration was used to minimize nonspecific binding to the chip surface.

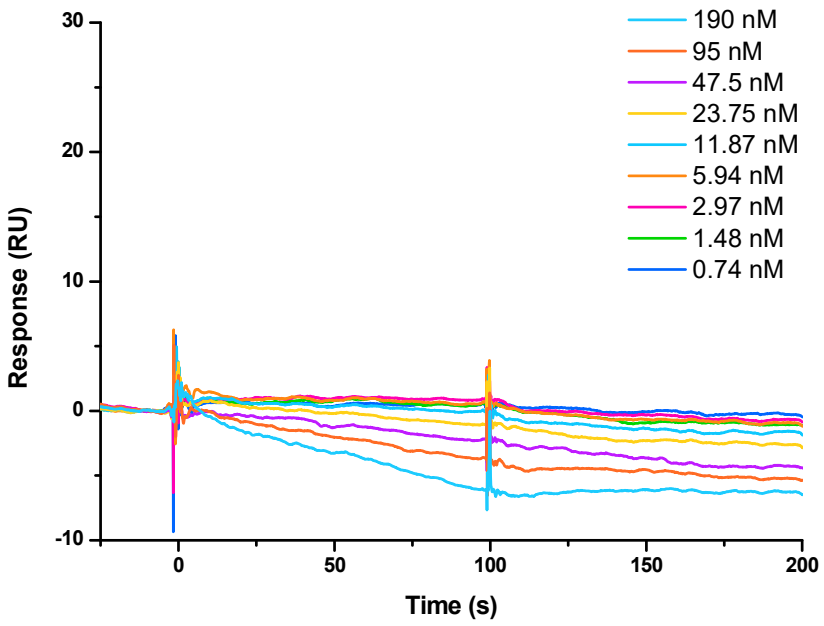

Figure S23. SPR sensogram of binding of 265 kDa CBP to [1064meLeu;1071meLeu]AD1-ACTR indicating no appreciable binding. Negative signal after reference and buffer subtraction is due to non-specific binding of CBP at higher concentrations.

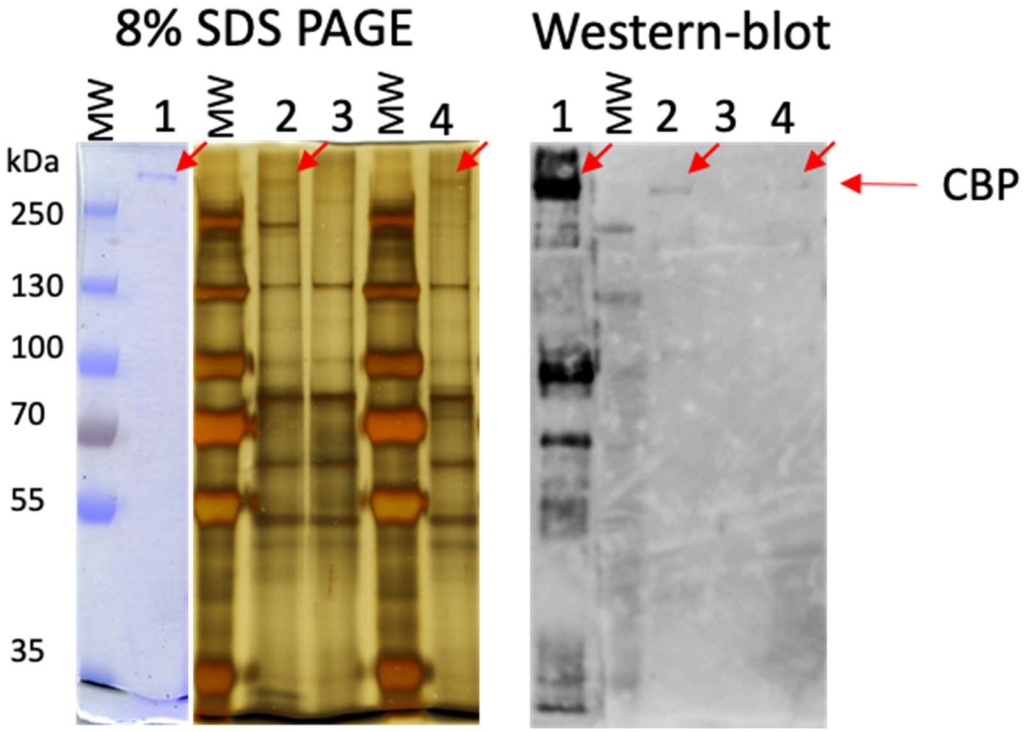

Figure S24. The MCF7 cell extract was treated with the biotin conjugated [1055meLeu;1076meLeu]AD1-ACTR or wild type peptide as a bait, then Strep-Tactin resin was used to pull down the proteins interacting with it. The SDS-PAGE and the Western-blot showing the full-length CBP confirming its interaction with the α-methylated peptide (lane 2) and the wild type peptide (lane 4) but absent in the control (lane 3, no peptide treatment). The purified CBP used as a control (lane 1). The results of the pull-down were analyzed by label free quantitative MS analysis (with the help of a Thermo Scientific Orbitrap Elite mass-spectrometer). The preliminary data showed the increased enrichment of CBP by > 2 fold for [1055meLeu;1076meLeu]AD1-ACTR variant versus wild type sample with the statistical significance (based on 3 technical replicates).

Figure S25. Analytical reverse phase HPLC chromatograms of proteins studied in this work (UV adsorption monitored at 220 nm). The conditions of analysis (HPLC column, gradient) varied for different groups of samples. This Figure is to show that all protein samples were homogeneous with purity ≥95% based on peak integration. The numbering and designation of proteins is according to Table S1 and Table S2. All samples were additionally analyzed by electrospray ionization mass-spectrometry (ESI-MS) and had correct molecular weights.

#1 wild type (WT) AD1-ACTR

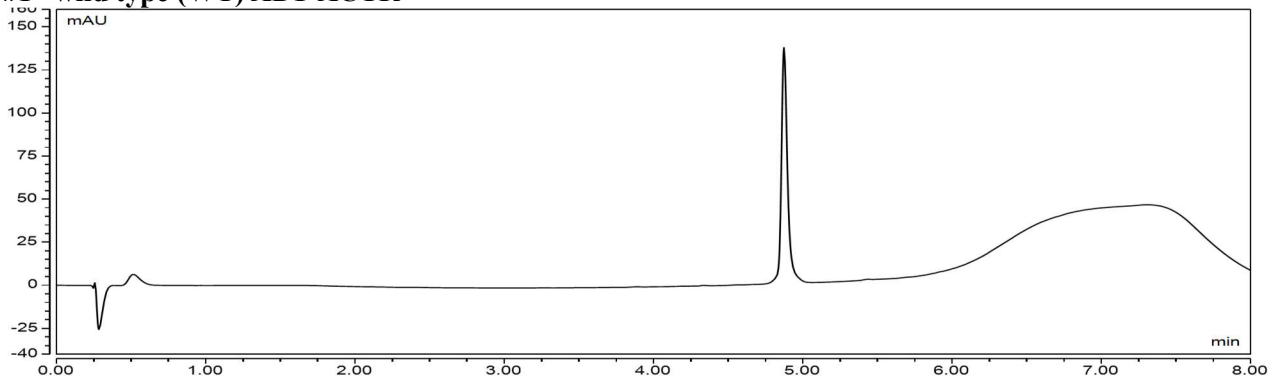

#2 [S1043M;D1050E;T1054Q]

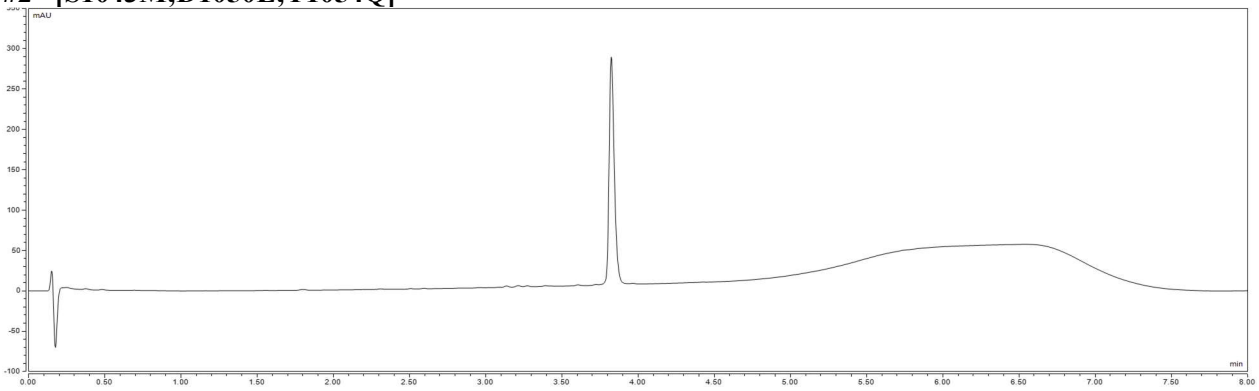

#3 [A1047G]

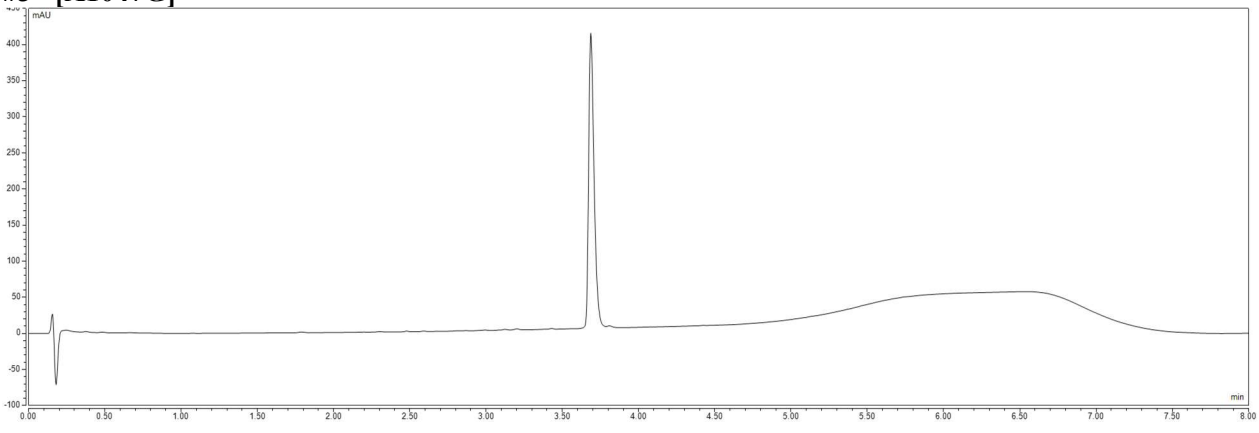

#4 [1047mA]

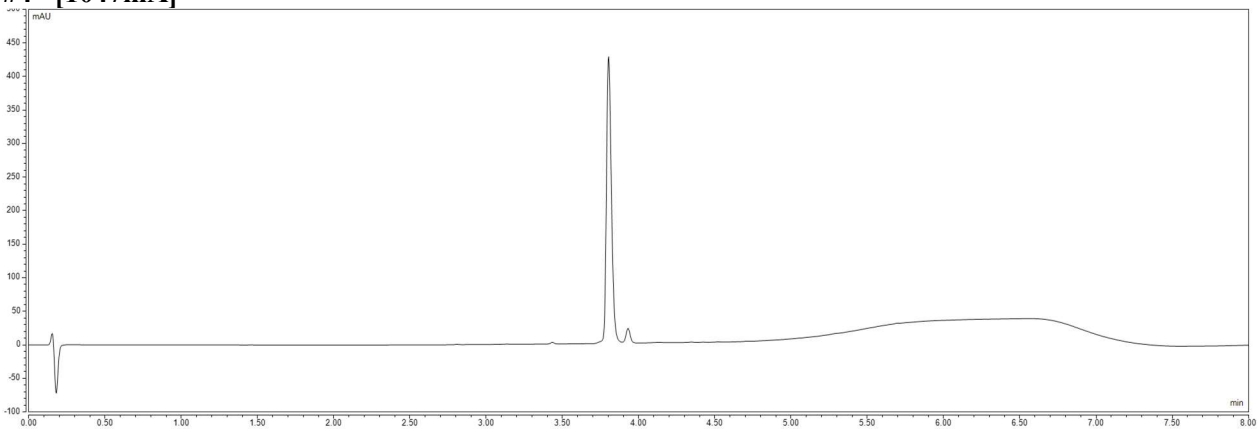

#5 [1048mL]

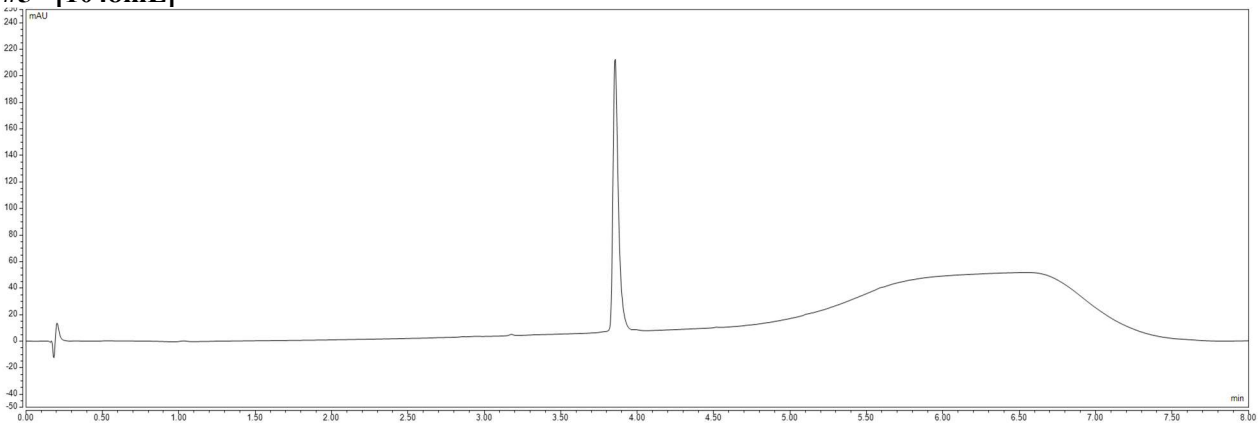

#6 [1049mL]

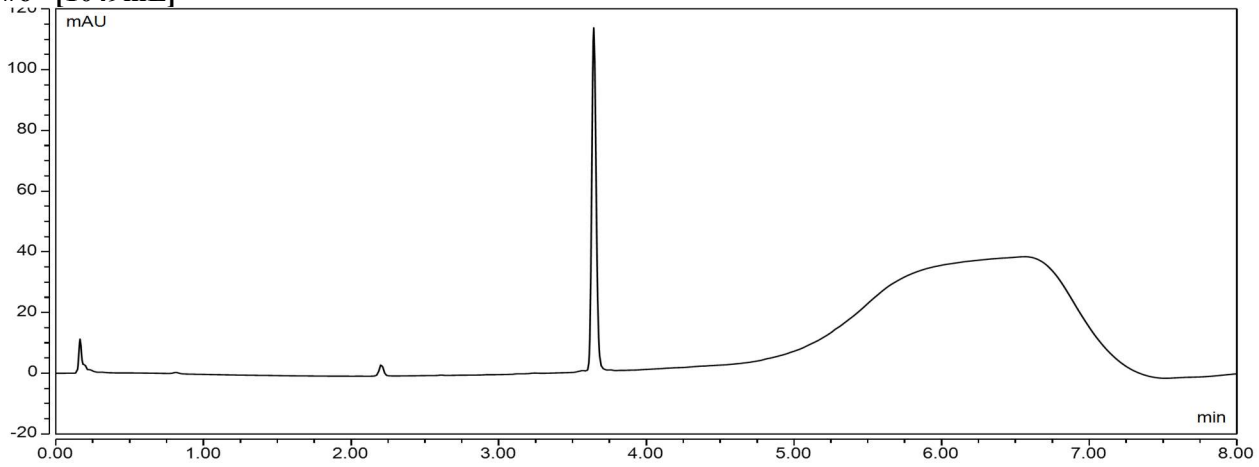

#7 [1050mD]

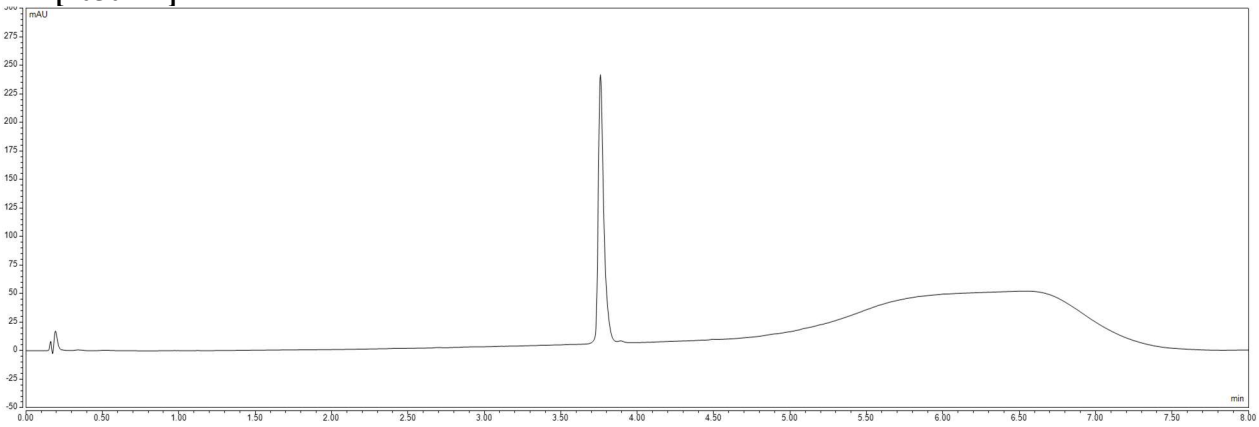

#8 [1052mL]

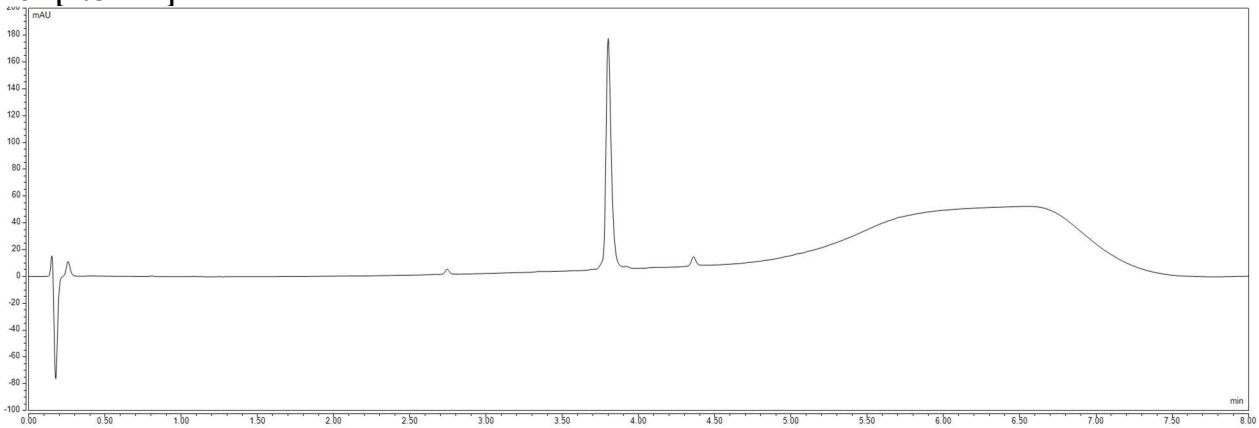

#9 [1055mL]

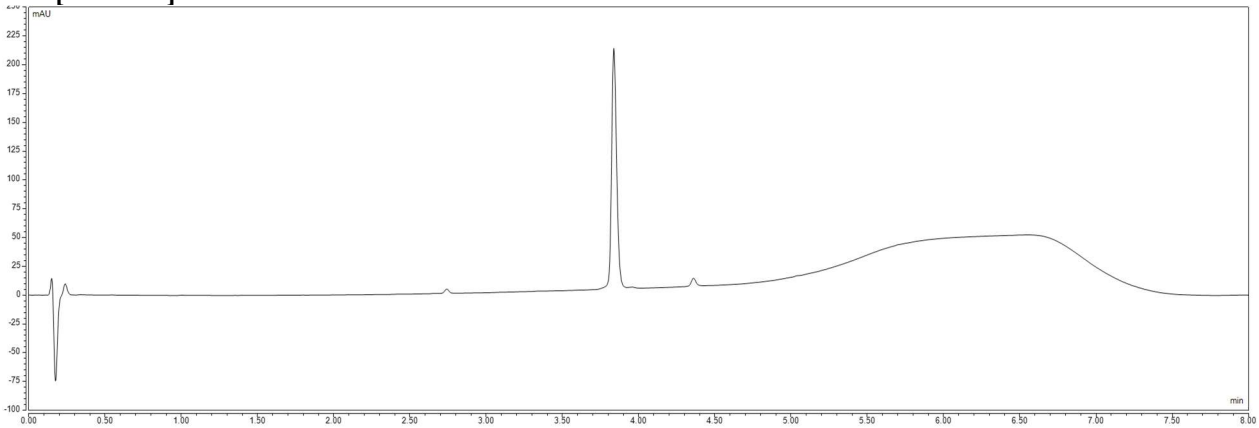

#10 [1056mL]

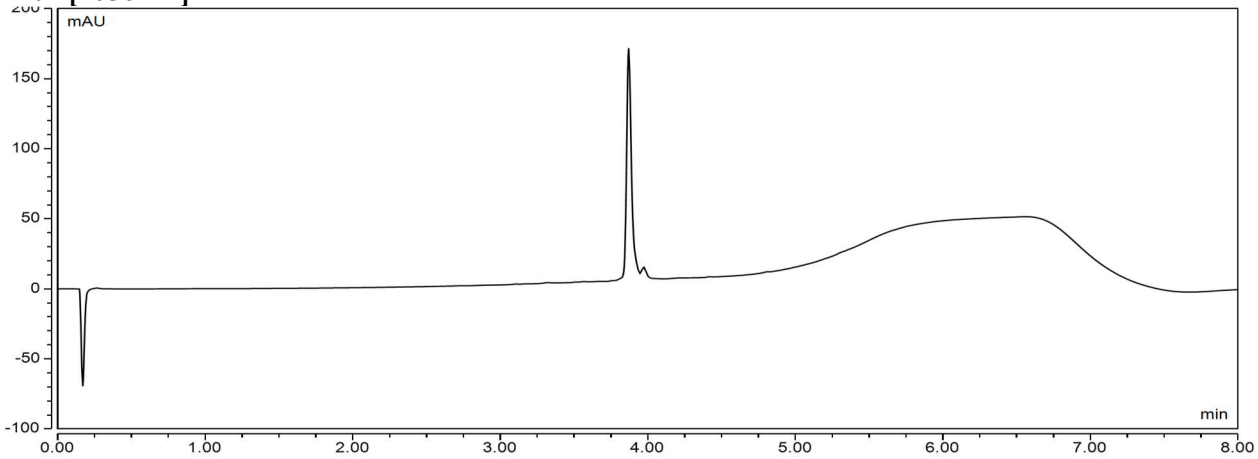

#11 [1061mA]

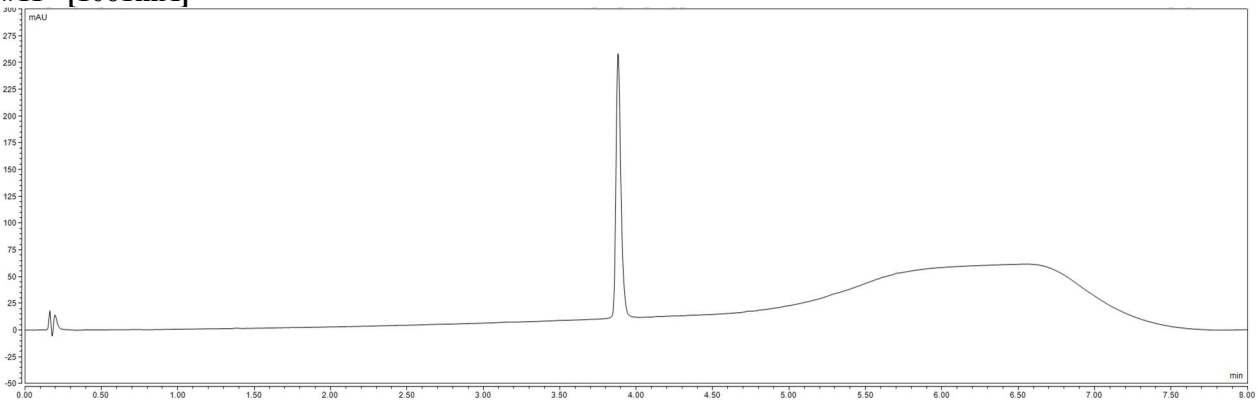

#12 [1064mL]

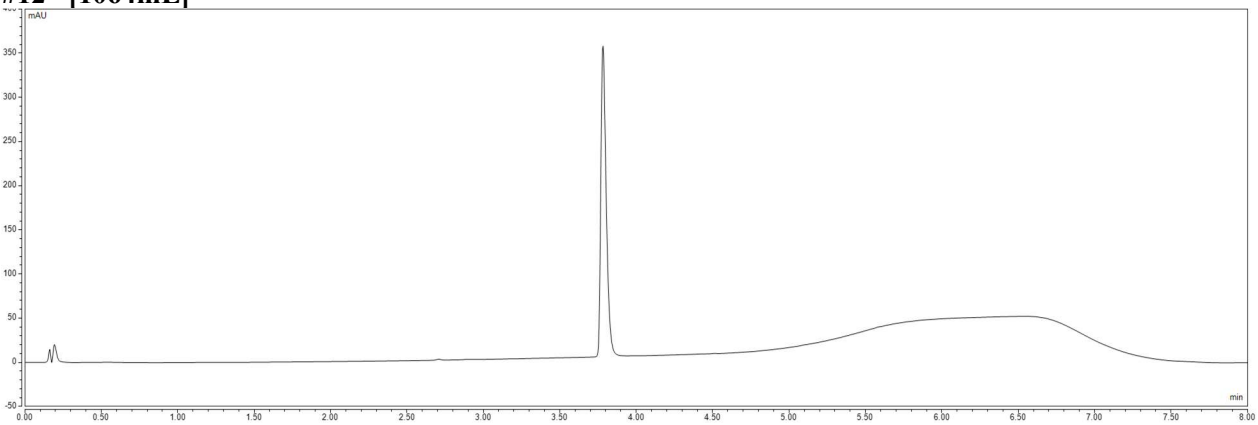

#13 [1071mL]

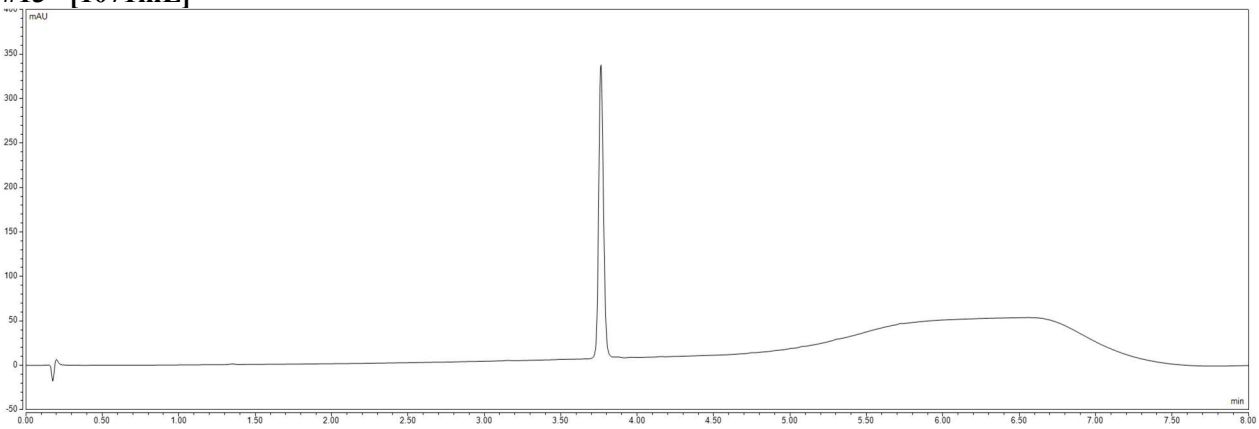

#14 [1072mA]

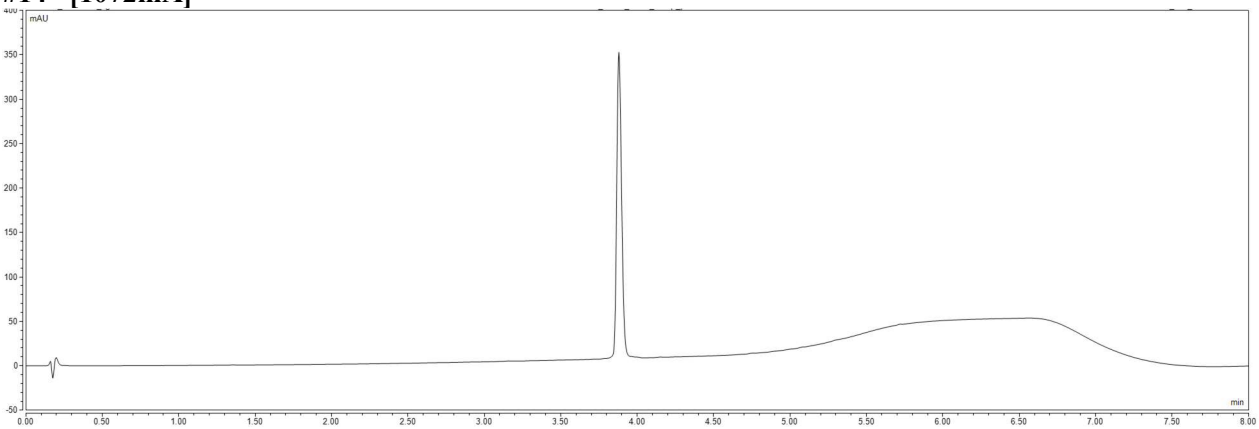

#15 [1076mL]

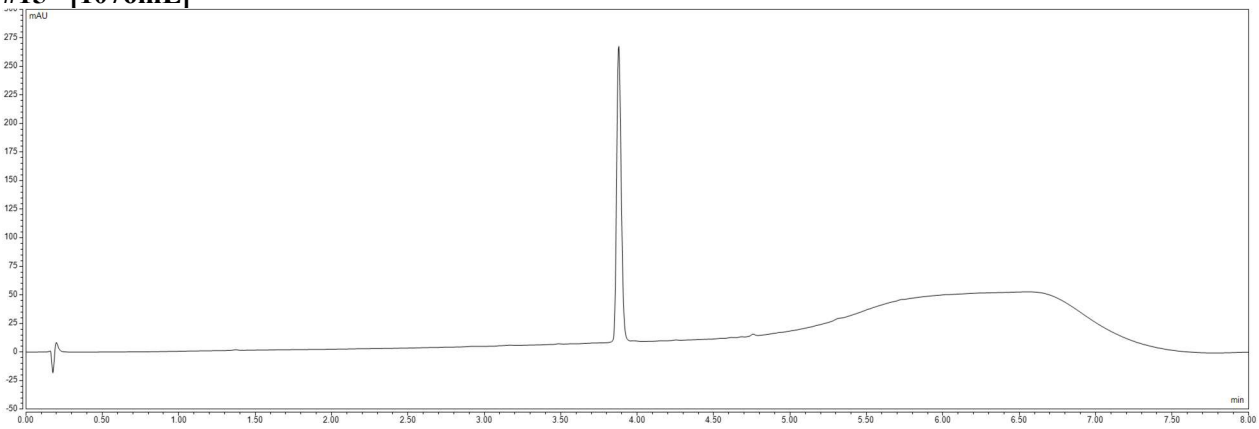

#16 [1077mV]

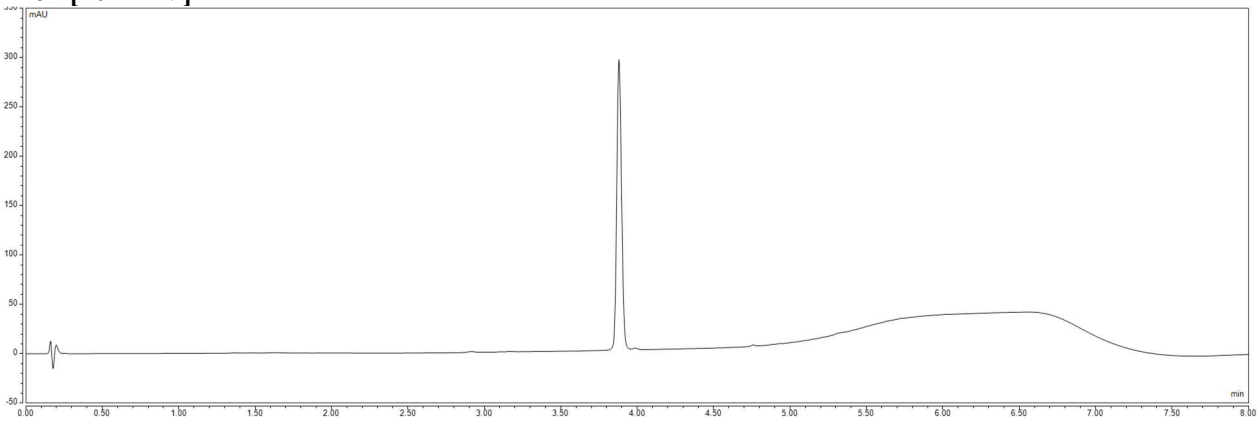

#17 [1080mA]

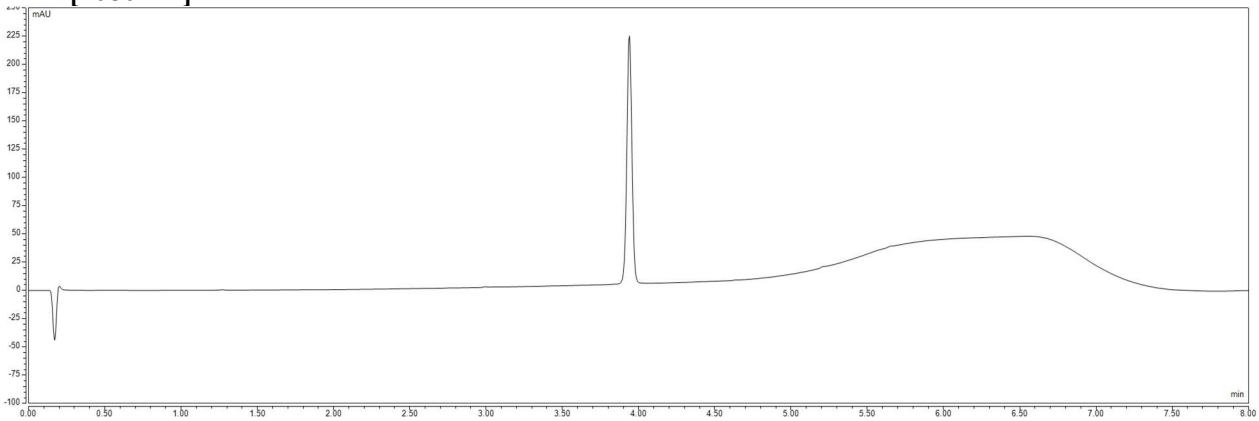

#18 [1082mA]

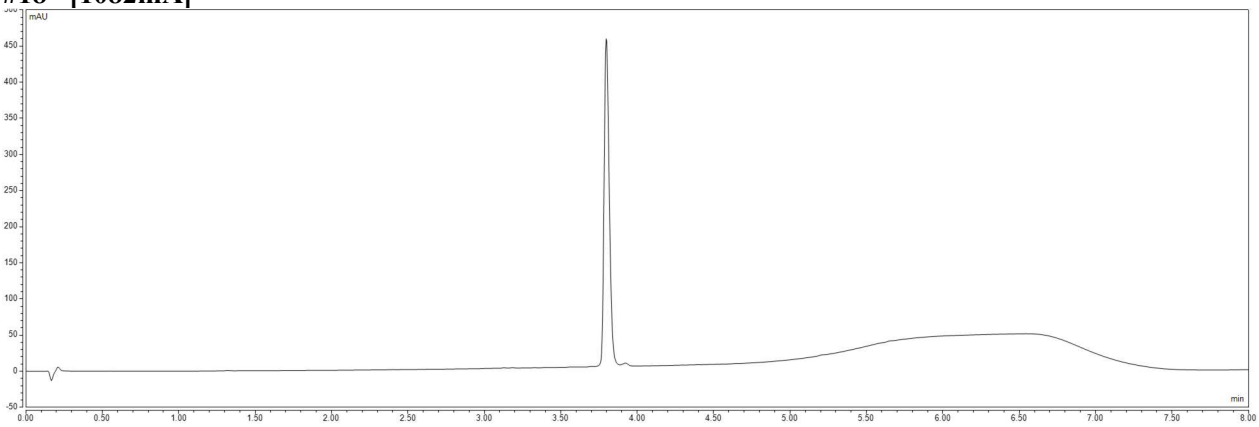

#19 [1083mL]

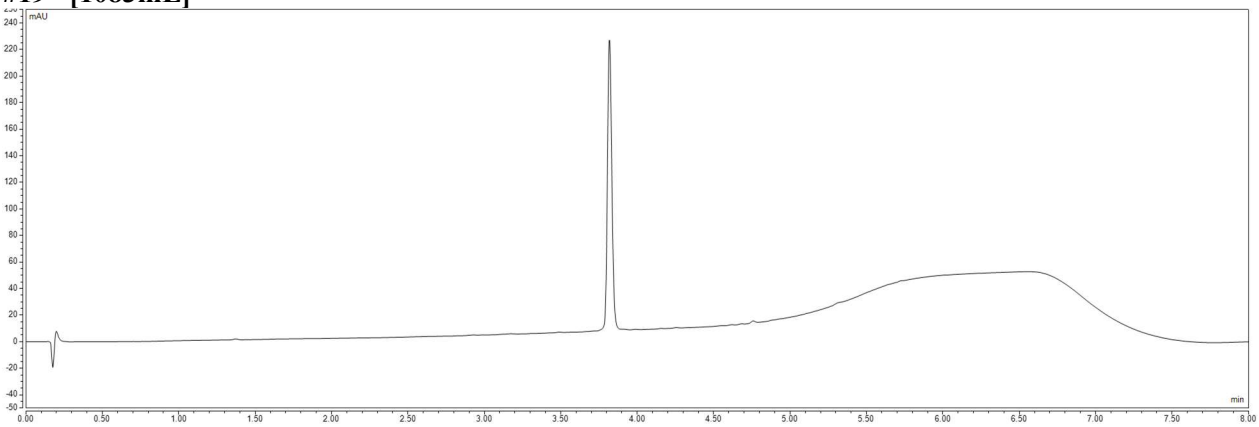

#20 [1085mP]

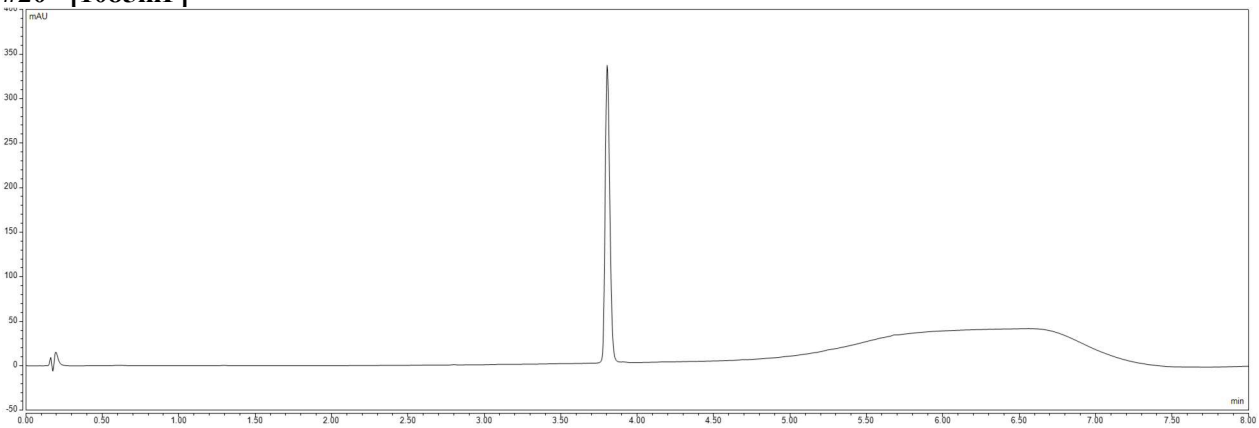

#21 [1047mA;1071mL]

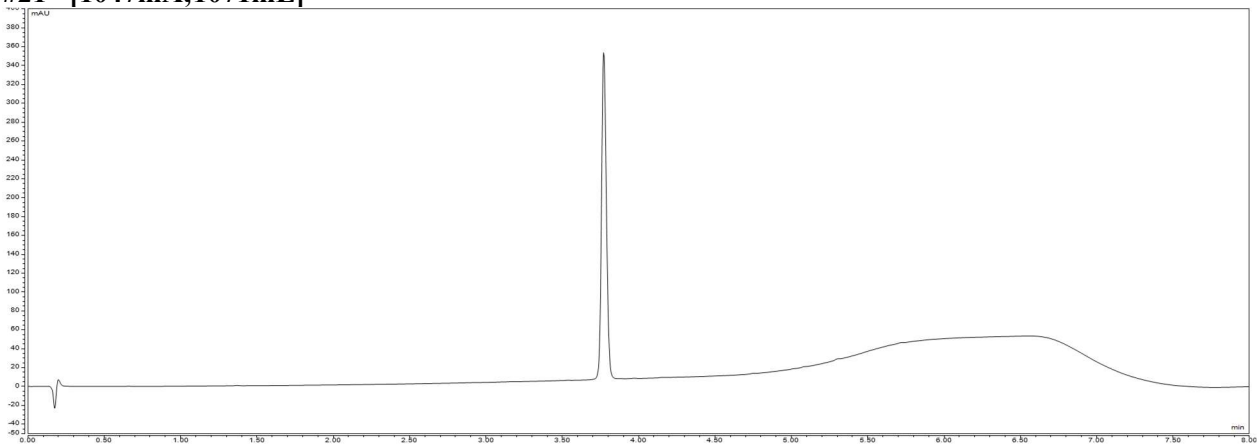

#22 [1047mA;1072mA]

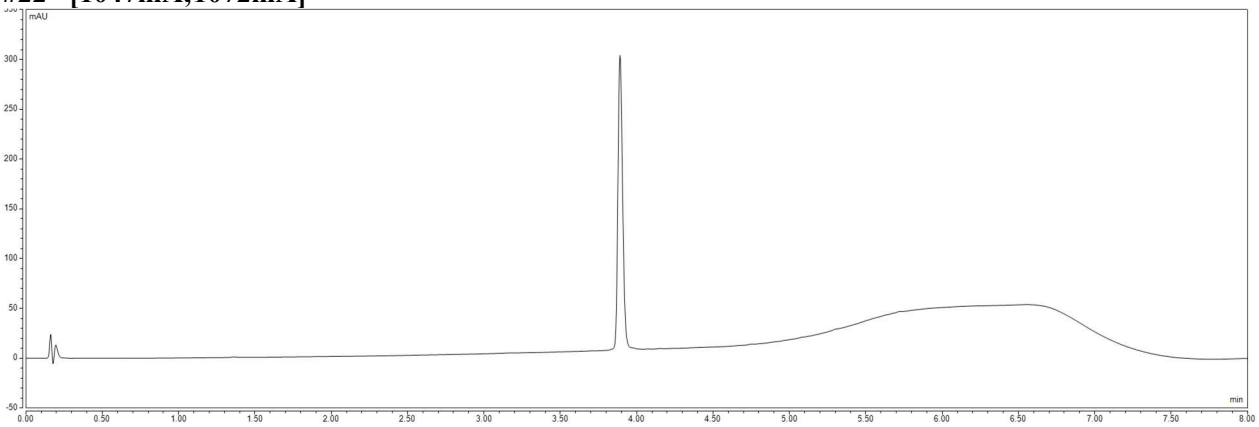

#23 [1047mA;1076mL]

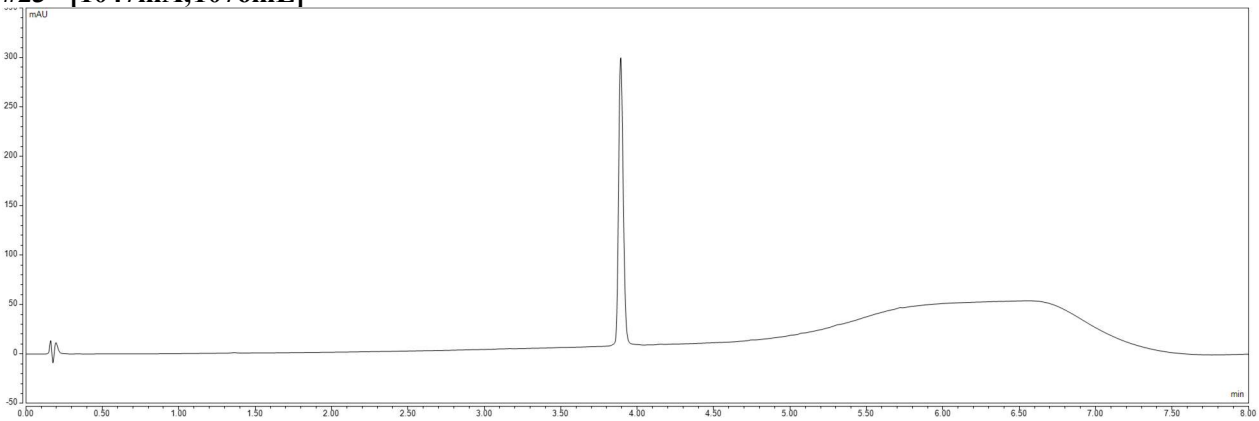

#24 [1047mA;1077mV]

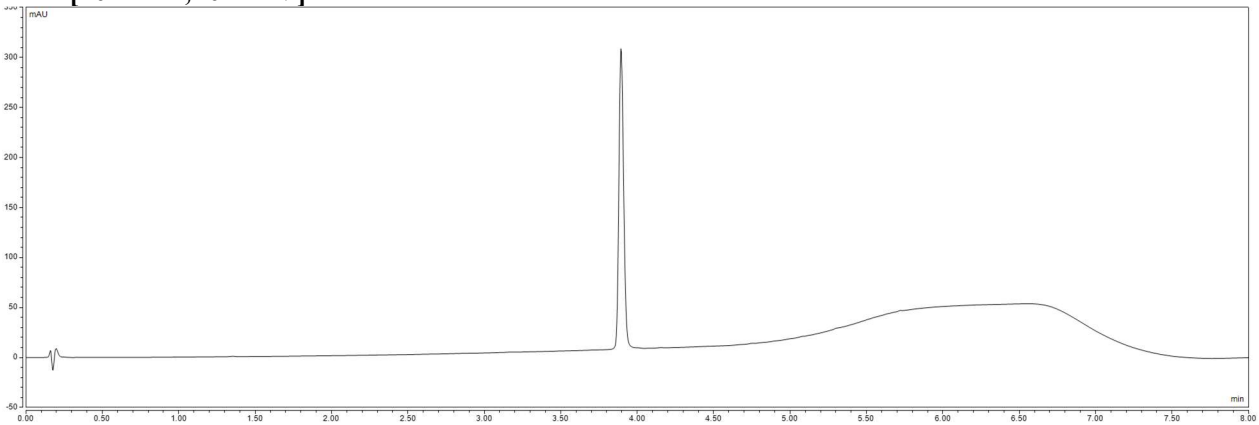

#25 [1047mA;1083mL]

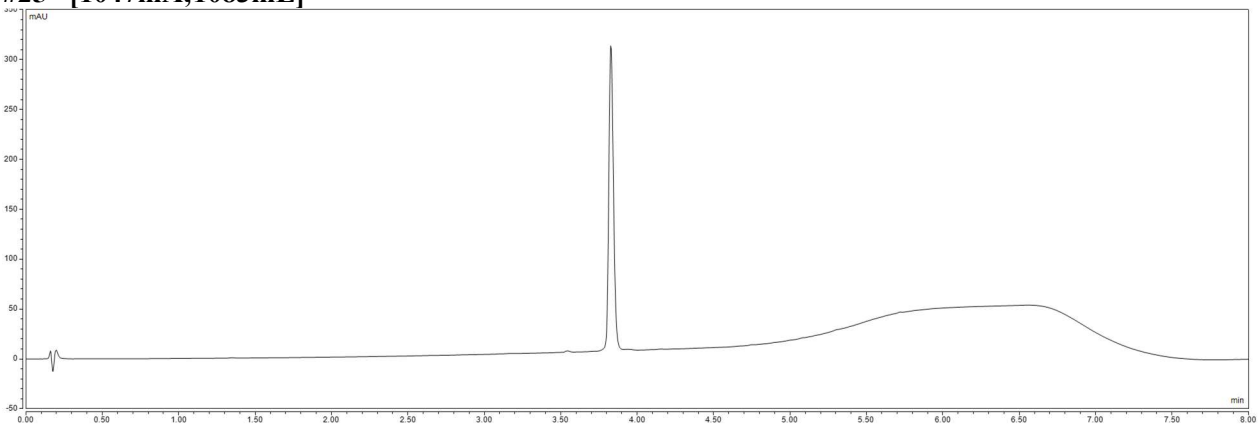

#26 [1048mL;1076mL]

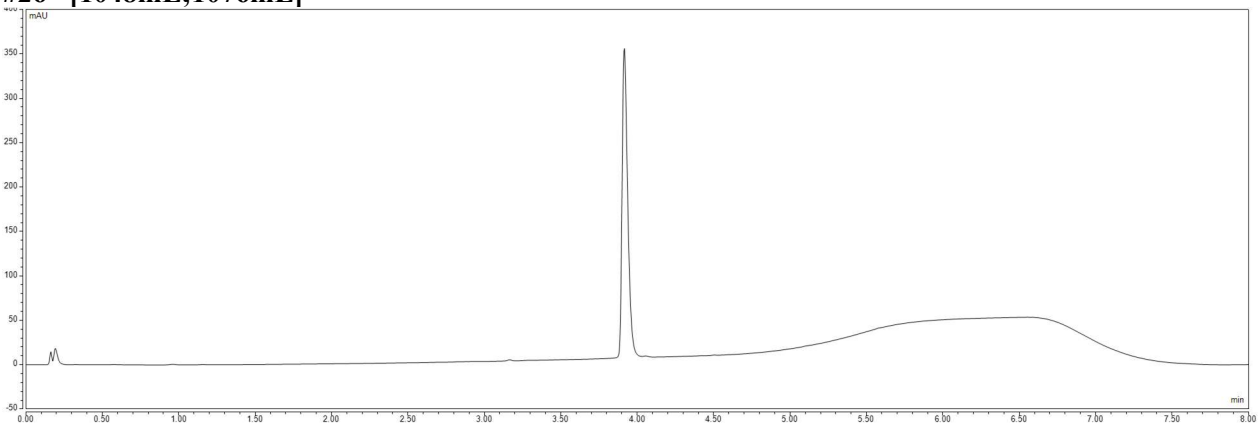

#27 [1048mL;1077mV]

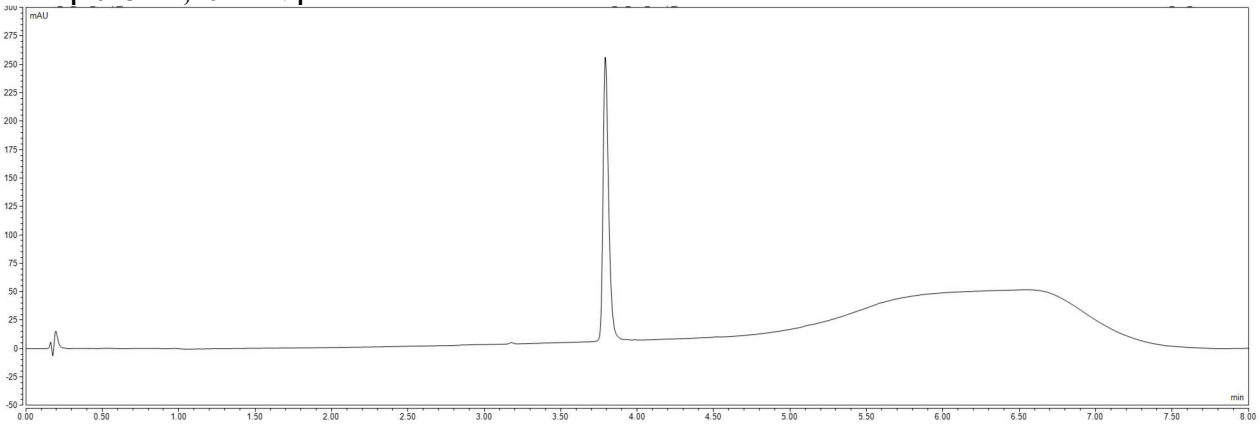

#28 [1048mL;1083mL]

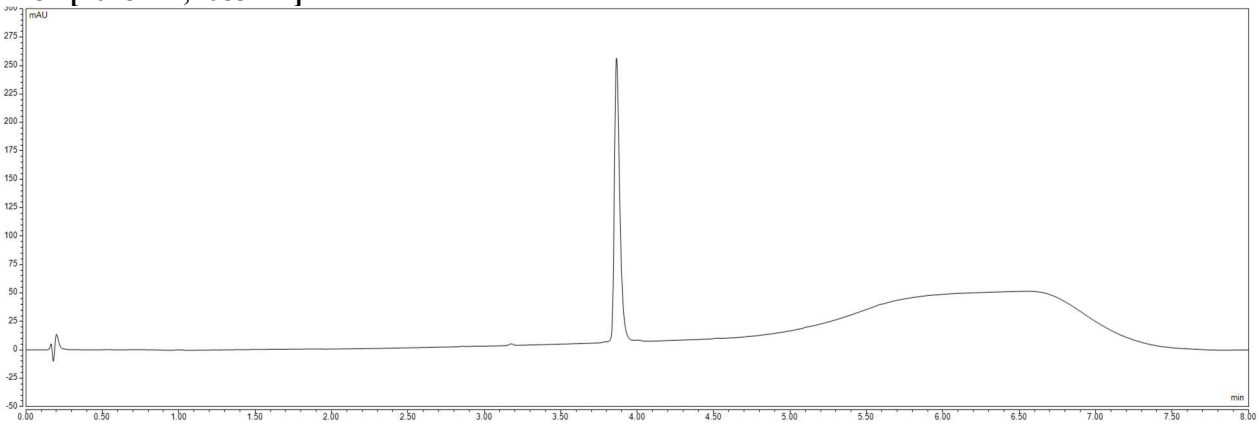

#29 [1050mD;1071mL]

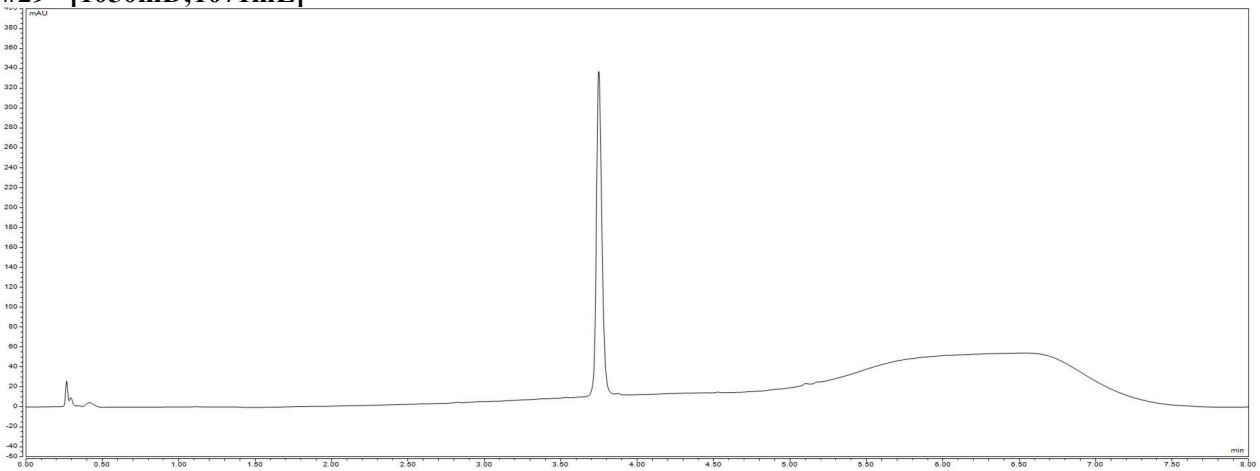

#30 [1050mD;1072mA]

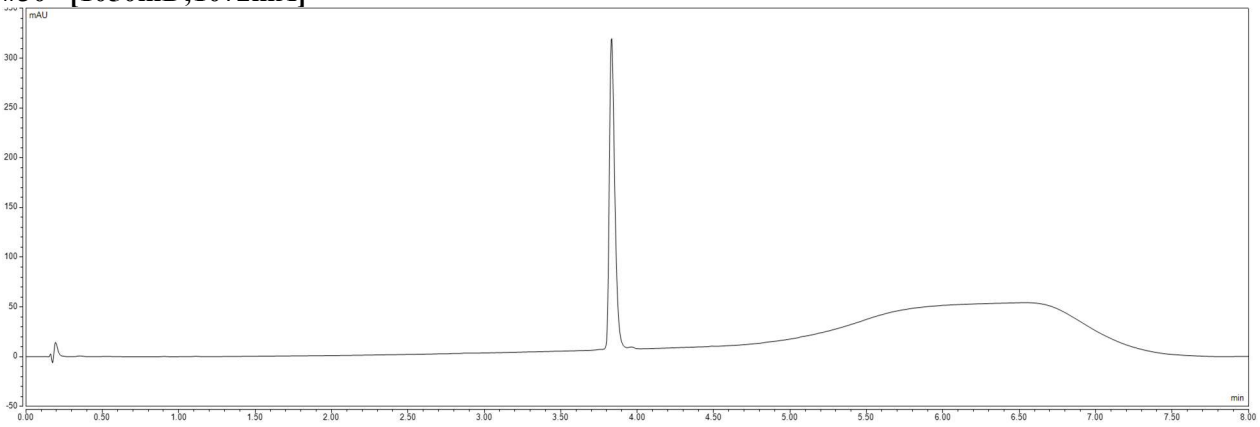

#31 [1050mD;1076mL]

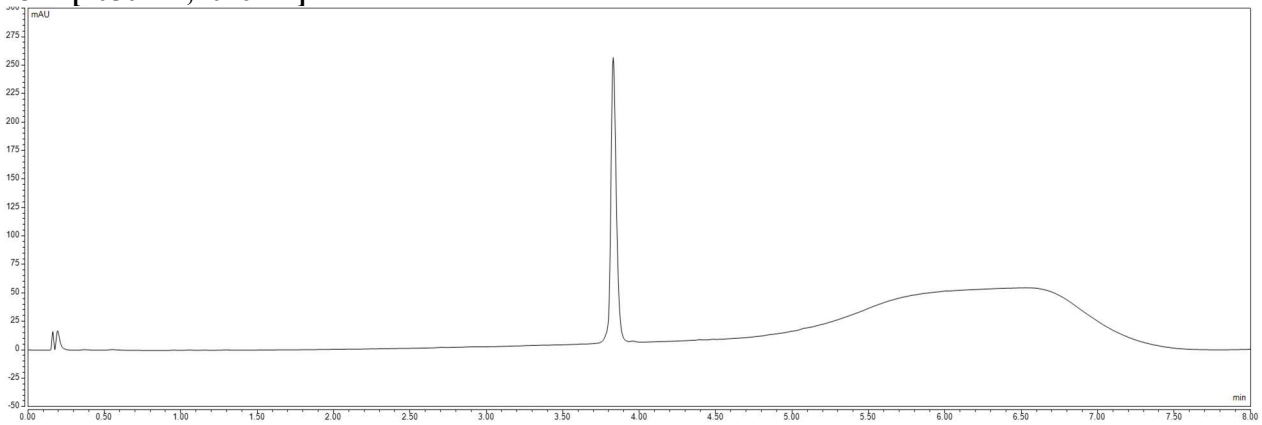

#32 [1050mD;1077mV]

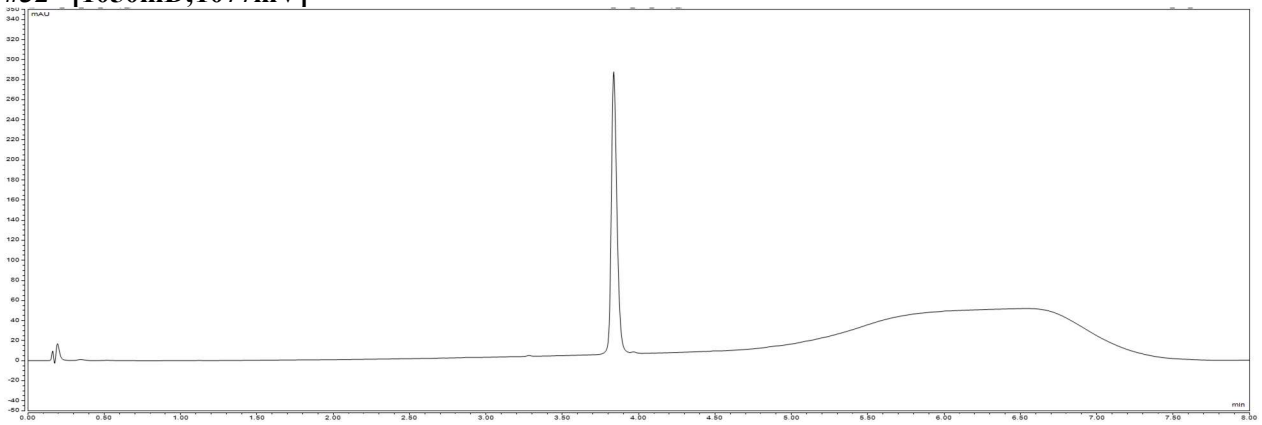

#33 [1050mD;1083mL]

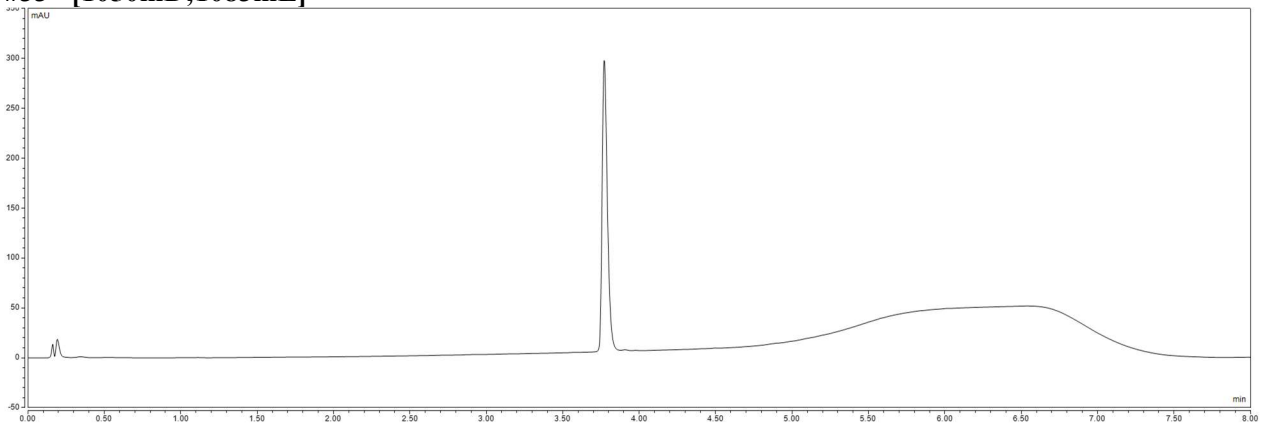

#34 [1055mL;1076mL]

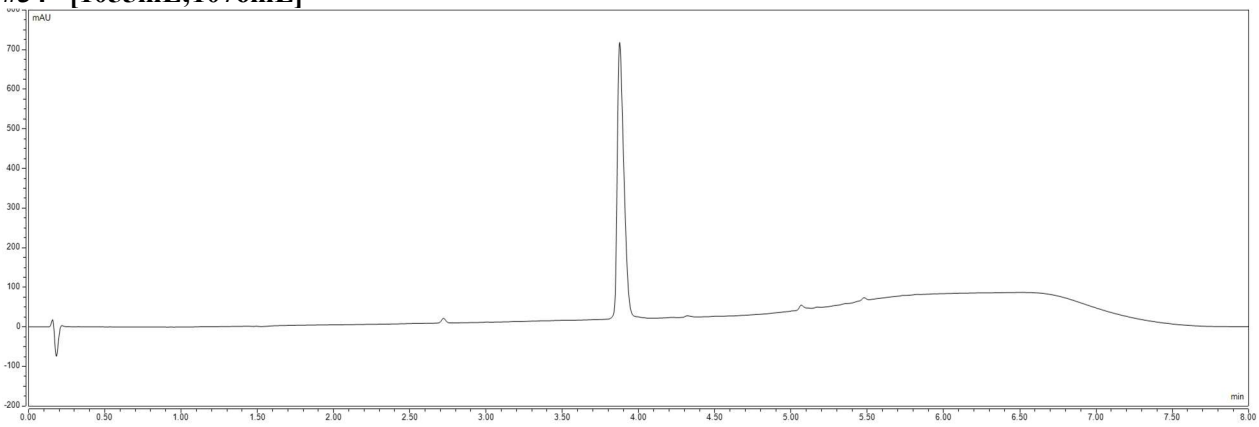

#35 [1061mA;1071mL]

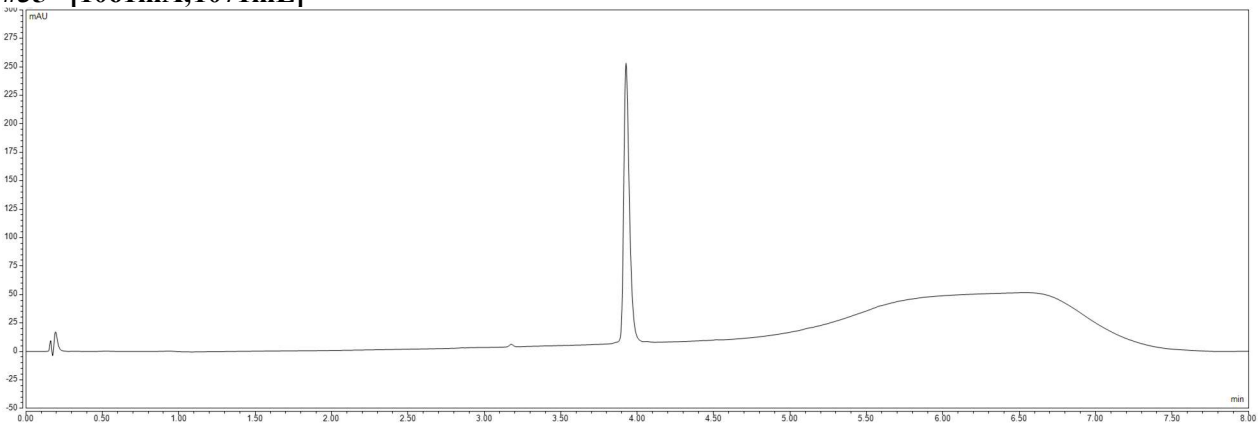

#36 [1061mA;1076mL]

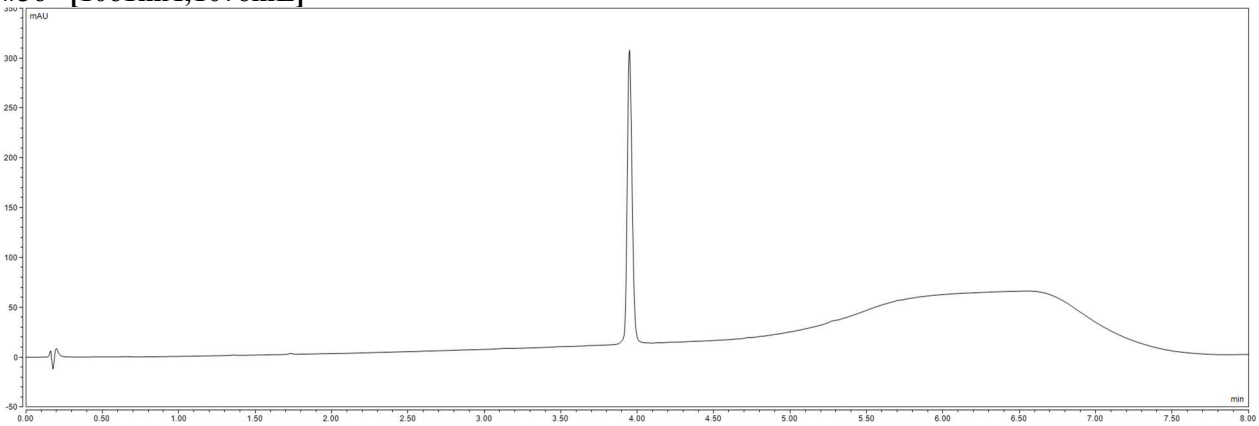

#37 [1061mA;1077mV]

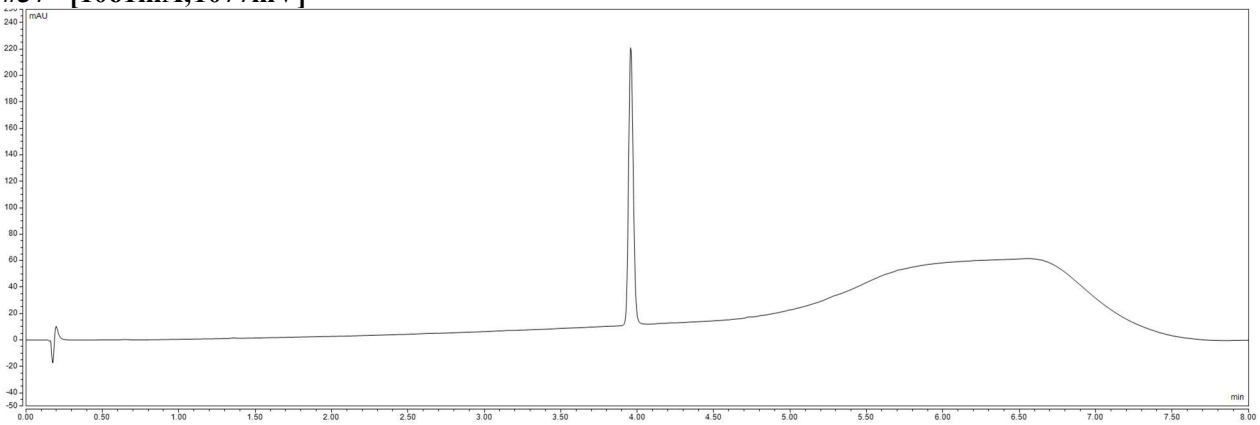

#38 [1061mA;1083mL]

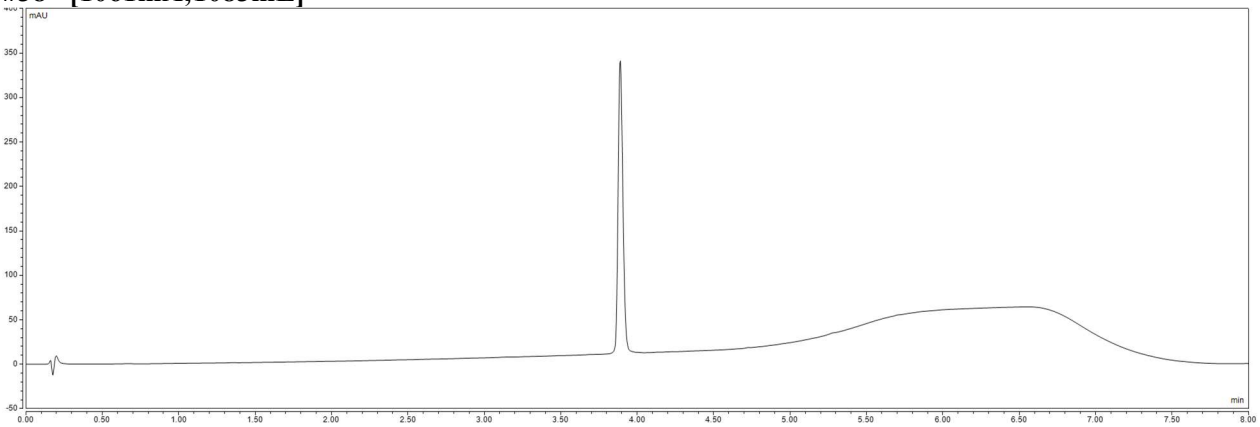

#39 [1064mL;1071mL]

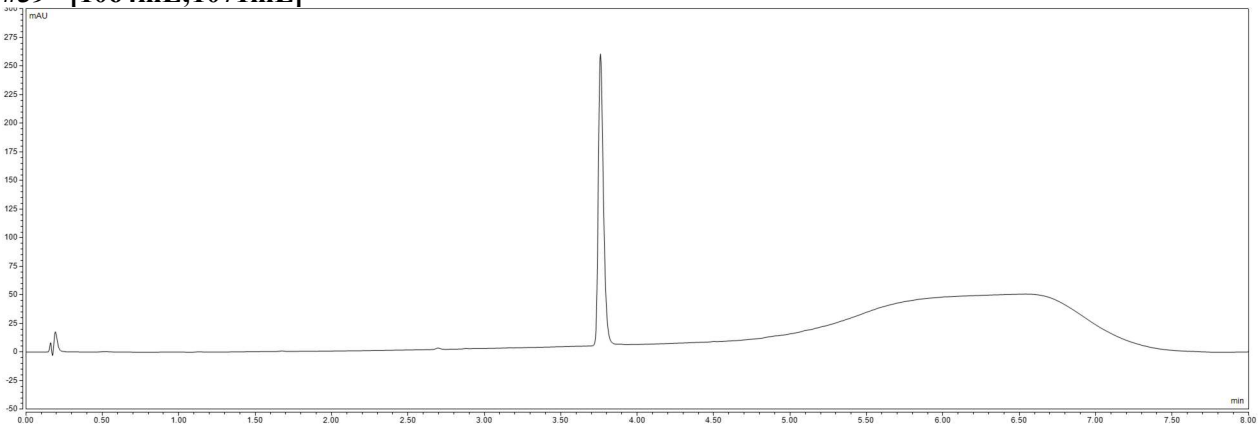

#40 [1064mL;1076mL]

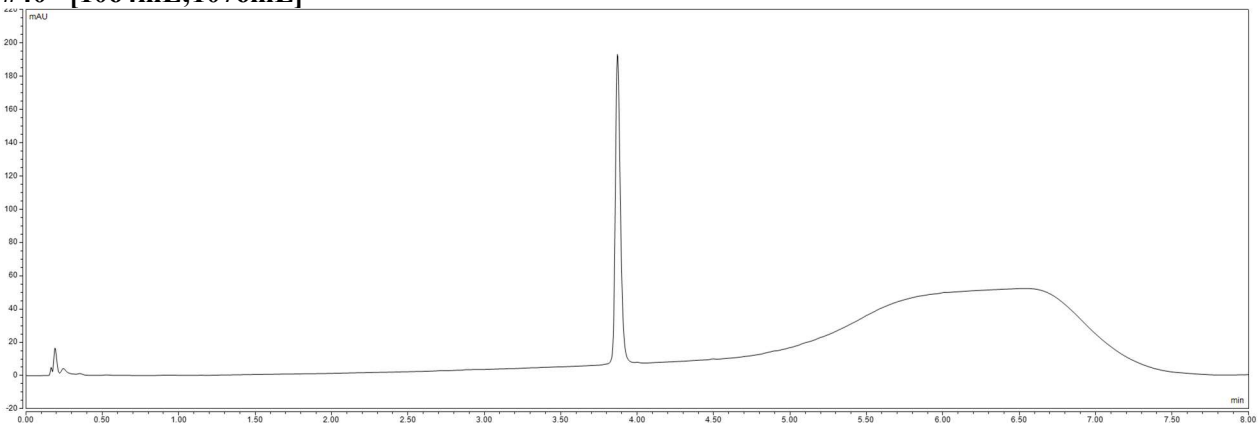

#41 [1064mL;1077mV]

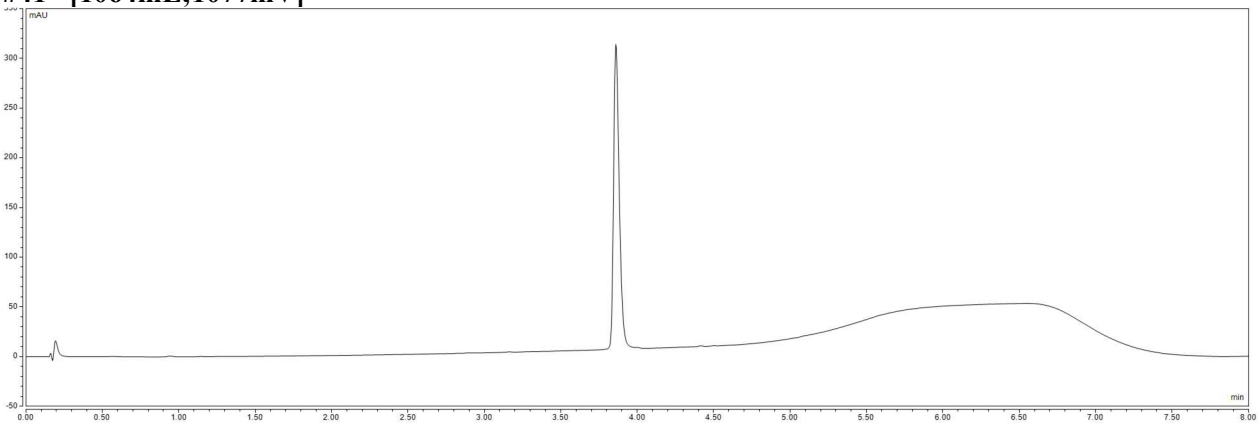

#42 [1064mL;1083mL]

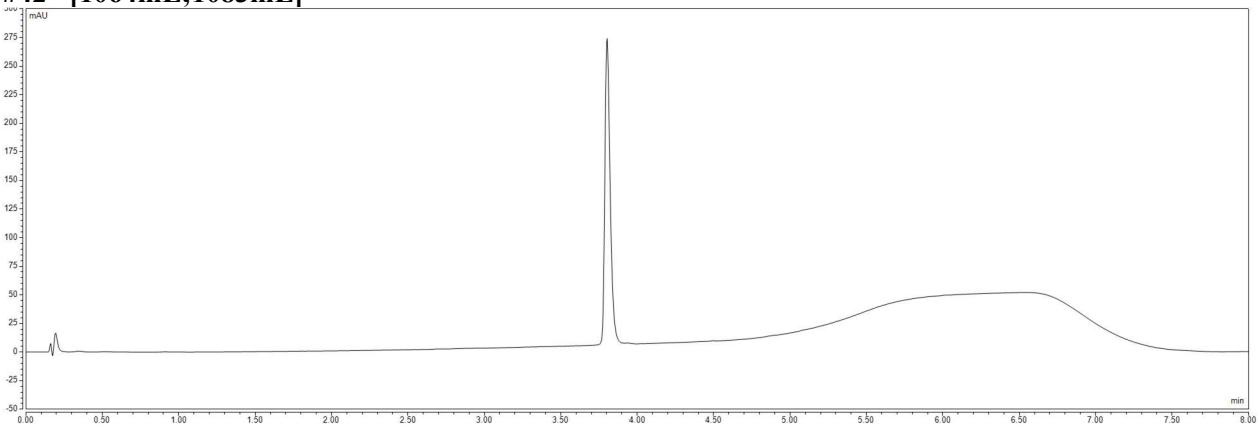

#43 [1047mA;1055mL;1061mA]

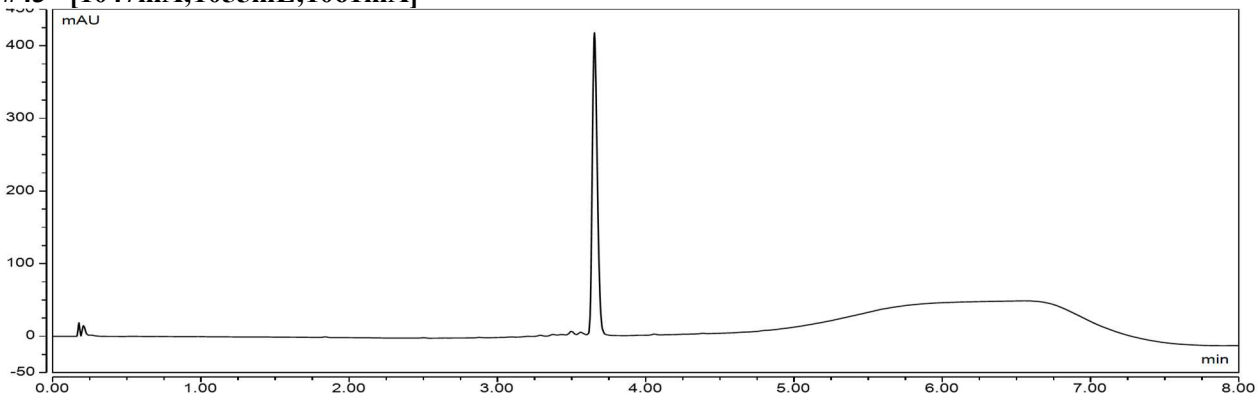

#44 [1055mL;1076mL;1083mL]

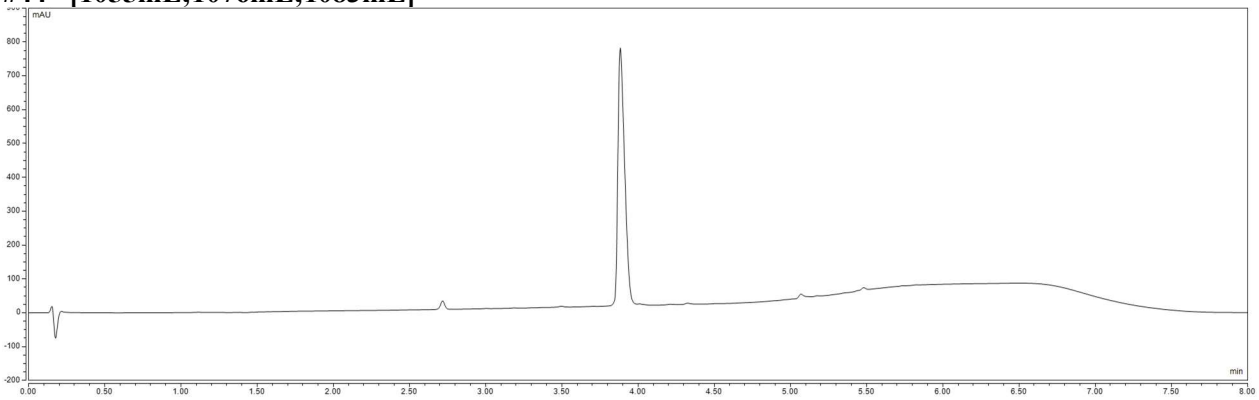

#45 [1047mA;1050mD;1061mA;1076mL]

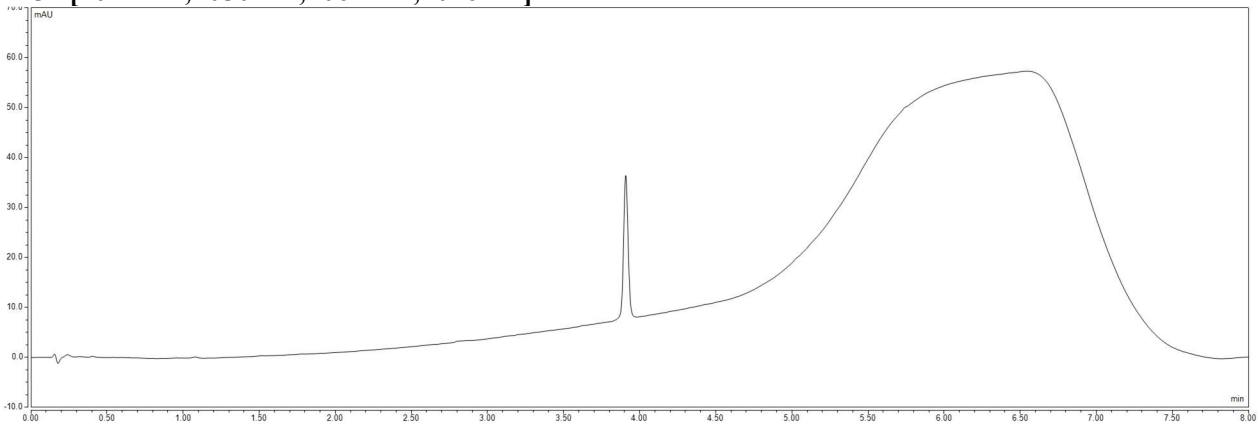

#46 [1047mA;1055mL;1061mA;1076mL]

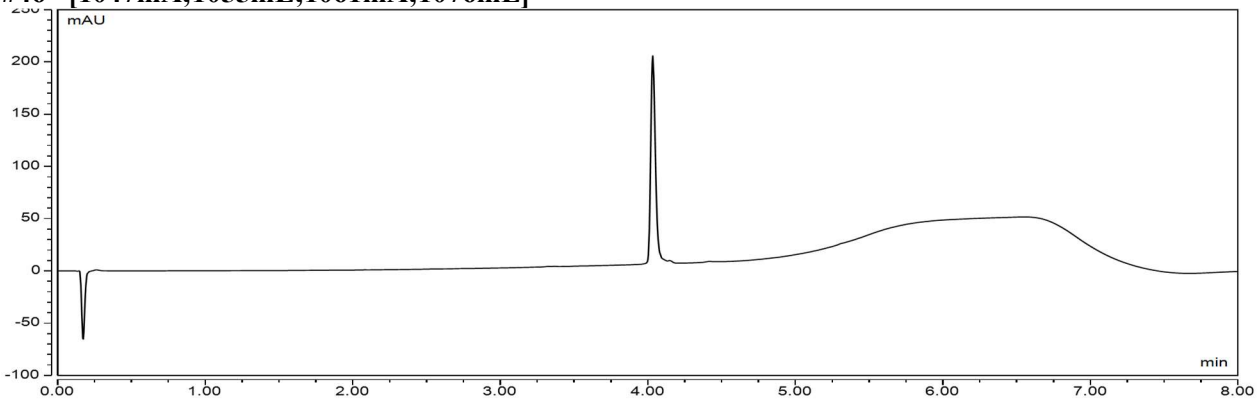

#47 [1047mA;1055mL;1076mL;1083mL]

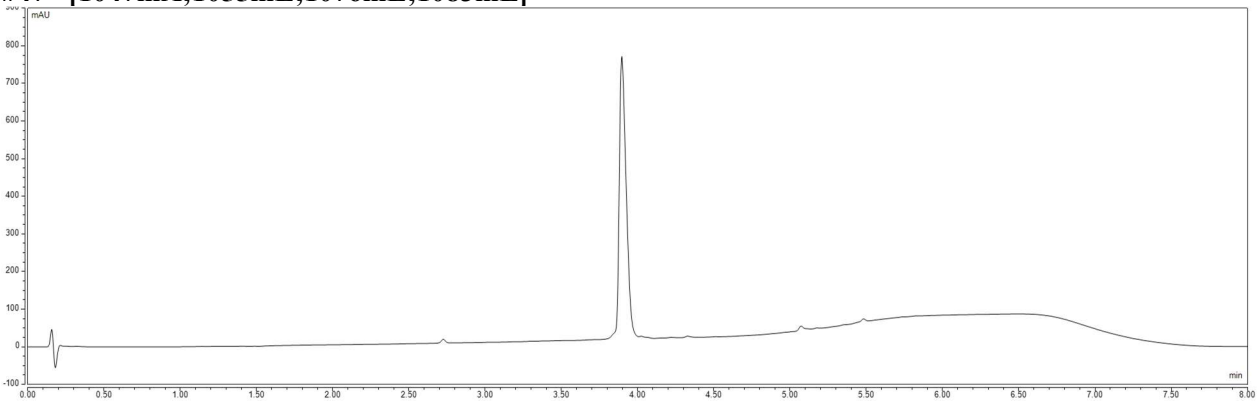

#48 [1047mA;1061mA;1076mL;1083mL]

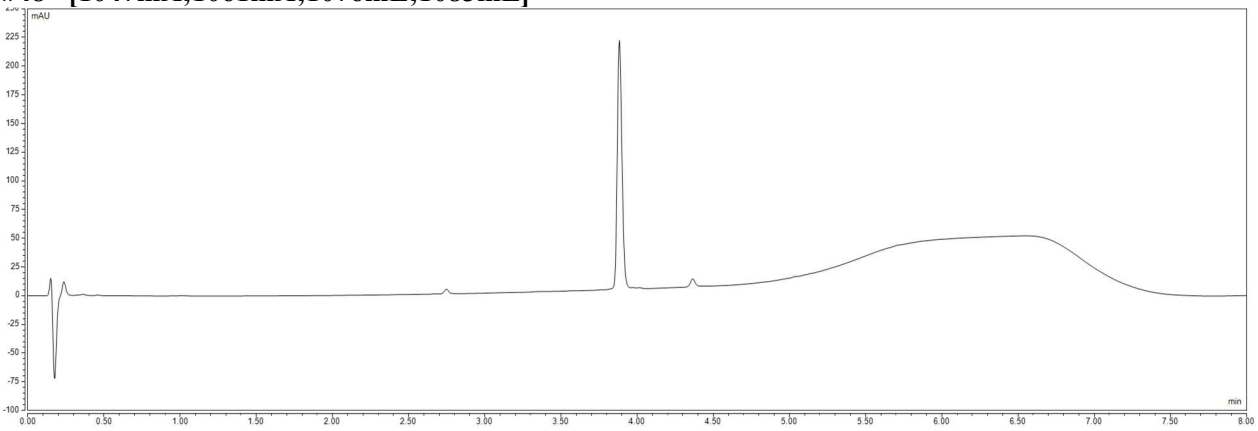

#49 [1047mA;1055mL;1061mA;1076mL;1083mL]

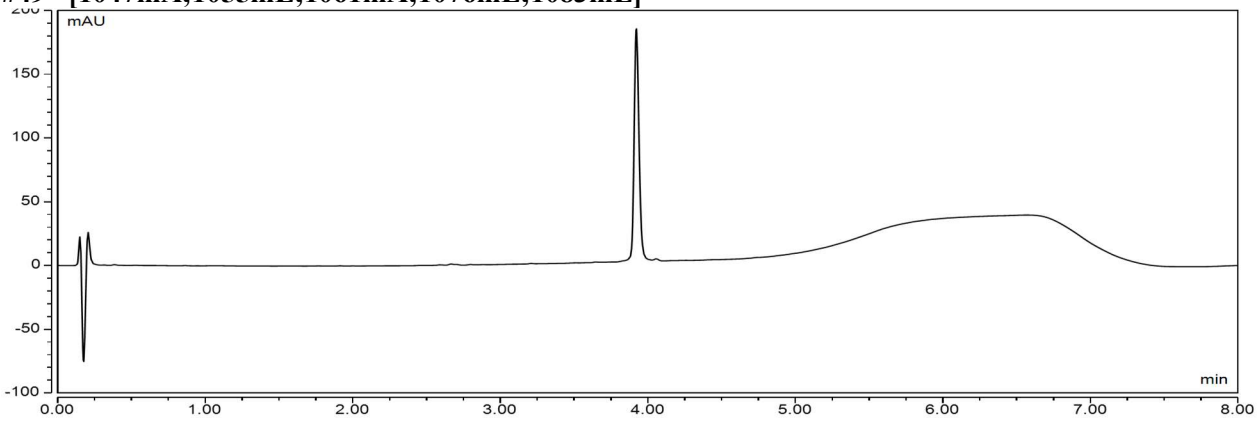

#50 [1047mA;1055mL;1061mA;1076mL;1083mL;1085mP]

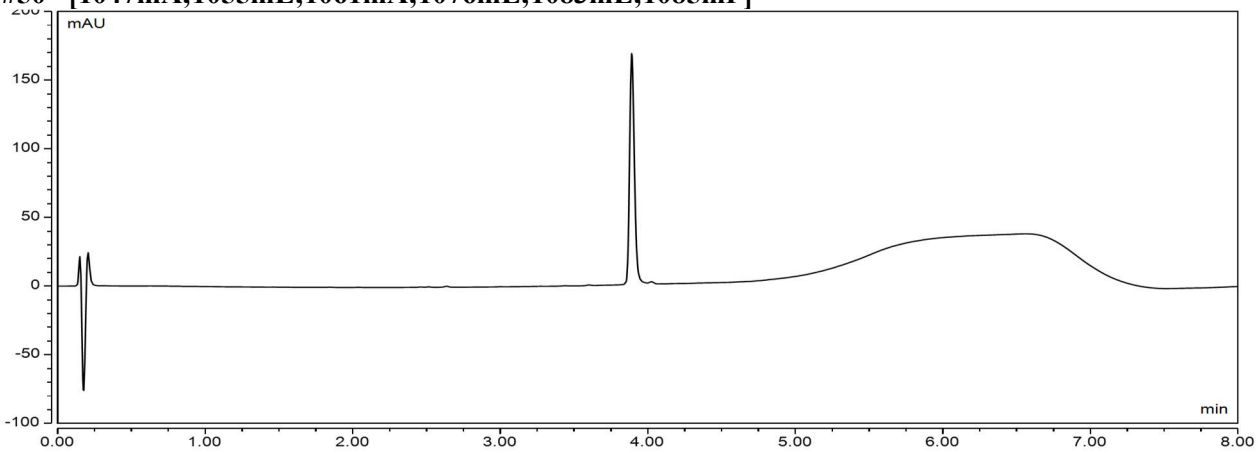

#51 NCBD

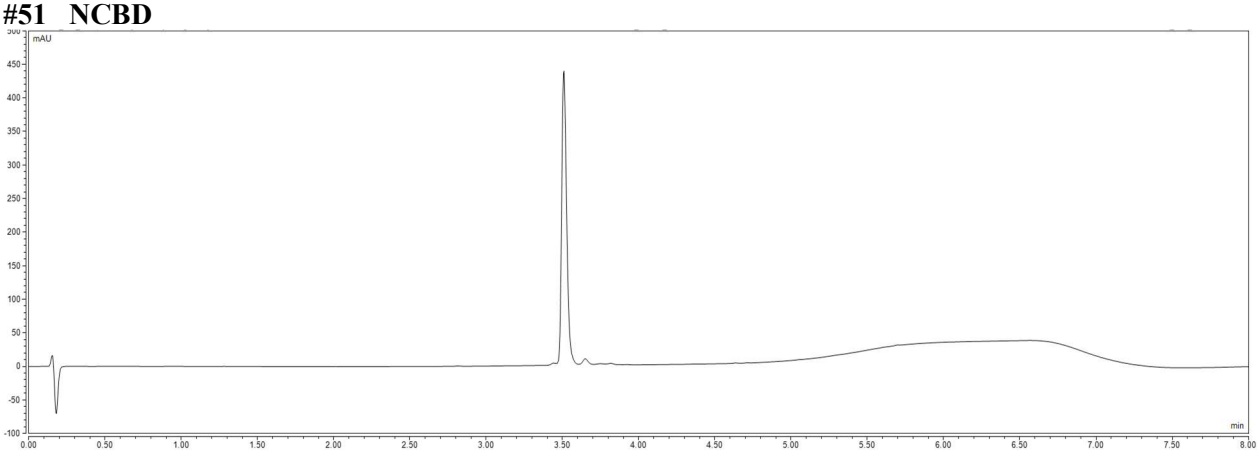

WT-AD1-ACTR-GGG-(PEG)$_3$-K(Biotin)-amide

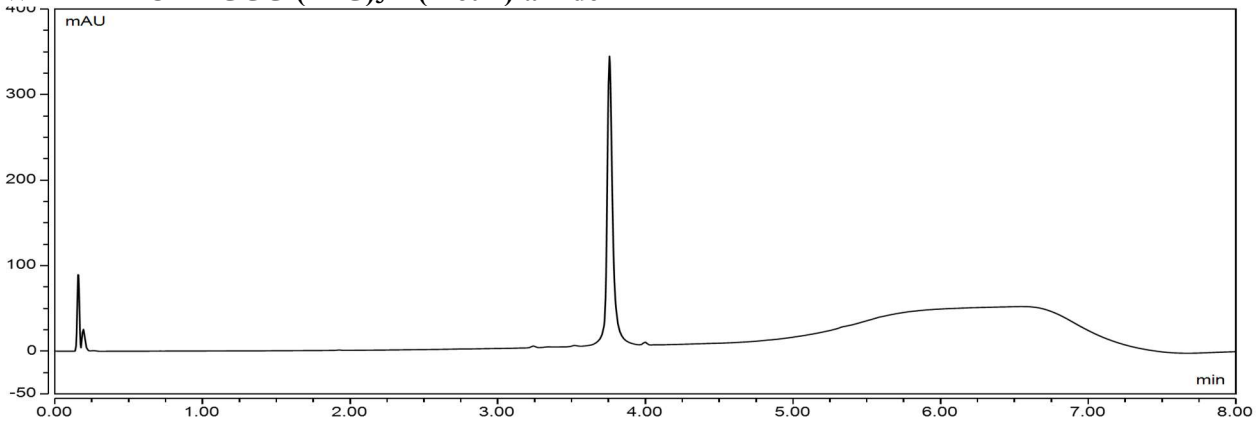

[1055mL]AD1-ACTR-GGG-(PEG)$_3$-K(Biotin)-amide

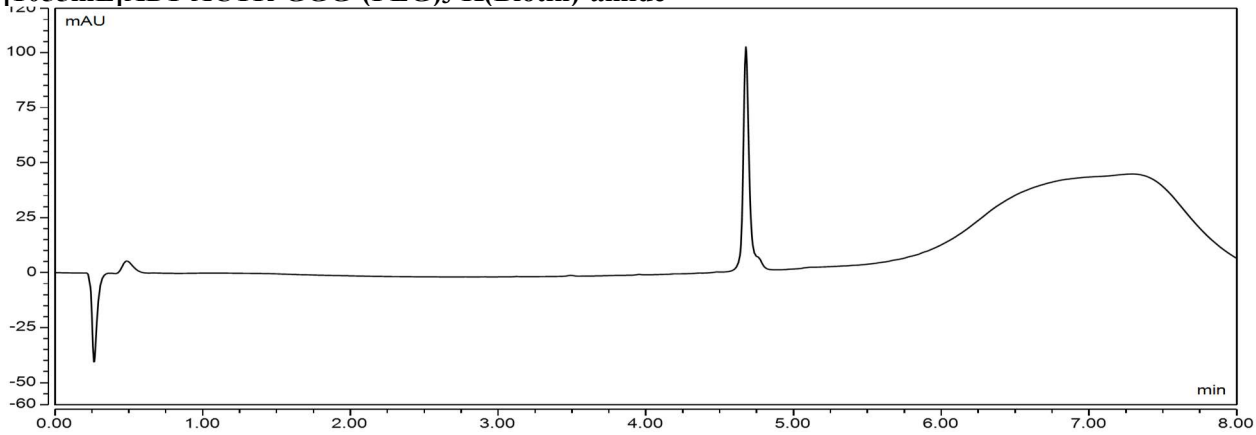

[1076mL]AD1-ACTR-GGG-(PEG)$_3$-K(Biotin)-amide

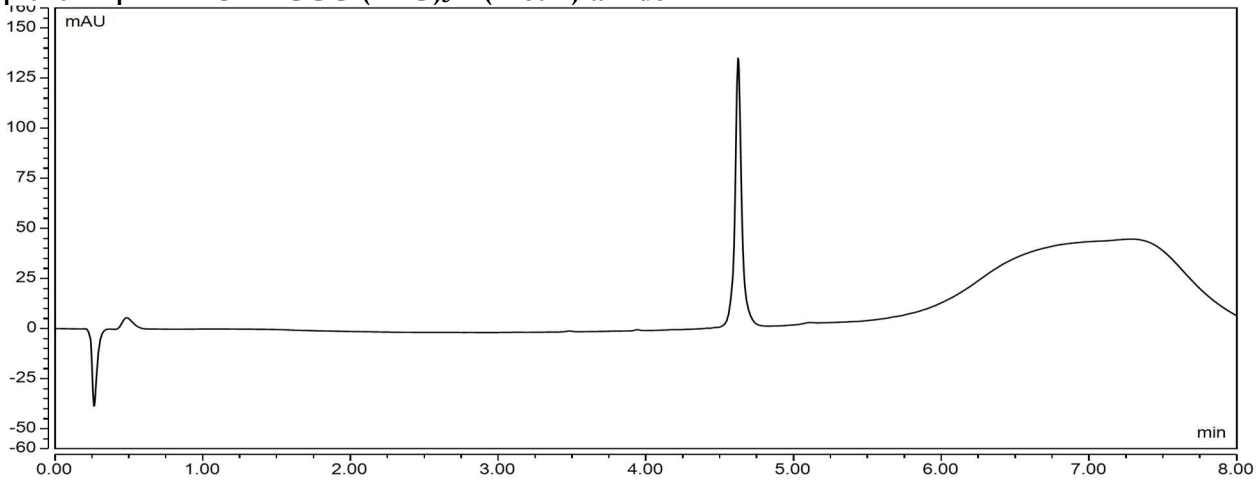

[1055mL;1076mL]AD1-ACTR-GGG-(PEG)$_3$-K(Biotin)-amide

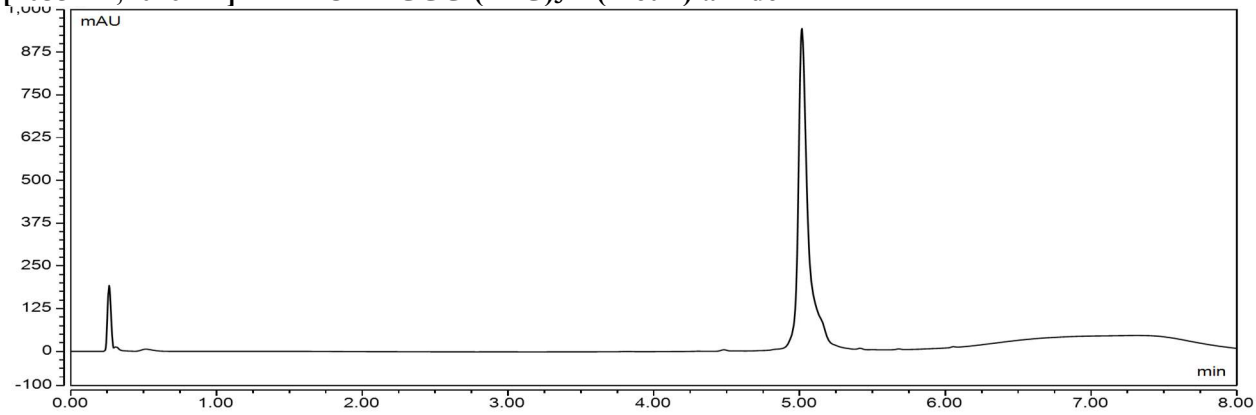

[1064mL;1071mL]AD1-ACTR-GGG-(PEG)$_3$-K(Biotin)-amide

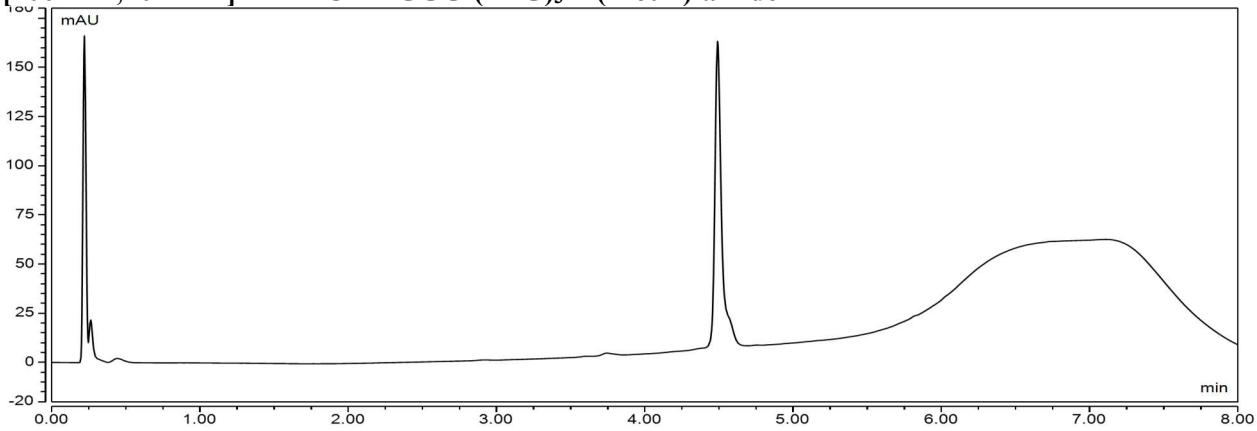

Fluo-(PEG)$_5$-WT-AD1-ACTR

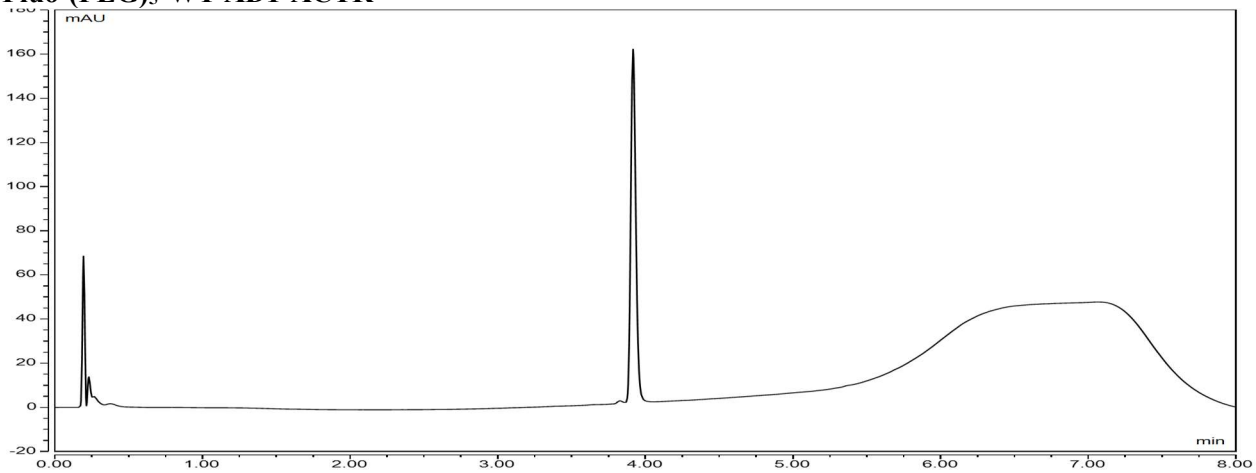

Fluo-(PEG)$_5$-[1055meLeu;1076meLeu]-AD1-ACTR

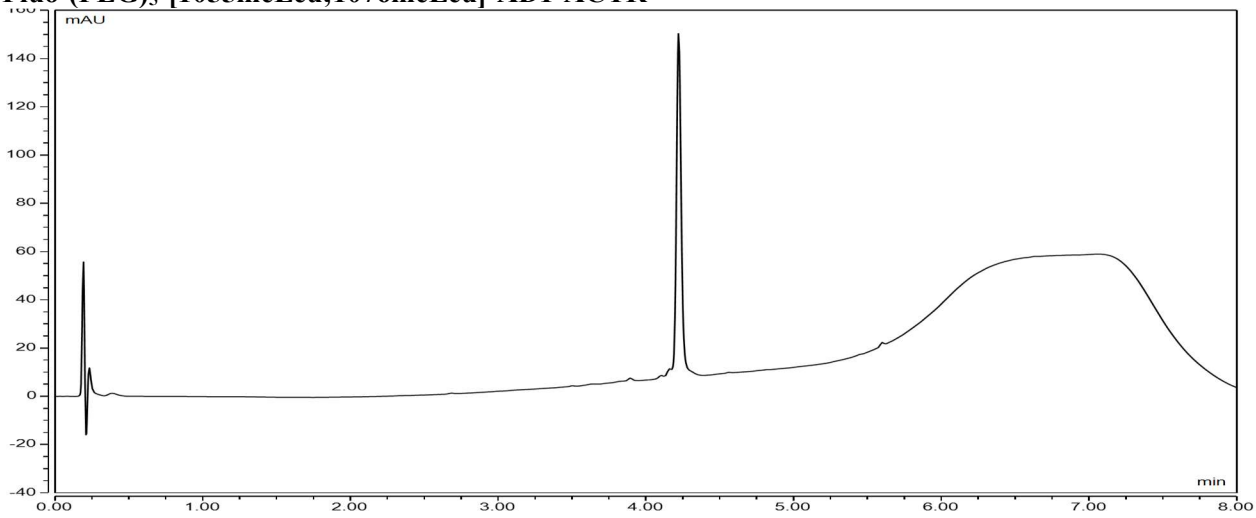

Supplementary References

1. G. Grigoryan, W. F. DeGrado, Probing designability via a generalized model of helical bundle geometry. *J. Mol. Biol.* **2011**, *405*, 1079-1100.
2. P. B. Harbury, J. J. Ptecs, B. Tidor, T. Alber, P. S. Kim, High-resolution protein design with backbone freedom. *Science* **1998**, *282*, 1462-1467.
3. J. Walshaw, D. N. Woolfson, SOCKET: a program for identifying and analysing coiled-coil motifs within protein structures. *J. Mol. Biol.* **2001**, *307*, 1427-1450.
4. P. Jemth, X. Mu, Å. Engström, J. Dogan, A frustrated binding interface for intrinsically disordered proteins. *J. Biol. Chem.* **2014**, *289*, 5528-5533.
5. B. Schmidtgall, O. Chaloin, V. Bauer, M. Sumyk, C. Birck, V. Torbeev, Dissecting mechanism of coupled folding and binding of an intrinsically disordered protein by chemical synthesis of conformationally constrained analogues. *Chem. Commun.* **2017**, 53, 7369-7372.
6. G. Stavropoulos, D. Gatos, V. Magafa, K. Barlos, Preparation of polymer-bound trityl-hydrazines and their application in the solid phase synthesis of partially protected peptide hydrazides. *Lett. Pept. Sci.* **1995**, *2*, 315-318.
7. J.-S. Zheng, S. Tang, Y. Guo, H. N. Chang, L. Liu, Synthesis of cyclic peptides and cyclic proteins via ligation of peptide hydrazides. *ChemBioChem* **2012**, *13*, 542-546.
8. G.-M. Fang, J. X. Wang, L. Liu, Convergent chemical synthesis of proteins by ligation of peptide hydrazides, *Angew. Chem. Int. Ed.* **2012**, *51*, 10347-10350.
9. A. Bekesi et al. Challenges in the structural–functional characterization of multidomain, partially disordered proteins CBP and p300: preparing native proteins and developing nanobody tools. *Methods Enzymol.* **2018**, *611*, 607-675.
10. S. Keller, C. Vargas, H. Zhao, G. Piszczek, C. A. Brautigam, P. Schuck, High-precision isothermal titration calorimetry with automated peak-shape analysis. *Anal. Chem.* **2012**, *84*, 5066-5073.
11. T. H. Scheuermann, C. A. Brautigam, High-precision, automated integration of multiple isothermal titration calorimetric thermograms: New features of NITPIC. *Methods* **2015**, *76*, 87-98.
12. C. A. Brautigam, H. Zhao, C. Vargas, S. Keller, P. Schuck, Integration and global analysis of isothermal titration calorimetry data for studying macromolecular interactions, *Nat. Protocols* **2016**, *11*, 882-894.
13. V. Iešmantavičius, J. Dogan, P. Jemth, K. Teilum, M. Kjaergaard, Helical propensity in an intrinsically disordered protein accelerates ligand binding. *Angew. Chem. Int. Ed.* **2014**, *53*, 1548-1551.
14. S. C. Kwok, R. S. Hodges, Stabilizing and destabilizing clusters in the hydrophobic core of long two-stranded alpha-helical coiled-coils. *J. Biol. Chem.* **2004**, *279*, 21576-21588.
15. D. S. Wishart, C. G. Bigam, J. Yao, F. Abildgaard, H. J. Dyson, E. Oldfield, J. L. Markley, B. D. Sykes, ^{1}H, ^{13}C and ^{15}N chemical shift referencing in biomolecular NMR. *J. Biomol. NMR* **1995**, *6*, 135-140.
16. L. E. Kay, D. A. Torchia, A. Bax, Backbone dynamics of proteins as studied by N-15 inverse detected heteronuclear NMR-spectroscopy - application to staphylococcal nuclease. *Biochemistry* **1989**, *28*, 8972-8979.
17. W. F. Vranken, W. Boucher, T. J. Stevens, R. H. Fogh, A. Pajon, M. Llinas, E. L. Ulrich, J. L. Markley, J. Ionides, E. D. Laue, The CCPN data model for NMR spectroscopy: development of a software pipeline. *Proteins* **2005**, *59*, 687-696.
18. J. T. Nielsen, F. A. A. Mulder, POTENCI: prediction of temperature, neighbor and pH-corrected chemical shifts for intrinsically disordered proteins. *J. Biomol. NMR* **2018**, *70*, 141-165.
19. W. Kabsch, XDS. *Acta Crystallogr. D (Biol. Crystallogr.)* **2010**, *66*, 125-132.

20. T. Jin, W. Chuenchor, J. Jiang, J. Cheng, Y. Li, K. Fang, M. Huang, P. Smith, T. S. Xiao, Design of an expression system to enhance MBP-mediated crystallization. *Sci. Rep.* **2017**, *7*, 40991.
21. A. J. McCoy, R. W. Grosse-Kunstleve, P. D. Adams, M. D. Winn, L. C. Storoni, R. J. Read, Phaser crystallographic software. *J. Appl. Crystallogr.* **2007**, *40*, 658-674.
22. P. D. Adams et al. PHENIX: a comprehensive Python-based system for macromolecular structure solution. *Acta Crystallogr. D (Biol. Crystallogr.)* **2010**, *66*, 213-221.
23. N. W. Moriarty, R. W. Grosse-Kunstleve, P. D. Adams, electronic Ligand Builder and Optimization Workbench (eLBOW): a tool for ligand coordinate and restraint generation. *Acta Crystallogr. D (Biol. Crystallogr.)* **2009**, *65*, 1074-1080.
24. J. Painter, E. A. Merritt, Optimal description of a protein structure in terms of multiple groups undergoing TLS motion. *Acta Crystallogr. D (Biol. Crystallogr.)* **2006**, *62*, 439-450.
25. N. Schmid, C. D. Christ, M. Christen, A. P. Eichenberger, W. F. van Gunsteren, Architecture, implementation and parallelisation of the GROMOS software for biomolecular simulation. *Comput. Phys. Commun.* **2012**, *183*, 890-903.
26. D. Poger, W. F. van Gunsteren, A. E. Mark, A new force field for simulating phosphatidylcholine bilayers. *J. Comput. Chem.* **2010**, *31*, 1117-1125.
27. N. Schmid, A. P. Eichenberger, A. Choutko, S. Riniker, M. Winger, A. E. Mark, W. F. van Gunsteren, Definition and testing of the GROMOS force-field versions 54A7 and 54B7. *Eur. Biophys. J.* **2011**, *40*, 843-856.
28. H. J. C., Berendsen, J. P. M. Postma, W. F. van Gunsteren, J. Hermans, Interaction models for water in relation to protein hydration. In *Intermolecular Forces*; Pullman, B., Ed.; Reidel: Dordrecht, The Netherlands, 1981; pp 331-342.
29. H. J. C. Berendsen, J. P. M. Postma, W. F. van Gunsteren, A. DiNola, J. R. Haak, Molecular dynamics with coupling to an external bath. *J. Chem. Phys.* **1984**, *81*, 3684-3690.
30. J. P. Ryckaert, G. Ciccotti, H. J. C. Berendsen, Numerical integration of the cartesian equations of motion of a system with constraints: molecular dynamics of n-alkanes. *J. Comput. Phys.* **1977**, *23*, 327-341.
31. I. G. Tironi, R. Sperb, P. E. Smith, W. F. van Gunsteren, A generalized reaction field method for molecular dynamics simulations. *J. Chem. Phys.* **1995**, *102*, 5451-5459.
32. A. Glättli, X. Daura, W. F. van Gunsteren, Derivation of an improved simple point charge model for liquid water: SPC/A and SPC/L. *J. Chem. Phys.* **2002**, *116*, 9811-9828.
33. A. P. Eichenberger, J. R. Allison, J. Dolenc, D. P. Geerke, B. A. C. Horta, K. Meier, C. Oostenbrink, N. Schmid, D. Steiner, D. Q. Wang, W. F. van Gunsteren, GROMOS++ software for the analysis of biomolecular simulation trajectories. *J. Chem. Theory Comput.* **2011**, *7*, 3379-3390.
34. X. Daura, W. F. van Gunsteren, A. E. Mark, Folding-unfolding thermodynamics of a β-heptapeptide from equilibrium simulations. *Proteins* **1999**, *34*, 269-280.
35. S. Fournane, S. Charbonnier, A. Chapelle, B. Kieffer, G. Orfanoudakis, G. Travé, M. Masson, Y. Nominé, Surface plasmon resonance analysis of the binding of high-risk mucosal HPV E6 oncoproteins to the PDZ1 domain of the tight junction protein MAGI-1. *J. Mol. Recognit.* **2010**, *24*, 511-523.
36. J. Walshaw, D. N. Woolfson, Open-and-shut cases in coiled-coil assembly: α-sheets and α-cylinders. *Protein Sci.* **2001**, *10*, 668-673.